Politecnico di Torino

Classe delle Lauree Magistrali LM-21

Master's Degree in Biomedical Engineering - Biomechanics

Master's Thesis

CFD ANALYSIS OF A CUSTOM MADE MOCK CIRCULATORY LOOP

Supervisors:

Prof. Umberto Morbiducci

Prof. Antonio D'Amore

Dr. Joan Dario Laubrie Soto

PhD student Elisa Lanzalaco

Candidate:

Provenzano Erika

A.a 2023/2024

Abstract

Valve prostheses are obtained through a design process involving in-vitro behavioural analysis with pulse duplicators that mimic the human heart and cardiac cycle. The pulse duplication device therefore plays an essential role during the in vitro analysis of a valve, which requires careful design. This last aspect is the focus of this thesis, in which supporting analyses were carried out for the creation of a new pulse duplicator model (currently under development at the Tissue Engineering Laboratory of the Rimed Foundation), which will be used to test a new mitral valve model in vitro. The customised pulse duplicator model aims to replicate left-sided chambers of the heart, consisting of atrial and ventricular chambers and offers the possibility to accommodate both the mitral valve (the main object of investigation) and the aortic valve.

Computational fluid dynamics (CFD) was used to evaluate the current design, adopting finite volume-based solver. Specifically, three models were investigated:

- a simplified model with the atrium, ventricle and mitral valve;
- two models based on the original complete design of the pulse duplicator and representing its preliminary and final versions, respectively, which differ in dimensions;

Once the CAD models were created, they were discretized by creating a mesh of quadrilateral elements, which reduced the error rate in the analysis phase. Simulations were then carried out with the aim of reproducing the cardiac cycle in its systole and diastole phases. The dynamic mesh method was used to take into account the movement of the mitral and aortic valves.

From the results obtained, velocity fields in two regions located before and after the mitral valve were analyzed to assess the prototype's ability to reproduce an environment suitable for the in-vitro analysis of a mitral valve.

Currently, the new pulse duplicator model can reproduce accurately the diastolic phase of cardiac cycle, while the obtainment of adequate behavior in the systolic phase is still object of research activity. To date, there is no work in the literature in which CFD has

been used to support the design phase of a pulse duplicator. This therefore turns to be an innovative work aimed at increasing the efficiency and effectiveness of the design cycle.

Acknowledgements

I would like to thank Professor Umberto Morbiducci for supporting me and giving me the opportunity to develop my Master Thesis.

I would like to thank the Ri.MED Foundation, in particular Professor Antonio D'Amore for having welcomed me into his team, giving me the opportunity to work alongside them, providing me with the instrumentation and tools necessary for my research, and sharing his knowledge with me. I would therefore also like to take this moment to thank his team, which has been of constant support throughout this journey and in particular postdoc Joan Dario Laubrie Soto and PhD student Elisa Lanzalaco, for supporting and advising me during the various stages of my research project.

Cardiovascular Tissue Engineering D'Amore Laboratory

Fondazione Ri.MED

Last but not least, I would like to thank my family: my mum, my grandmother, my aunt and uncle, my cousin. I thank my mother for all the sacrifices she made in order to give me this opportunity in life, for always being by my side, for being a reference and support whenever I needed it. I thank my grandmother for always being a shoulder to lean on. I thank my friends for supporting (and putting up with) me, bringing me joy even in difficult times. I thank my family and friends for the love and support they always showed me!

Sommario

Chapter 1

Introduction

1.1 Cardiovascular disease: epidemiology

Cardiovascular disease (CVD) occurs due to the improper functioning of cardiovascular system's components, which affects its normal activity. These cardiovascular disorders are the leading causes of morbidity and mortality in the world, particularly in developed countries[1]. The onset of these diseases is related to the presence of cardiovascular risk factors. This subsequently lead to vascular damage to the target organ, terminal organ failure and death. Risk factors include hypertension, smoking, obesity, and low physical activity[2]. The incidence of these diseases is rising even among young people due to an increased unhealthy risk profile[3]. According to statistics in the United States, 57 million people are affected by cardiovascular diseases, resulting in treatment costs of around 260 billion. These disorders include heart valve disease, for which an estimated 60,000 operations are performed, of which 15,000 are related to congenital problems[4]. According to data published by the American Heart Association, in 2003 there were 19,989 deaths whose primary cause was heart valve (HV) disease and 42,590 ones for which it was a contributing factor[5].

1.2 Prosthetic valves and pulse duplicator for in-vitro testing

Heart valve diseases can affect all four valves, leading to their incorrect functioning related to stenosis or regurgitation problems. These disorders also alter the normally present hemodynamics[6], which considerably influence the functioning mechanisms of the valves. Therefore, it is essential to know the interactions that occur between valves and local haemodynamics in order to understand the functioning of valves and their pathologies[5]. Among valvular heart diseases, those affecting mitral valve are the most common, especially in older people, with an estimated 10% for people over 75 years of age[7]. Their treatment involves surgery in which the compromised valve is repaired or

replaced with a heart valve prosthesis[8]. However, all valves in use today experience flows that differ from those physiologically present in the cardiovascular system, with regions of high velocity values and shear stresses. These are all factors that are unsuitable for blood constituents and contribute to the formation of recirculation regions and clots. Due to the complex environment in which heart valves operate, their design requires a synergy between experimentation and computational techniques [9]. With regard to in vitro testing, standards indicate that valves should be subjected to pulsatile flow testing. For this purpose, pulse duplicators devices are used to analyse the hydrodynamic behavior of the valve, taking into account parameters such as heart rate and pressure values. Several models of these devices have been produced over the years[10]. The use of computational fluid dynamics (CFD) to simulate the pulse duplicator could allow important information such as velocity profiles to be obtained[11]. Indeed, CFD appears to be a valuable tool that, alongside experimentation, can lead to important information that will enable the development of ideal valve prostheses, including tissue prostheses[9]. Specifically, in this thesis, CFD will be used as a tool for the design cycle of a new Pulse duplicator model.

1.3 Outline of the Thesis

The aim of this thesis is to support the design phase of a new Pulse duplicator model developed by the Cardiovascular Tissue Engineering Laboratory operating within the Ri.MED Foundation, which will then be used to conduct in vitro analyses on a new mitral valve model currently under development with the Biomitral project. To this end, innovative research has been carried out, in which computational fluid dynamics has been used as a tool to support the evaluation of the pulse duplicator prototype design. To conduct the analysis, the numerical solver Ansys Fluent 2022 R2 was used, which is based on the finite volume method.

The thesis is structured as follows:

Chapter 1 – Introduction: an overview will be given of the anatomy and physiology of the cardiovascular system, the heart valves that make it up, and in particular mitral valve disorders and the treatments currently in use

Chapter 2 - Background: Computational fluid dynamics and its applications in the biomedical sector will then be presented, followed by an overview of pulse duplicator models presented in the literature;

Chapter 3 - Materials and Methods: The Finite Volumes method and the pulse duplicator experimentation conducted on Ansys Fluent will be presented;

Chapter 4 - Results and discussion: the results obtained in the investigation carried out will be shown and commented on;

Chapter 5 - Conclusion;

1.4 An insight into the heart

The heart has a trapezoidal shape; its position can be easily identified within the rib cage by means of landmarks [Figure 1]:

- At the level of the fifth intercostal space, on the mid-clavicular line, is the apex of the heart;
- The lower edge is positioned between the sixth left and right ribs;
- The upper edge is located at the second and third and behind the sternum;
- On the right, between the sixth and third cartilage, the right edge is placed[12];

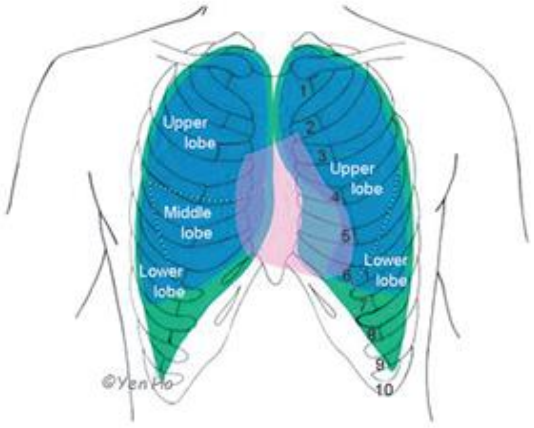

Figure 1 – Position of the heart in the rib cage [12]

The heart is formed by 4 chambers divided into 2 atria and 2 ventricles. The first collect blood from the body, specifically the left atrium collects blood from the lungs, while the right atrium receives blood from the rest of the body. The ventricles direct blood to the body, more precisely the right ventricle to the lungs, while the left one pumps blood throughout the rest of the body.

The blood flows unidirectionally due to the presence of four valves: pulmonary, aortic and the valves separating the atria and ventricles, which are the tricuspid and mitral[13].

The cardiovascular system deals with the nutritional and immunological needs of various cells through what can be considered a closed circuit; blood from the left heart, through the aorta, reaches the arterial system, then returns through the venous system to the vena cava, which carries it to the right heart. From there, through the pulmonary artery, the blood goes to the lungs and, through the pulmonary vein, returns to the left side of the heart[14]. [Figure 2].

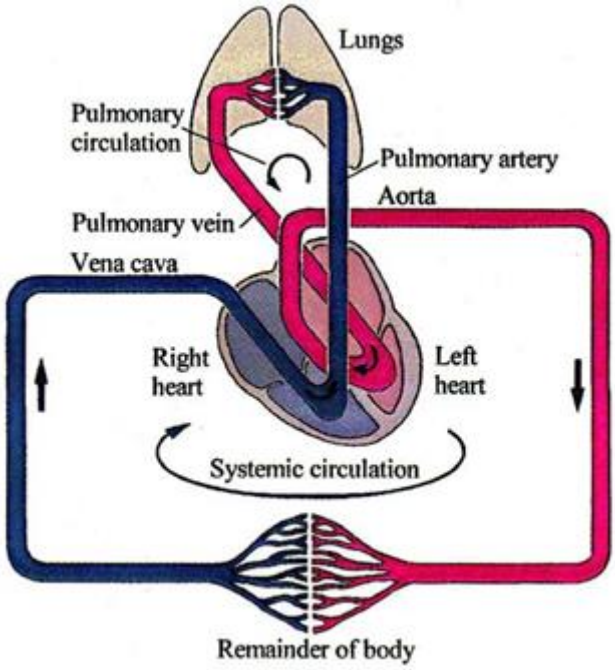

Figure 2 – Organization of cardiovascular system[14]

The heart chambers are characterised by different shapes and thicknesses, as they adapt to the volume of blood they must accommodate and to the pressures they are subjected to. In fact, the right side of the heart is generally subject to less pressure than the left side. For this reason, the walls that make up the right atrium are thinner, undergoing an average pressure of 2-6 mmHg, and are able to accommodate about 60 ml of blood. The shape of its walls facilitates flow towards the tricuspid valve, which opens when the ventricular pressure is lower than the atrial pressure, allowing blood to flow into the right ventricle. Pressure values are also lower than the left counterpart, with values around 8-12 mmHg. From the right ventricle, blood is pumped by contraction to the pulmonary valve, which is called the semilunar valve. Then the blood reaches the pulmonary artery, which is the only artery in the body that carries deoxygenated blood.

The left atrium generally collects about 60-70 ml of blood, which is conveyed to the left ventricle through the mitral valve. This is composed of two leaflets, papillary muscles and chordae tendineae that enable it to be attached to the walls of the ventricle. This one has a thickness of 8-10 mm and collects 100-120 cc of blood. From here, the blood passes through the aortic valve, to the aorta and then to the subclavian, branchicepphalic and carotid arteries, and into the systemic circulation[15].

Within the walls of the heart, three layers can be distinguished; starting from the inside and going outwards there are: endocardium, myocardium and epicardium. The walls of the heart are supplied with blood through the coronary arteries, which are classified into the right coronary artery, the left anterior descending artery and the left circumflex artery[13].

In order to distribute the right supply of blood to all cells, pumping action is required, which occurs through the heartbeat, which consists of two phases: systole and diastole. Diastole is identified by the passive passage of blood from the atria to the ventricles (which corresponds to what is called the E wave) and atrial contraction (which corresponds to the A wave), while in systole it is the ventricles that contract in order to send blood to the corresponding arteries. The inverse of the duration of a heartbeat is the heart rate (HR) which identifies the number of beats per minute. Another key parameter is the cardiac output, which indicates the volume of oxygenated blood

supplied by the left ventricle in one minute. Under resting conditions, physiological HR values are around 60-100 bpm (beats per minute) [Figure 3].

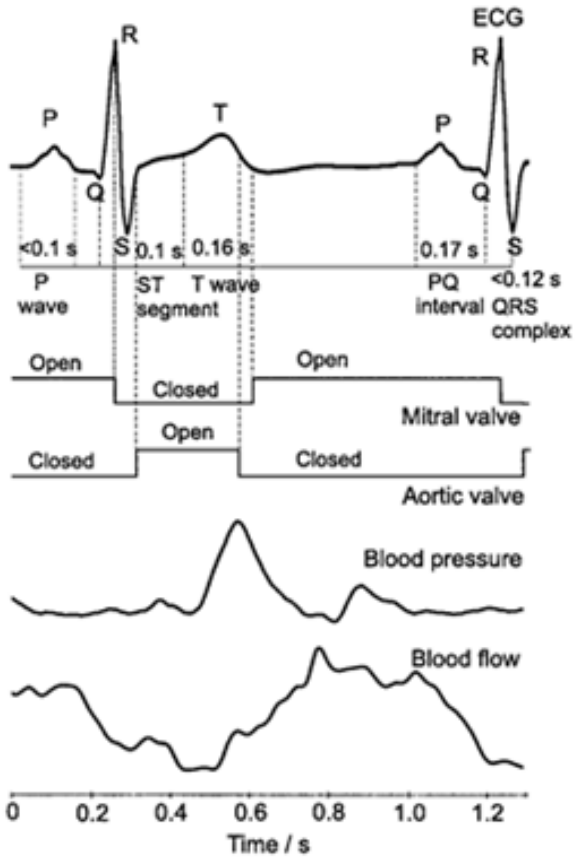

Figure 3 - Electrocardiographic signal of a heart in a normal state and trends in blood pressure and flow[14]

When HR values are below 60 bpm a bradycardia occurs, where the decrease in beats leads to a reduction of blood flow and thus oxygen to the various organs, as a result of which symptoms such as fatigue and fainting may occur. When HR is greater than 100 bpm, tachycardia is associated with an increase in inflammatory molecules and mechanical stress on the heart, resulting in an increased risk of mortality [16] [Figure 4].

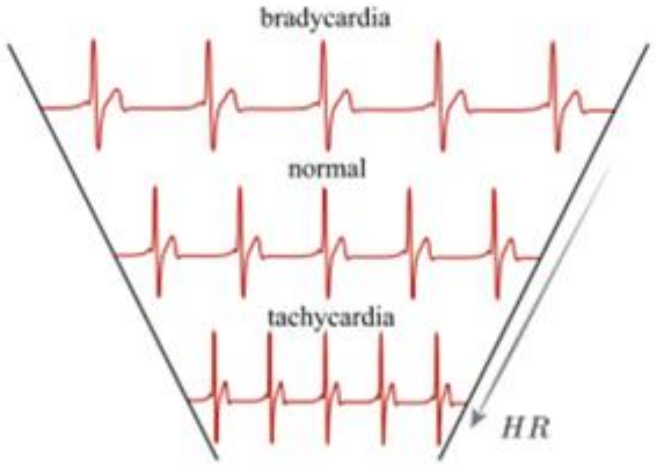

Figure 4 - Electrocardiographic signal related to a brachycardial, normal and tachycardiac state[16]

1.4.1 Heart valves: anatomy and fisiology

Heart valves (HV) play a complex biomechanical role. Their main task is to allow blood to flow in a single direction, reacting passively to the forces applied by the blood. Based on their function, valves can be classified into:

- Semilunar valves: pulmonary and aortic valves, which obstruct the passage of backward blood flow during diastole;
- Atrioventricular valves: tricuspid and mitral valves prevent the passage of backward flow from the ventricles to the atria during the period of systole;

These actions are performed for each heartbeat, so considering the entire lifespan, it is possible to estimate an opening and closing of the HV of about 3 x 10^9 times[17]. The four heart valves are positioned in a plane that can be considered the base of the heart and constitutes its fibrous skeleton. It's in fact composed mainly of collagen fibers that enable its stability. [Figure 5].

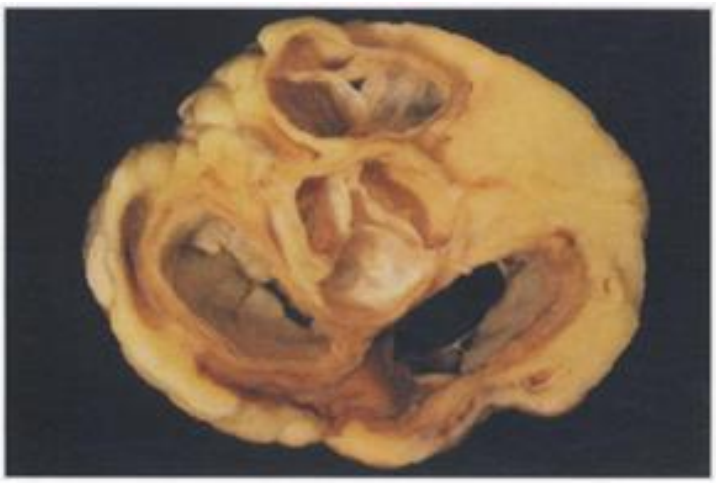

Figure 5 – The positioning of the four valves[18]

Each valve can be considered connected to the others, but at the same time has its own anatomical and physiological characteristics specific to the context in which it must work[18] [Figure 6].

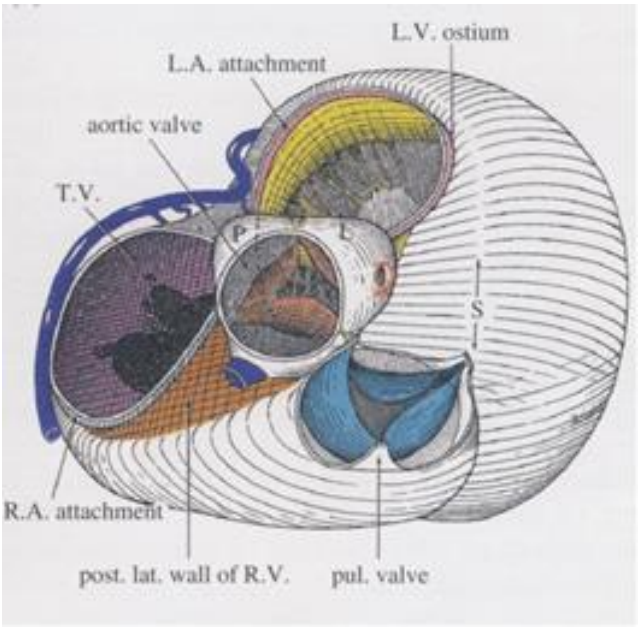

Figure 6 – Valve position in relation to the heart chambers[18]

1.4.1.1 Mitral valve

The mitral valve's name comes from its resemblance to the liturgical headdress used by Bishops and called 'mitre'. As explained above, it is housed in the left side of the heart and precisely between the atrium and ventricle.

Compared to the other left valve, it has a greater extension and is also subject to greater pressure. Its apparatus is composed by the annulus and the chordae tendineae that bind the leaflets to the papillary muscles[19] [Figure 7,8].

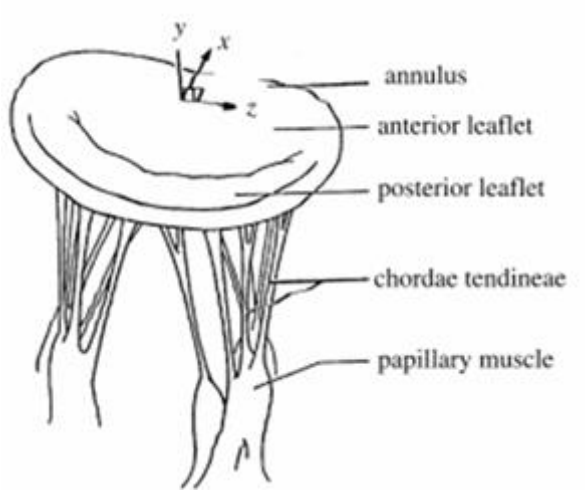

Figure 7 – Mitral valve apparatus[20]

The mitral annulus (MA) is composed of parallel-oriented collagen fibers and has a so-called saddle shape. It consists of an anterior and a posterior section that is less attached to the surrounding tissue, making it capable of movement in relation to the cycle of contraction and relaxation[21]. Regarding leaflets, two areas can be distinguished: the translucent zone and the rough zone.

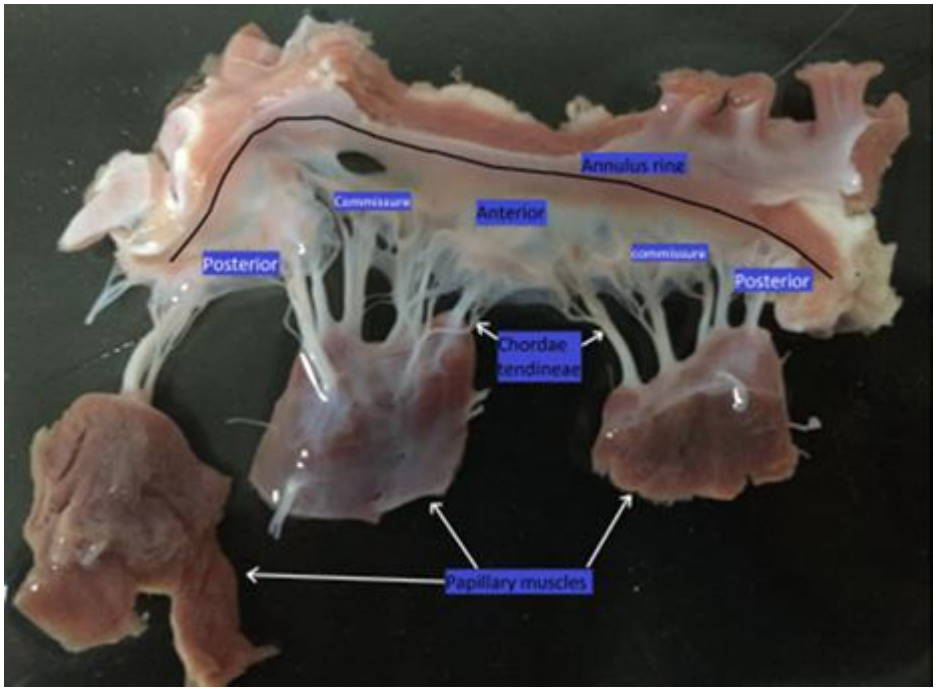

Figure 8 - Mitral valve explanted from a pig heart[19]

The posterior leaflet is connected to the annulus and covers about 2/3 of its perimeter, although it is the anterior leaflet that contributes almost entirely to the closure of the orifice[18] [Figure 9].

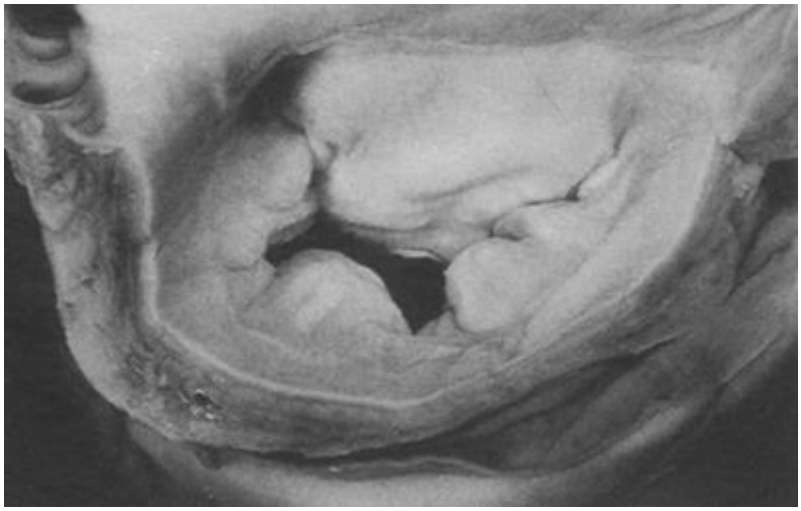

Figure 9 – MItral valve' s anterior and posterior leaflets[18]

Based on the composition of the leaflets, three layers can be distinguished: fibrosa, spongiosa and atrialis[21];

Their connection to the papillary muscles is enabled by the presence of the chordae tendineae that also transmit their contraction. The chordae can attach to the leaflets in the portion connected to the annulus, or in the case of the commisural chordae the attachment occurs in the interleaflet area[18] .

The mitral valve leaflets, in comparison to those of other valves, must withstand higher pressure values, this condition can lead to degeneration of the valve. This also occurs under other circumstances related to infection and old age. In severe cases of diseased valve, its repair or replacement is necessary[22] .

1.4.1.2 Aortic valve

The aortic valve is a part of the aortic root, which conveys blood to the systemic circulation and controls its perfusion[18]. By opening, the aortic valve allows unidirectional flow of blood to the systemic circulation, while by closing it prevents reverse flow to the ventricle. The most important components that form the valve are the three sinuses of Valsalva, three interleaflet triangles and three aortic leaflet. Valve closure is enabled by the overlapping of the free edges of the three leaflets[23] [Figura 10], the size of which varies between individuals. Moreover the leaflets are not completly symmetrical[24]. The three sinuses of Valsalva represent protusions located between the leaflets and the walls of the aortic root, near them are also the 3 interleaflet triangles. The sinuses also form a ring-shaped structure called the sinotubular junction that identifies the transition point to the aorta[23] .

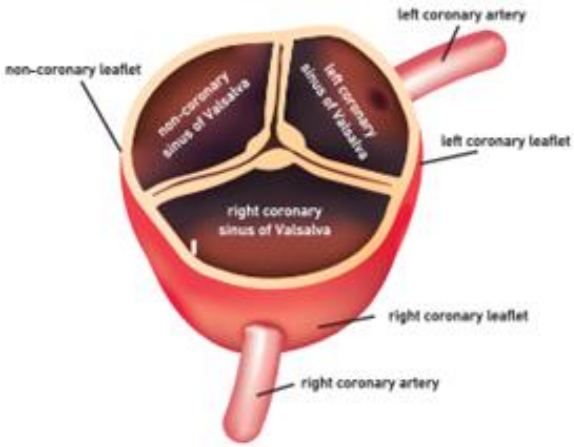

Figure 10 - Aortic valve in closed position[23]

1.4.1.3 Pulmonary valve

The pulmonary valve is located on the right side of the heart. It has the task, during systole, of allowing blood to flow from the ventricle to the pulmonary trunk, while during diastole, it must prevent backward flow by closing[25]. Like the aortic valve, the pulmonary valve must also be considered together with the structure to which it is connected, which is the pulmonary root. The elements that characterise this complex are the sinus trunci pulmonalis, the structure of the annulus, three leaflets and their respective commissure, and the sinotubular junction[18] [Figure 11]. It is separated from the other valves by a muscular sleeve[26] and no chordae tendineae or papillary muscles are present.

Figure 11 – Pulmonary valve's leaflets[25]

1.4.1.4 Tricuspid valve

The tricuspid valve is located on the right side of the heart and is an atrioventricular valve. The most important components are the annulus, chordae tendineae, leaflets (anterior, posterior, and septal), and papillary muscles, which may be in different numbers[18,26]. Usually, the large anterior papillary muscle is connected to both the anterior and posterior leaflets, while the posterior papillary muscle only to the posterior leaflet and a to a portion of septal one; moreover, its structure can take on a bi/trifurcated form [Figure 12].

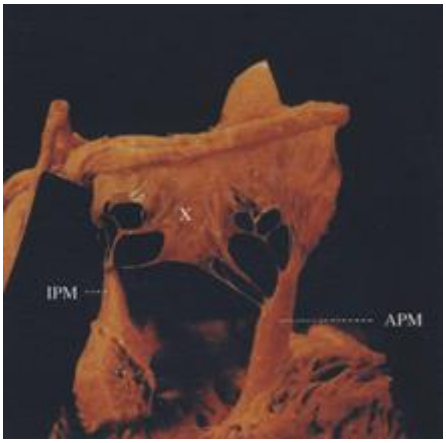

Figure 12 – Tricuspid valve image showing the septal leaflet (X), the chorda tendinae, inferior papillary muscle (IPM) and anterior papillary muscle (APM)[18]

The annulus has a lack of fibrous tissue and collagen that makes it dynamically active in the passage of blood from the atrium to the ventricle. In fact, a conformational change occurs in which its structure assumes a flat shape and returns to its original saddle shape during distole[27].

1.4.2 Mitral valve disease

Heart valve dysfunction is a condition that is largely present in the ageing part of the population, with a correlated risk of morbidity and mortality.

This is clear from a study conducted on two population samples of which echocardiographic reports were analysed. The first sample consisted of 11911 randomly subjects, and the second one consisted of 16501 people, for whom echocardiography had been clinically indicated. In the first sample, the results show the presence of valvular disease in 5.1% of cases. This percentage varies when the various age groups are analyzed separately. In particular, the highest percentage (13%), is found with people over 75 years of age.

In the second sample, the highest percentage (11.7%) also correlates with individuals in the same age group. Furthermore, this study showed that the valve most frequently affected was the mitral valve (9.3%) with the problem of mitral regurgitation (MR)[28,29] [Figure 13].

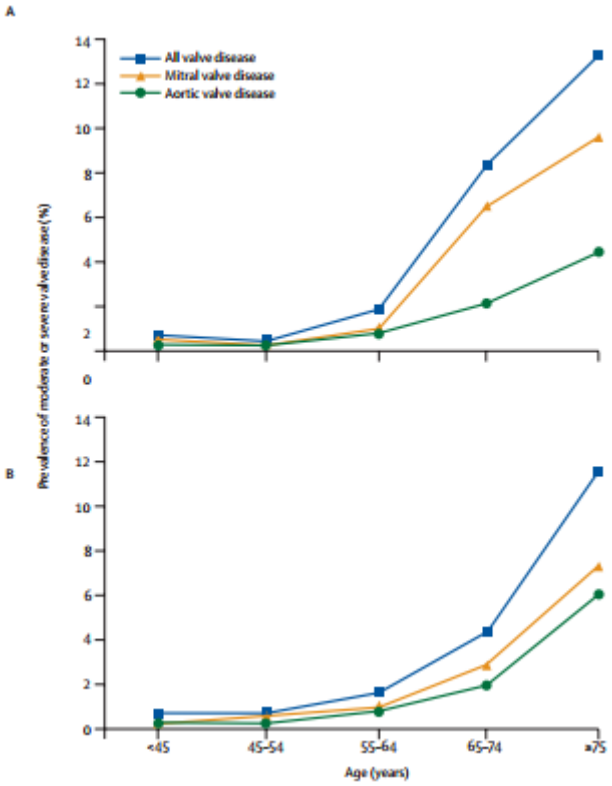

Figure 13 – Diagram of heart valve disease based on age for the first group (A) and for the second one (B)[29]

The disorders affecting the heart valves can be divided into two main types:

- Stenosis: manifested by the difficulty for the blood to flow through the valve;
- Regurgitation: occurs as an imperfect closure of the valve, which therefore fails to prevent backward flow[26];

Regurgitation is caused by misalignment of the leaflets due to the degeneration of their tissue and termed 'myxomatous' [Figure 14]. In other cases, abnormalities of the ventricle may be involved.

Statistics predict that the number of mitral valve cases will roughly double in 2030 compared to 2000.[6,7].

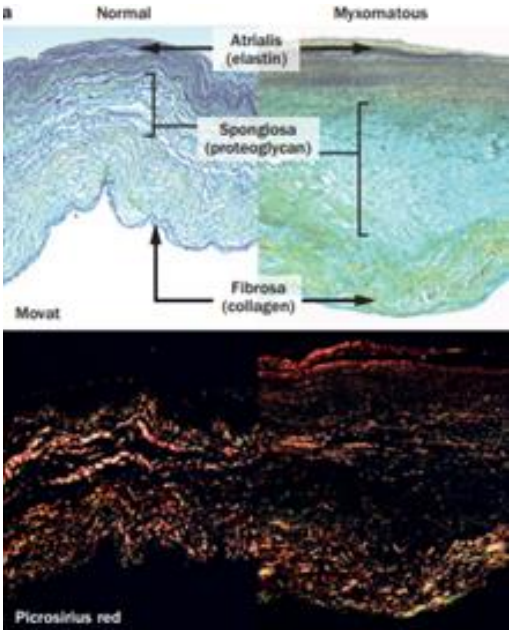

Figure 14 - Morphological analysis of normal and myxomatous mitral valves (Movat pentachrome and Picrosirius red staining)[30]

It is possible to distinguish 3 types of MR [Figure 15]:

- The first type involves a still functional leaflets mobility, but there is a lack of coaptation due to dilatation of the atrium and annulus or perforation of the leaflets;
- The second type is due to chordal rupture;

– The third type is associated with reduced leaflet motion[21];

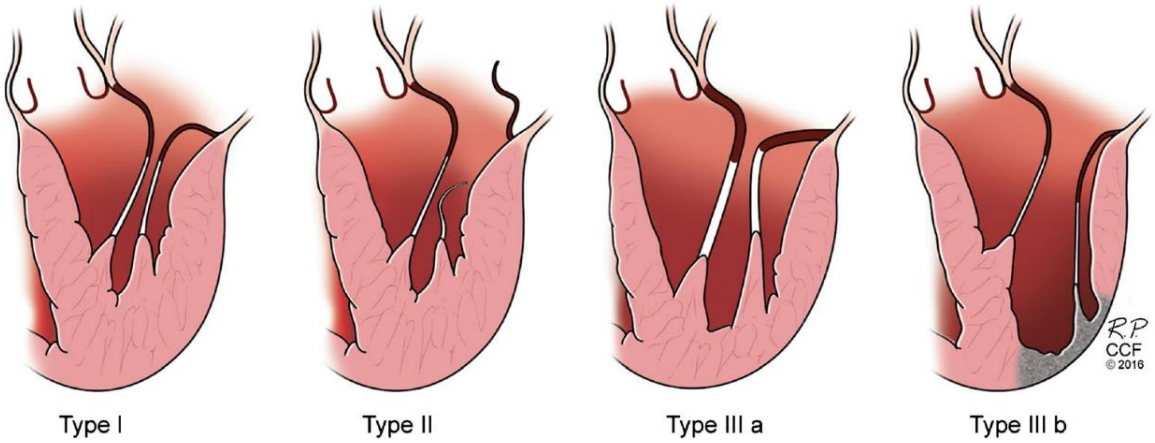

Figure 15 - Classification of mitral regurgitation.

Type I: normal leaflet motion. Type II: high mobility of leaflets. Type III: limitade leaflet motion during systole and diastole (type a) and during systole only (type b)[31]

Depending on the degree of severity of mitral insufficiency, the size of the ventricle may increase[32].

Therefore, this pathology leads to significant consequences such as arrhythmia, endocarditis, heart failure and ultimately death[30].

The other pathology affecting the mitral valve is stenosis. This is related to an increase in the level of fibrosity of the commisure, an increase in the thickness of the leaflets and a reduction in the length of the chordae tendineae.

Stenosis is a common consequence of acute rheumatic fever [Figure 16], which develops an inflammatory state due to infection by the bacterium Streptococcus pyogenes, which mimics cardiac proteins[31,33].

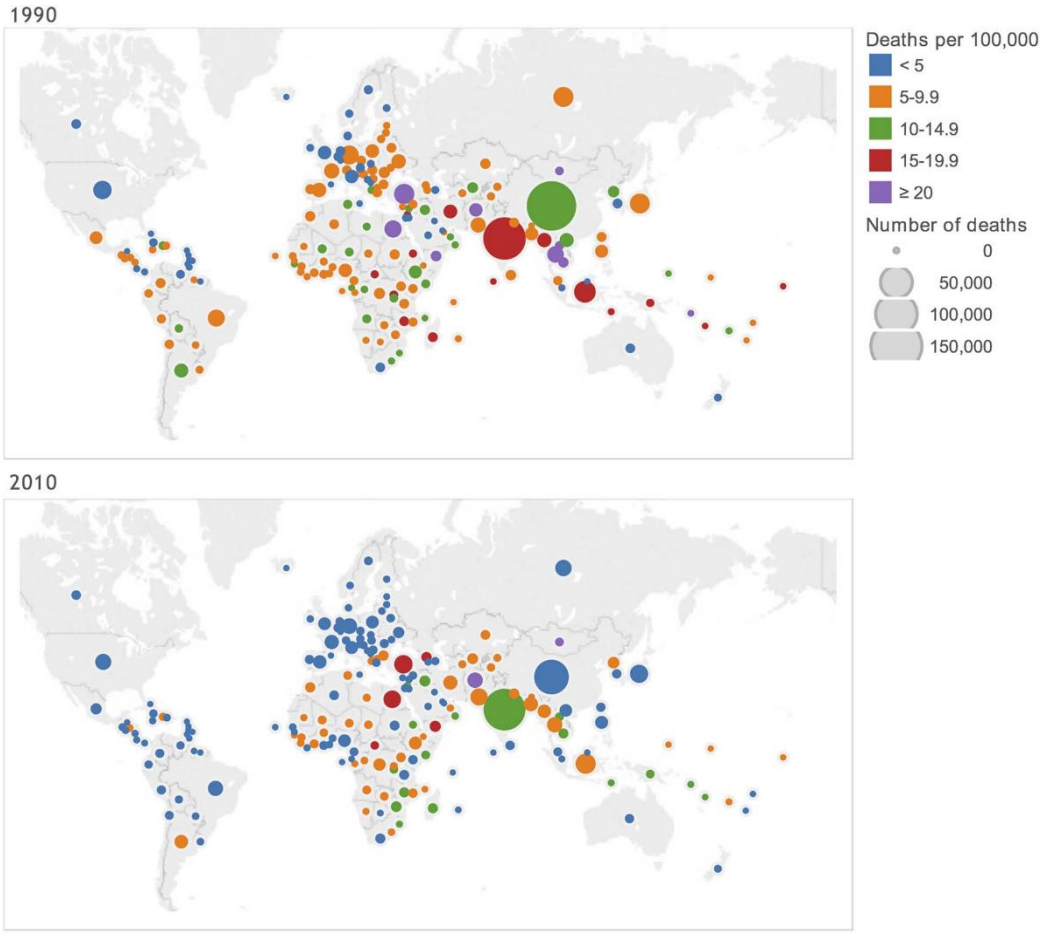

Figure 16 - mortality rate due to rheumatic heart disease from 1990 to 2010[33]

A study of 1,000 people with rheumatic fever showed that 2/3 of them had asymptomatic stenosis in the first 10 years, followed by a reduction in the size of the valve orifice with consequences such as increased pressure, breathing difficulties and death[32,34] [Figure 17].

Stenosis can also be caused by factors such as calcification of the annulus, radiation or anatomical abnormalities due to congenital malformations related to the surrounding haemodynamics[31,35].

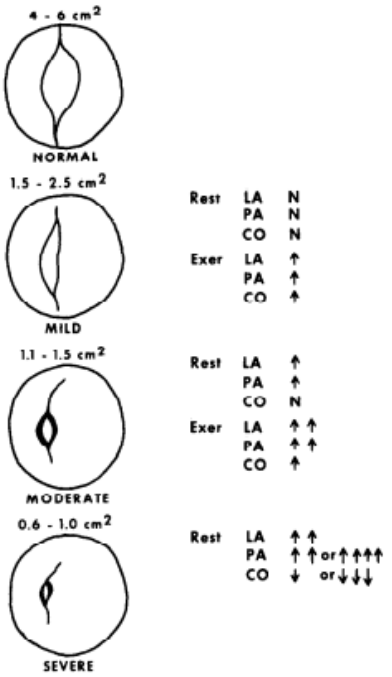

Figure 17 - various grade of severity of mitral stenosis.
(CO = cardiac output; Exer = exercise: LA = left atrial pressure: N = normal; PA = pulmonary arterial pressure)[32]

1.4.2.1 Treatments and future perspective

A malfunctioning mitral valve can be repaired or replaced using various surgical techniques, including the percutaneous approach, minimally invasive surgery, transcatheter replacement and sternotomy[36].

When the valve is replaced with a prosthetic one, the haemodynamic environment is compromised with flow regions separation, high shear stresses and pressure drops. These conditions can induce clotting and red blood cell injury, especially when biomechanical prosthetic valves are used (the most commonly used model is the bileaflet valve). Consequently, patients must follow anti-coagulant therapy[37,38,39]. Thrombotic risk is closely linked to high shear stress, which causes damage to blood components and hyperactivation of platelets. According to the study conducted by Harker and Slichter, this context was already present in early ball-and-cage and tiltingdisc valve designs. Furthermore, Skoularigis et al. found elevated blood

haemoglobin levels, serum concentrations of LDH and haptoglobin in patients with Jude Medical and Medtronic-Hall valves [9,40,41].

Alternatively, bioprosthetic valves can be used. However, this type of valve has a relatively short lifespan of about 10 years. This is related to the high stresses to which the leaflets are subjected, leading to structural degradation over time[37].

The limitations of the two types of valves presented, have increased the interest of the scientific community in creating new valves through tissue engineering. This category of valves involves the use of biomaterials and cells that interact with the native tissue in a biocompatible manner, allowing reactivation of proper function[42,43]. Both success and failure cases have been encountered, but integration with computational techniques could allow the creation of new models capable of achieving this vision[42].

Chapter 2

Background

2.1 Computational Fluid Dynamics

Computational fluid dynamics (CFD) is a technique that allows the equations governing fluid dynamics to be solved using numerical methods by means of computer simulations.

Its applications are many and cover different areas of engineering, including aerospace, chemical, construction and architectural, environmental, energy and biomedical sectors. Its potential is used during the design phase of new devices and in their optimization process[44,45].

In particular, in the biomedical field, with reference to the cardiovascular context [Figure 18], it is exploited for the production of biomedical devices such as heart valves, stents, but also in the study of diseases such as atherosclerosis.

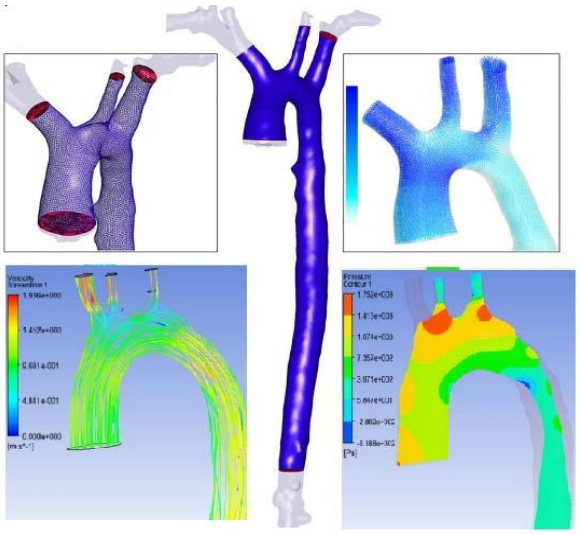

Figure 18 – Example of CFD application to the cardiovascular context[44]

Underlying the power of this methodology is its ability to solve the laws that describe fluid behaviour, i.e. the principles of conservation of mass and momentum, which are incorporated into the Navier-Stokes equations:

- $\nabla \cdot \vec{V} = 0$ (2.1)
- $\rho \frac{\partial \vec{V}}{\partial t} + \rho(\vec{V} \cdot \nabla)\vec{V} = -\nabla p + \nabla \cdot \tau$ (2.2)

Where:

- ρ: fluid density;
- τ: viscous stress tensor;
- p: pressure;
- $\vec{V}$: velocity vector;

These constitute a system of non-linear partial differential equations, which cannot be solved analytically, but whose solution can be obtained numerically[46,47] by means of approximations, in which the integrals are calculated as a sum of finite small elements or volumes (finite element method and finite volume method). These form a mesh that allows the continuous system to be discretized [Figure 19].

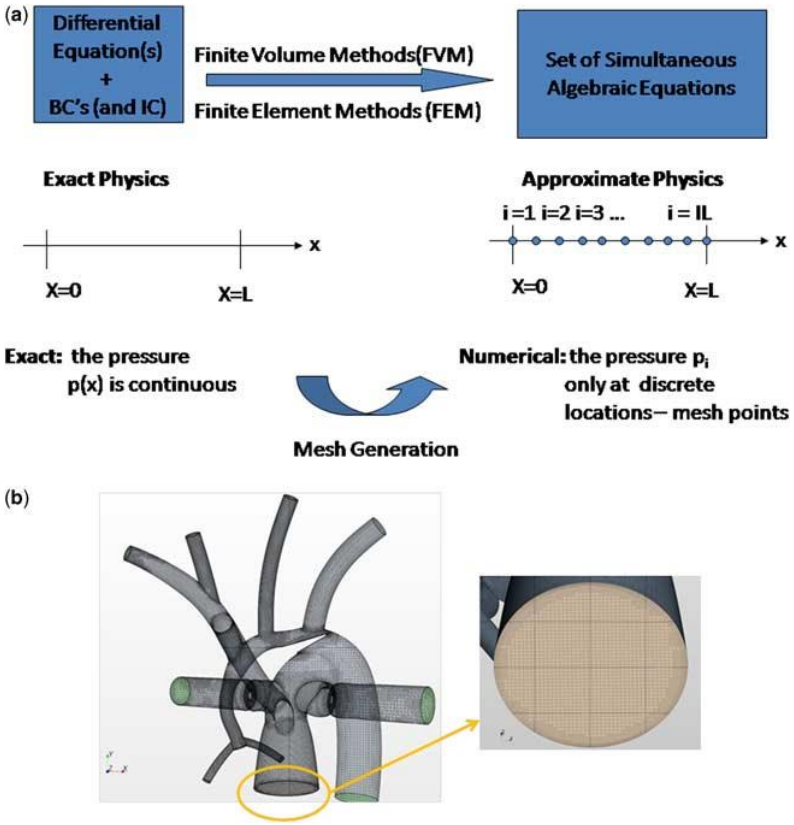

Figure 19 - (a) Numerical procession (b) Example of mesh created with a finite volume method for haemodynamics analysis of pulmonary root mesh. (BC: boundary conditions; IC: initial conditions)[46]

Among the necessary conditions to be imposed, in order to obtain solutions, are boundary conditions in which the velocity and pressure values, corresponding to certain temporal and spatial instants, are usually defined [Figure 20]. It is thus possible to iteratively arrive at the result[46].

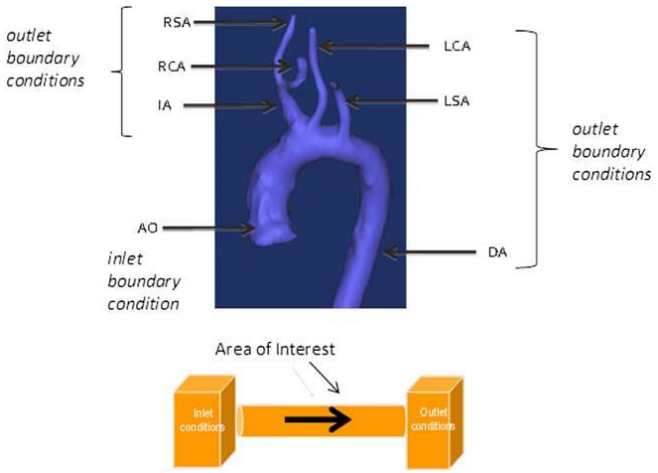

Figure 20 – Example of identification of boundary conditions to the inlet and outlet regions

(AO: aorta; DA: descending aorta; IA: innominate artery; LCA: left carotid artery; LSA : left subclavian arteries; RCA: right carotid artery; RSA: right subclavian artery) [46]

2.1.1 Biomedical applications: state of the art

Numerical simulations are an important tool during the design phase of a biomedical device, such as a heart valve prosthesis, as they can lead to significant advantages in terms of time and cost, obtaining information not easily attainable through classic experimentation, and possibly allowing modifications to the design to improve performance and reduce associated risks. The data obtained on the flow can be used to confirm the effectiveness of the device and obtain regulatory approval, with the support of a verification and validation process[48,49].

Its potential is not only limited to the design process, but also finds applications in the field of imaging diagnostics, as its haemodynamic analysis capability can allow factors such as wall shear stress and regions of stagnation to be assessed, making predictions about thrombus formation and any associated diseases. In fact, their recognition in adequate time makes it possible to reduce the risks to which the patient is subjected[50].

The earliest studies using CFD in the analysis of heart valve prostheses date back to around 1970, where simplified axisymmetric or two-dimensional models were used,

while 3D analyses were not implemented until two decades later, thanks to technological advances that allowed the development of suitable workstations.

To find simulations with less simplified analyses, one has to look at more recent times, such as the study conducted by Ge et al.11 where no symmetry assumptions were made to investigate the geometry of a bileaflet valve with open flaps[37,51].

Another interesting study, where CFD has been used in the analysis of heart valves, is the one carried out by McQueen and Peskin[52] on a bileaflet valve in mitral position, coming to the conclusion that an optimal situation in terms of velocity and pressure drop is represented by a curved leaflets shape [Figure 21].

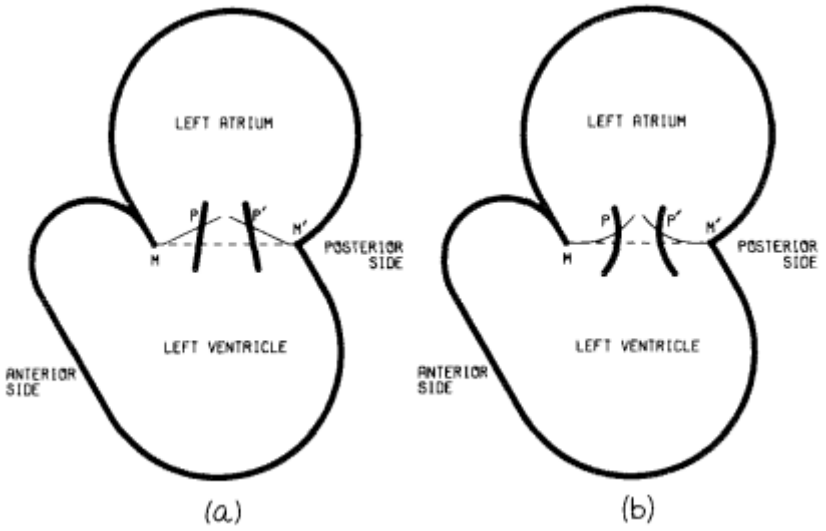

Figure 21 – Bileaflet valve model in opened configurarion, with (a) flat and (b) curved leaflets [52]

Computational fluid dynamics also finds advantageous use in investigating the opening and closing movements of valves, which normally at an experimental level yields not much information in addition to high cost and time consumption. An example is the research conducted by Lai et al. which demonstrates the usefulness and effectiveness of CFD, which was applied in the examination of six different leaflets geometries in order to assess their effect on flow during valve closure[53]. Also of interest is the study presented by King et al.[54], where a bileaflet valve in aortic position was investigated using a 2D computational model, the results of which were compared with those obtained by laser Doppler velocimetry on a 3D experimental model. Despite some

differences, both analyses led to the identification of the same optimal valve opening angle.

Computational fluid dynamics can also be used to study mitral regurgitation, as was done by Collia et al. by coupling CFD with clinical imaging[55] [Figure 22].

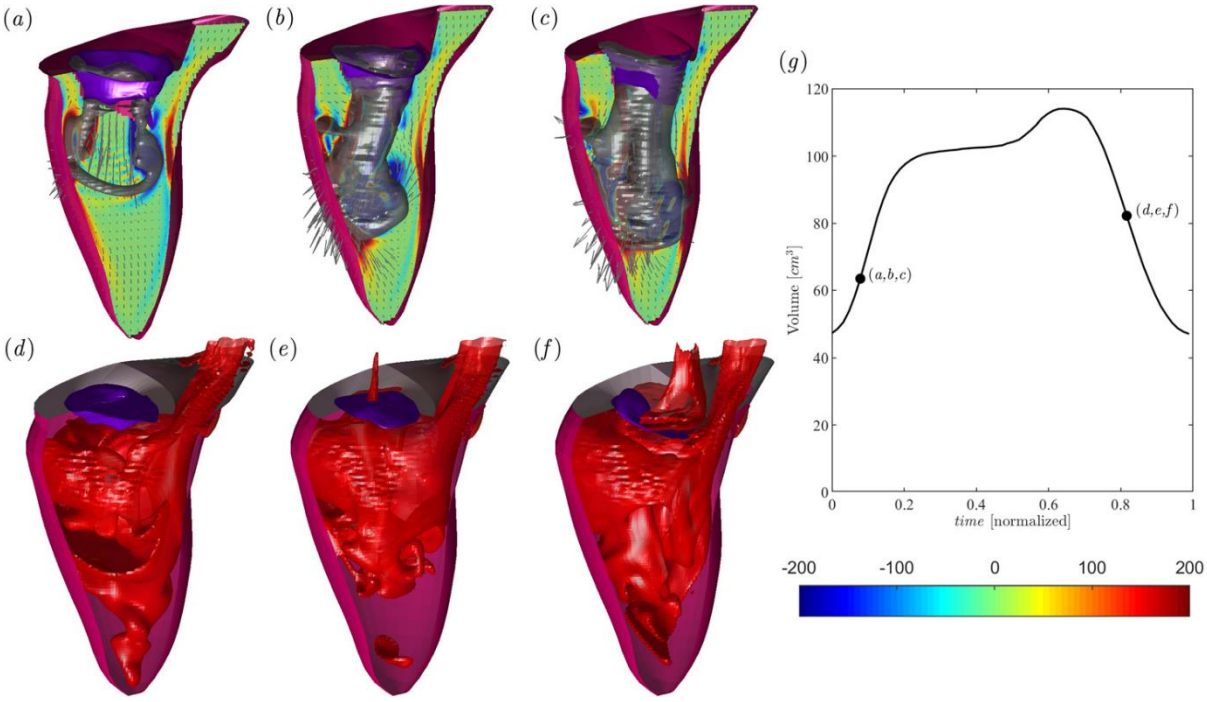

Figure 22 – Flow analysis for the identification of mitral regurgitation for different case: (a) and (d) healthy valve; (b),(c),(e),(f) prolapsed valve. [55]

2.2 Cardiac Pulse Duplicator: state of art

Advances in heart valves and the need to test them in an environment that mimics the one physiologically present in the heart led to the development of the Cardiac Pulse Duplicator[56,57]. This is a device capable of replicating the left side of the heart and the systemic circulation, using lumped resistances and compliances[11]. The first models were developed around 1950 with the aim of studying haemodynamics and the circumstances that can induce pathology. A decade later they proved essential in the field of valve prostheses. In addition, the recent development of numerical techniques such as CFD

or FSI (fluid-structure interaction), which have enabled a better understanding of the valve context, has once again highlighted the need to create devices capable of bridging the differences between physiologically present conditions and those currently reproducible in vitro[58]. Bjork et al.[56] proposed a pulse duplicator model on the basis of certain characteristics considered essential for the correct testing of a valve prosthesis, such as a variable frequency and end-volume, and a pressure pattern similar to the physiological one.

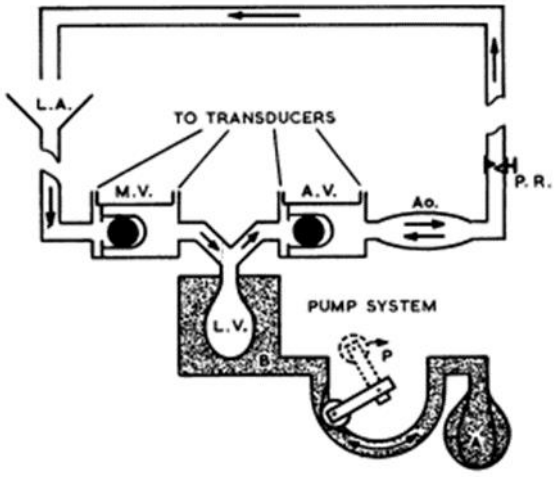

Figure 23 – Pulse duplicator model proposed by Bjork et al. and composed by L.A.: left atrium; M.V:mitral valve; L. V :left ventricle; A. V :aortic valve; A: elastic container; B: rigid container; P:pump; P.R.:peripheral resistance. [56]

As can be seen from the figure [Figure 23], there is a pumping system and a system that constitutes the left heart chambers, the aorta and the peripheral resistors. The frequency and waveform of the pulses depend on a roller pump, driven by a motor. The liquid used for experimentation is water (or alternatively a glycerine solution), which is passed from reservoir A (atrium) to reservoir B (ventricle), and then back to A via the peripheral circuit of the aorta, formed by a rubber tube 28 cm long and approximately 3 cm in diameter.

In this system, mitral and aortic test valves can be placed in the respective inflow and outflow positions of B (in which a check valve is placed in the first instance). The

pressures within the 'heart chambers' are regulated by means of a clamp, which manages the voltage at the head of the peripheral resistors.

In the presented study, atrial pressure values of 10 mmHg and pressure differences of 100/45 mmHg for systole and 300/150 mmHg for diastole were used in the aorta.

The pulse duplicator thus realised was functional and met the expectations set by its creators, although it did have some limitations such as the use of water or a glycerine solution instead of blood and the lack of instrumentation components capable of imitating the movement of the annulus.

Haaf et al.[59] tested a new model of stent valved by means of a pulse duplicator that had been calibrated using a human aortic valve, and with which they then tested various commercially available prosthetic valves and others of new design.

The device, developed by the Institute of Experimental and Applied Physics at Kiel University (Germany), consists of a drive complex capable of reproducing the cardiac impulse through a piston, whose movement is regulated by a screw connected to a computer-controlled motor. As can be seen from the figure [Figure 24], a reduction in cross-section at the point where the valve should be placed has been realised in order to obtain a flow velocity profile similar to the physiological one.

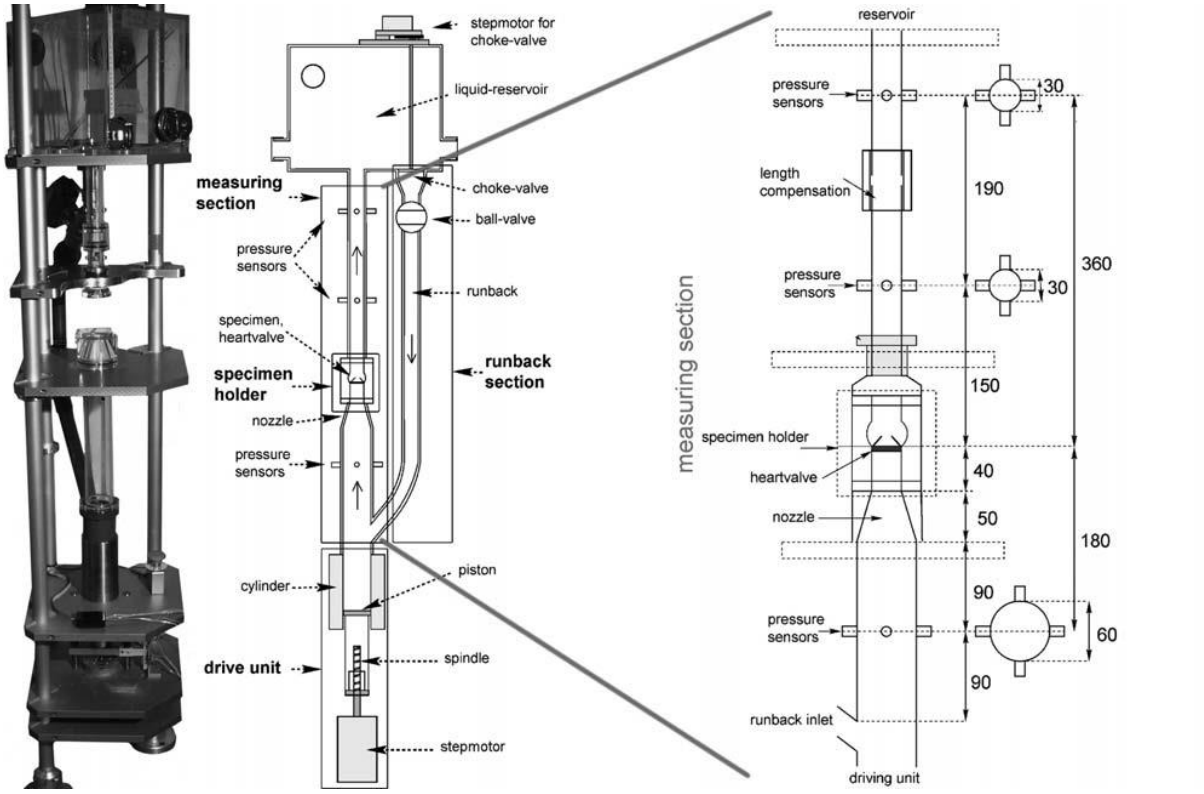

Figure 24 – Pulse duplicator used by Haaf et al. [59]

There are also four piezoresistive sensors whose function is to detect the pressure to which the valve is subjected during the simulation of the cardiac cycle, which was reproduced using a frequency of 60 beats/min and an ejection volume of 73 ml, while the pressure is regulated by means of a butterfly valve. No blood was used as fluid, but distilled water.

A simpler pulse duplicator model used to test an aortic prosthetic valve is the one presented by J. Fredrick Cornhill and D.Phil.[60] [Figure 25]. It consists only of the chamber representing the ventricle and the peripheral pathway. The fluid used is air contained in a pexiglass box, and it enters the ventricular chamber (when the pressure is about 0 mmHg) through the opening of an inlet valve. It then passes through the aortic valve into the peripheral circulation, which is realised by means of a resistance, a capacitance and another resistance, which model the aorta, the arterial system and the peripheral resistance respectively.

The air finally passes into two reservoirs. This device has a frequency range of 40 to 240 bpm.

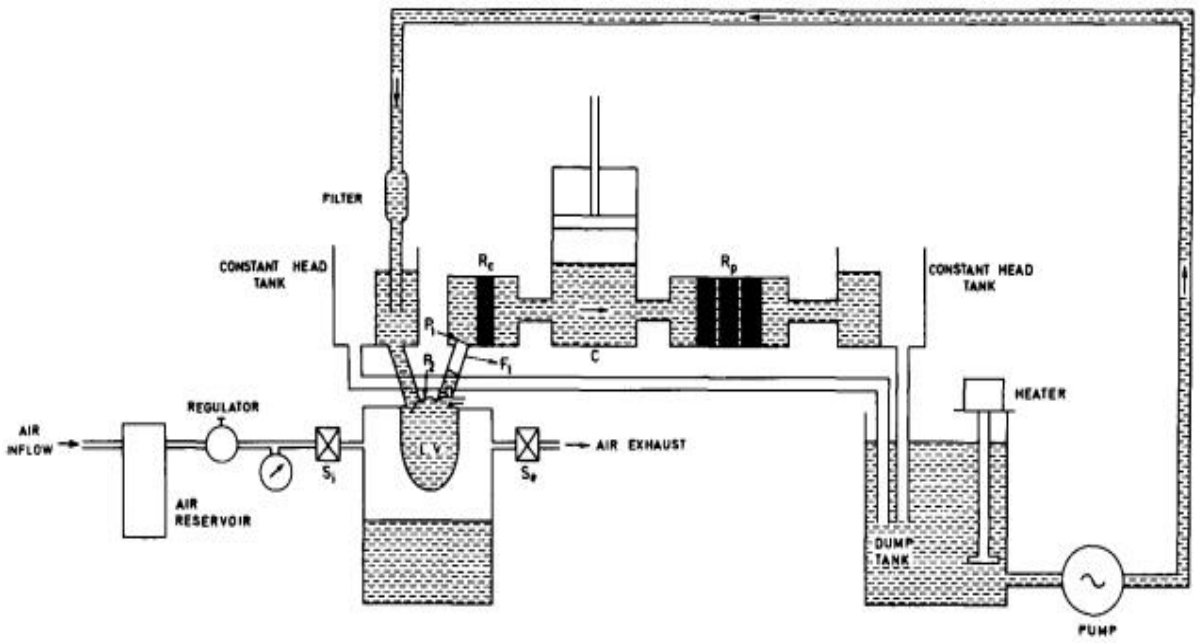

Figure 25 – Pulse duplicator scheme used by J. Fredrick Cornhill and D.Phil[60]

Pulse duplicator models used to test prosthetic valves in the mitral position can also be found in the literature, as in the case of the work by P. R. Verdonck et al.[61] who tested St. Jude Medical, CarboMedics, ATS Medical and Medtronic Parallel valves.

Their pulse duplicator model [Figure 26] consists of two chambers (atrium and ventricle) surrounded by a chamber connected to the reservoir, and a circuit representing the pulmonary veins and aortic arch.

The fluid used is an aqueous solution consisting of 30% glycerol. The cardiac cycle is electronically controlled and is at a rate of 70 bpm, with a flow rate of 4 l/m and maintaining aortic pressure values around 120 mmHg for systole and 70 mmHg for diastole.

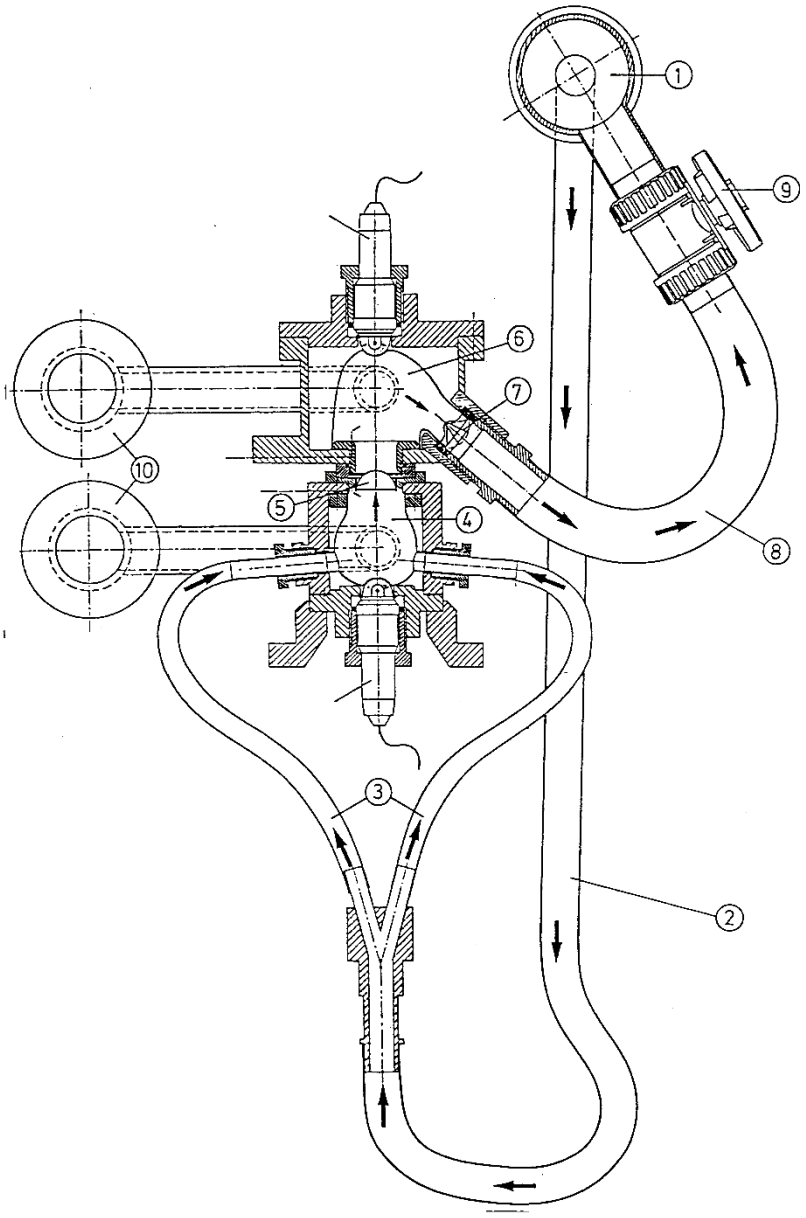

Figure 26 – Scheme of Pulse duplicator used by P. R. Verdonck et al.[61]

Mashari et al.[62] tested a patient-specific mitral valve model made using 3D printing, using a pulse duplicator [Figure 27]. It consists of a circuit comprising an atrial reservoir and a chamber representing the ventricle connected via rings to a piston controlled by an Arduino device, which allows them to control the contractility of the system and the passage of ultrasound fluid into the ventricle via the mitral valve.

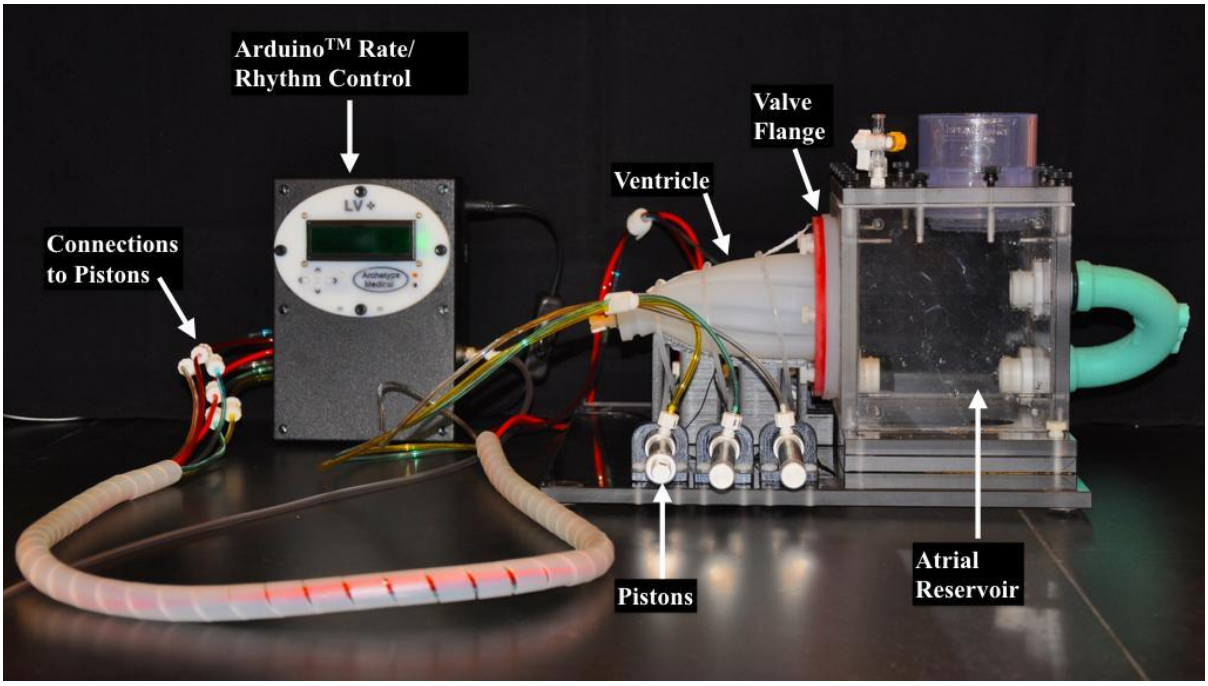

Figure 27 – Pulse duplicator used by Mashari et al. [62]

The device made it possible to obtain pressure values similar to those found in reality, but it has limitations. It is only capable to reproduce the ventricular diastole phase, as it does not have an apparatus that models the aortic section.

Instead, Manzoni et al.[8] present in their study a more complete and customizable pulse duplicator [Figure 28], which is currently used in the Healing Research Laboratory at the University of Padua, and whose components can be adapted according to the type of experimentation to be performed. The fluid is set in motion by a computer-controlled piston. The frequency and heart rate are managed by an electronic unit and human control. There are three chambers with fluid inlets and outlets: atrial, ventricular and aortic. The atrial one is maintained at a pressure of 10 mmHg and houses a constant fluid level, while the aortic chamber contains pressure transducers.

Next there is the model of the aortic arch and the peripherals schematized through compliance and resistance.

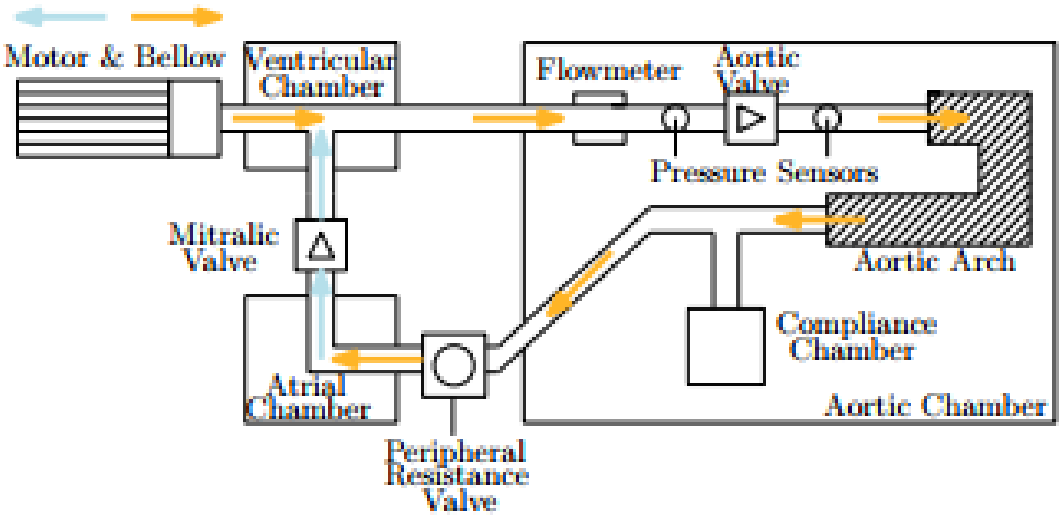

Figure 28 – Scheme of pulse duplicator used by Manzoni et al. [8]

C. G. Duran et al.[57] propose a pulse duplicator model [Figure 29] that exhibits a number of features that, in their opinion, distinguish it from other prototypes currently in use. These include its simplicity and cost-effectiveness, the possibility of using both water and gas as fluid, and the presence of two removable viewing chambers of the same size.

The latter are connected to the systemic circuit and to the cardiac chamber in which, in addition to the holes that allow the passage of fluid, there is also an opening to accommodate a ventricular cannula. There are also the mitral and aortic cannulas, and two solenoid valves which, with their opening and closing, allow the chamber to be filled by gravity, with flow rates of 3 L/min.

The configuration of the cannulas and observation chambers can be modified in the case of insertion of a prosthetic valve to be tested and the flow rates can reach values of 6 L/min in this case.

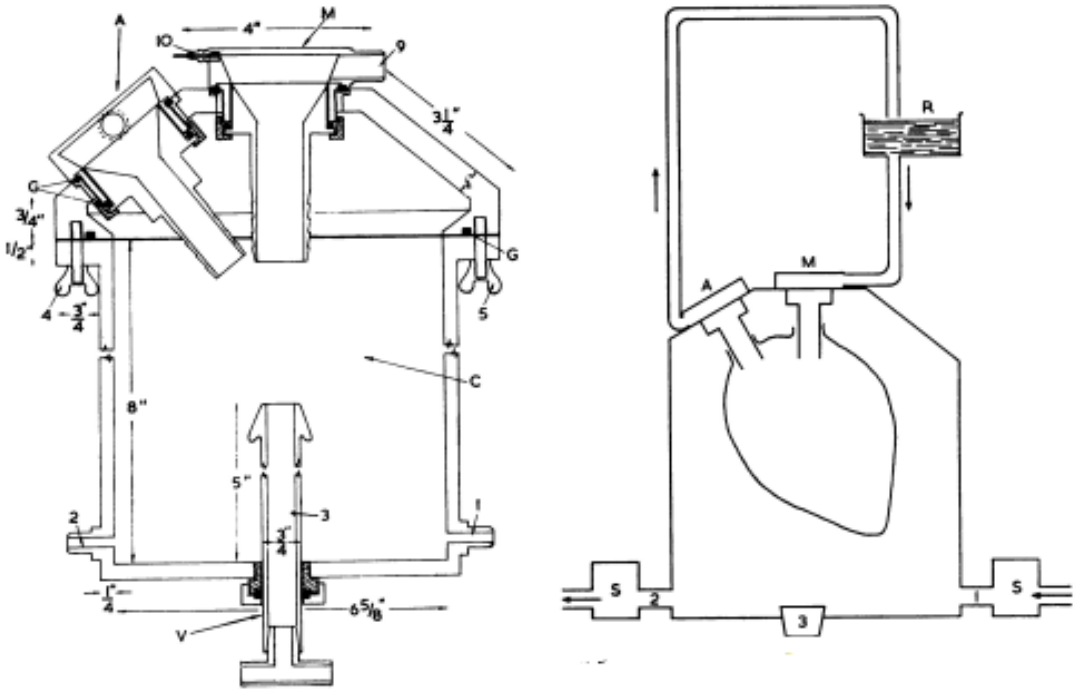

Figure 29 – Pulse duplicator model proposed by C. G. Duran et al [57]

There are also studies in the literature where the pulse duplicator has been associated with the use of numerical techniques for the analysis of valve prostheses. As in the research published by Jae H. Lee et al.[48] and by G. Ranjith and C. V. Muraleedharan.[11]

In the case of the first research, the developers analysed bioprosthetic valves made from pig and bovine tissue (aortic valves) by combining the potential of the FSI with the ViVItro pulse duplicator and a customised pulse duplicator [Figure 30]. In both pulse duplicators, no blood was used as it was considered temperature-influenced, instead saline was used[48].

In the second research mentioned earlier[11], CFD (specifically the Ansys CFX 13.0 solver) was used to simulate the behaviour of a tilting disc aortic valve. with the aim of obtaining values for velocity profiles, stagnation zones and pressure drops, which were then validated through in-vitro experimentation with the pulse duplicator.

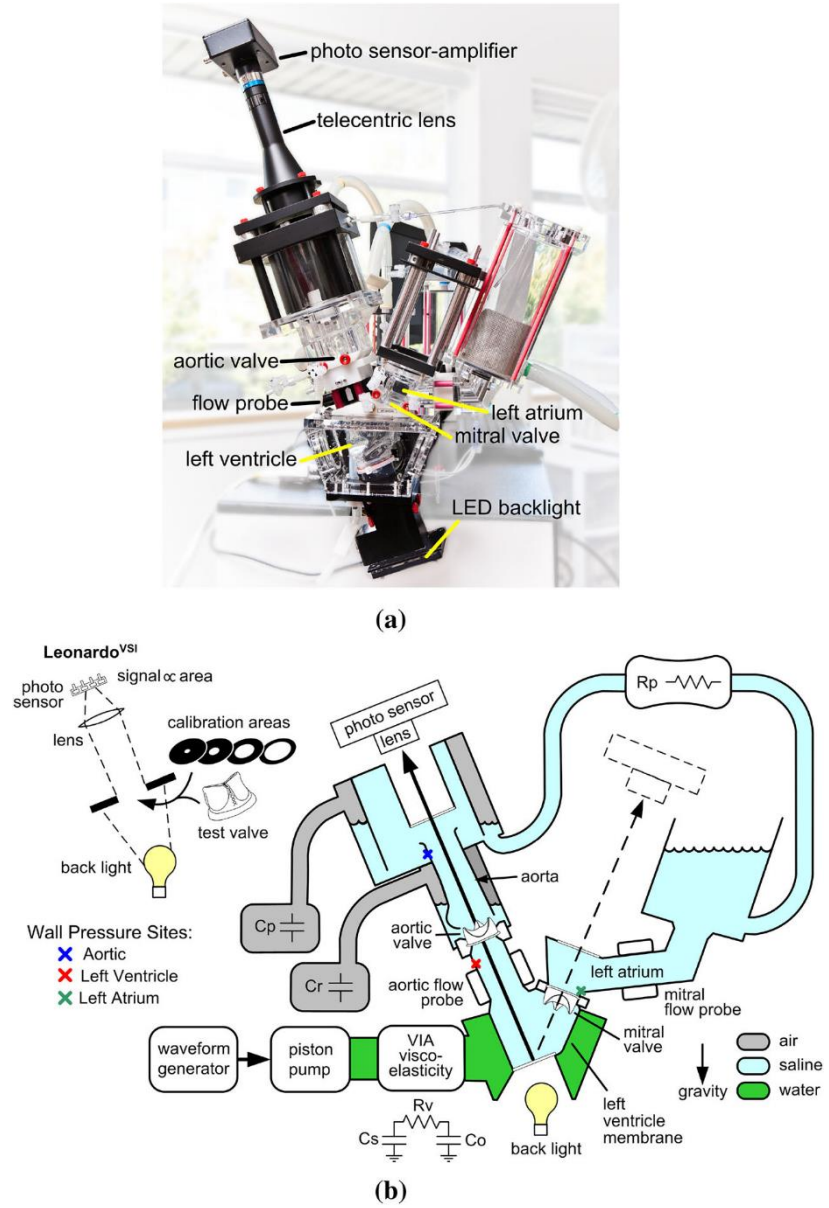

Figure 30 - Jae H. Lee et al. 's customized pulse duplicator [48]

The latter [Figure 31] consists of an atrium modelled by a reservoir, a chamber corresponding to the ventricle and two balloons performing the pumping action. The peripheral circuit is modelled by compliance and resistance.

The experimentation was conducted at a frequency between 40-150 bpm. The valve during the numerical simulations was considered as a rigid hinged body whose movements were restricted. Values obtained from the pulse duplicator were used as boundary conditions for the numerical simulation, while the rheological characteristics of blood were set for the definition of the fluid.

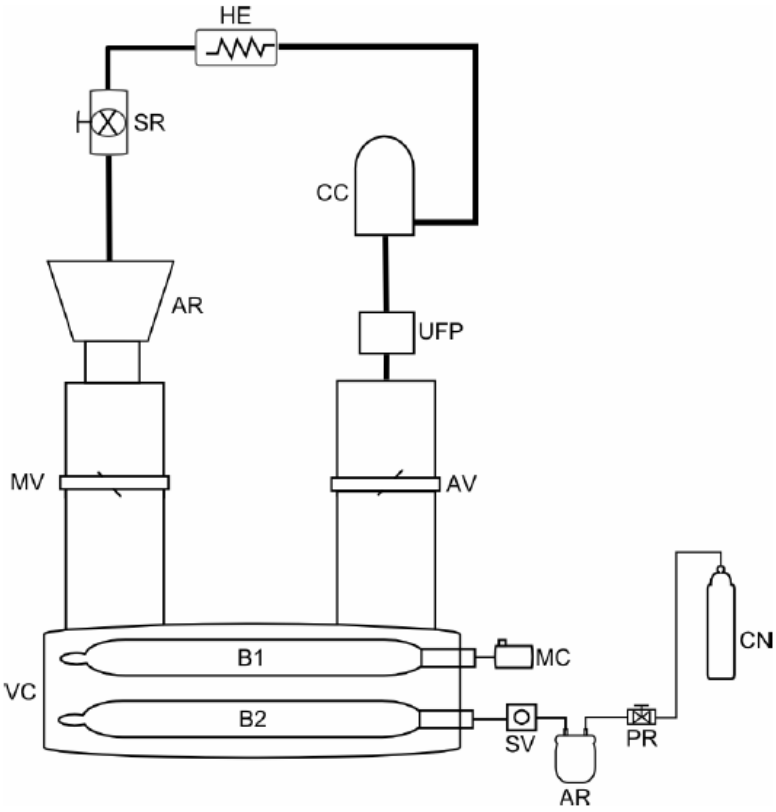

Figure 31 - G. Ranjith and C. V. Muraleedharan 's pulse duplicator setup[11]

Chapter 3

Materials and methods

3.1 The theory of Computational Fluid Dynamics

In a CFD analysis, the study of a physical problem is achieved through its idealisation and modelling in a mathematical model.[63] This process consists of several steps [Figure 32]:

1. Model definition: the analysed system's geometry is realised;[64,65]

2. Discretization: this consists in subdividing the domain under examination into small elements or volumes, called 'cells'. These can take the form of tetragonal, hexagonal, polyhedral, quadragonal etc.. The set of cells and their nodes form the 'mesh'. A well-designed mesh allows for more conformal and accurate results. The degree of discretization must be high enough to allow for adequate processing of the model, but without increasing the computational costs. It is up to the user to design the mesh following a proper compromise. A mesh can also present a uniform appearance when it is made up of rectangular elements, equally dimensioned and realised following a second-order accuracy criterion. Alternatively, a non-uniform mesh can be created, consisting of cells whose size varies according to the area of the geometry in which it is positioned, for example with a smaller size in the vicinity of sudden and complex changes in the geometry;[47,64,65,66]

3. Definition of boundary conditions, physical and chemical characteristics: The properties of the fluid under investigation are expressed, the physical limits of the model, such as the inlet and outlet regions, are identified and conditions are applied to these ones to define the state of the system;
4. Simulation: Given the initial conditions, the transport equations governing the fluid-dynamic system are solved. These equations cannot be solved analytically,

so it is necessary to use numerical methods which can be explicit, implicit (iterative process). In the latter case, the process is slower but also more robust and it allows convergence of residuals, representing the conservation of properties;

5. Post-processing: the information obtained, such as velocity and pressure, is processed; it is possible to represent the results in graphic form with 2D or 3D visualizations, analysis of the vector fields, the motion of the particles and the distribution of the quantities under investigation (such as pressure and velocity);[47,64,65]

6. Validation: A comparison is made with reference data, which can be obtained through in-vitro experimentation, in order to demonstrate validity; [47]

The above steps are carried out by 3 components: pre-processor, solver and post-processor. The pre-processor takes care of the processing of the first 3 steps, the solver is responsible for obtaining solutions and is therefore associated with step 4, the post-processor takes care of step 5. [44,64,65,66]

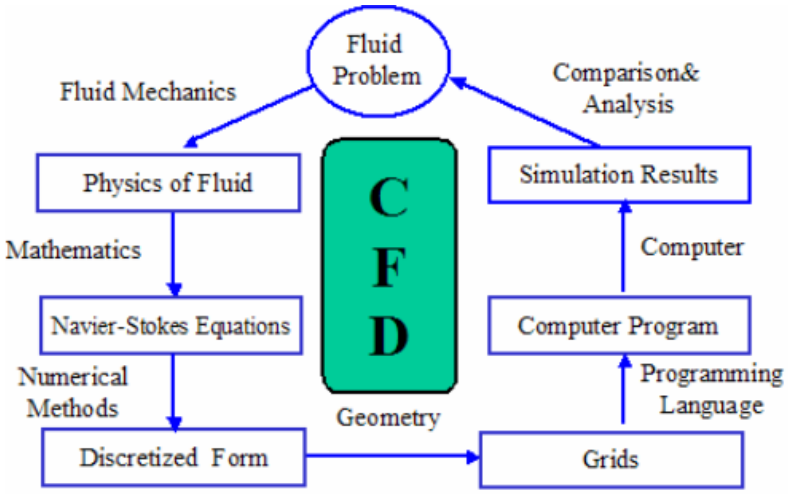

Figure 32 – CFD process scheme[66]

3.1.1 The Navier-Stokes equations

CFD allows the equations of fluid dynamics, which are partial differential equations, to be solved using numerical techniques that consist of discretizing the domain of interest into small elements and applying boundary conditions to the system, thus allowing the values of pressure and velocity of the system to be obtained.

The system can thus be represented as the volume in the figure [Figure 33], where u, v and w represent the velocities along the 3 directions, which together with the pressure constitute 4 unknowns, for the solution of which the same number of equations are needed.

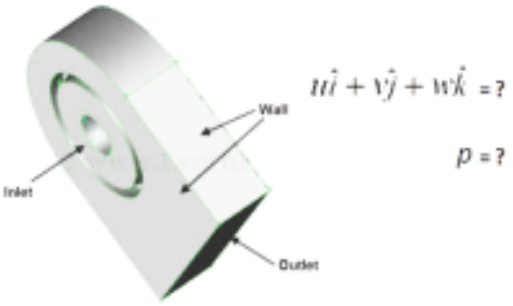

Figure 33 -Fluid-dynamic domain[66]

The first one is found by the principle of conservation of energy, according to which the increase in mass is given by the difference between the inflow and outflow[66] [Figures 34,35]:

Rate of change of ϕ in the control volume with respect to time	=	Net rate of increase of ϕ due to convection into the control volume	+	Net rate of increase of ϕ due to diffusion into the control volume	+	Net rate of creation of ϕ inside the control volume

Figure 34 - principle of mass conservation[64]

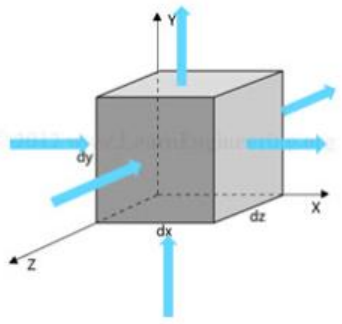

Figure 35 – Flow through control volume[66]

- $\frac{\partial \rho}{\partial t} + \frac{\partial (\rho u)}{\partial x} + \frac{\partial (\rho v)}{\partial y} + \frac{\partial (\rho w)}{\partial z} = 0$ (3.1)

From the conservation of momentum (Newton's second law), considering one equation for each vector component, it's possible to obtain the 3 missing equations:

- $\frac{\partial (\rho u)}{\partial t} + \frac{\partial (\rho u^2)}{\partial x} + \frac{\partial (\rho uv)}{\partial y} + \frac{\partial (\rho uw)}{\partial z} = -\frac{\partial p}{\partial x} + \frac{\partial}{\partial x}\left(\lambda \vec{V} \cdot \vec{V} + 2\mu \frac{\partial u}{\partial x}\right) + \frac{\partial}{\partial y}\left[\mu\left(\frac{\partial v}{\partial x} + \frac{\partial u}{\partial y}\right)\right] + \frac{\partial}{\partial z}\left[\mu\left(\frac{\partial u}{\partial z} + \frac{\partial w}{\partial x}\right)\right] + \rho f_x$
- $\frac{\partial (\rho v)}{\partial t} + \frac{\partial (\rho uv)}{\partial x} + \frac{\partial (\rho v^2)}{\partial y} + \frac{\partial (\rho vw)}{\partial z} = -\frac{\partial p}{\partial y} + \frac{\partial}{\partial x}\left[\mu\left(\frac{\partial v}{\partial x} + \frac{\partial u}{\partial y}\right)\right] + \frac{\partial}{\partial y}\left(\lambda \vec{V} \cdot \vec{V} + 2\mu \frac{\partial v}{\partial y}\right) + \frac{\partial}{\partial z}\left[\mu\left(\frac{\partial u}{\partial z} + \frac{\partial w}{\partial x}\right)\right] + \rho f_y$
- $\frac{\partial (\rho w)}{\partial t} + \frac{\partial (\rho uw)}{\partial x} + \frac{\partial (\rho vw)}{\partial y} + \frac{\partial (\rho w^2)}{\partial z} = -\frac{\partial p}{\partial z} + \frac{\partial}{\partial x}\left[\mu\left(\frac{\partial u}{\partial z} + \frac{\partial w}{\partial x}\right)\right] + \frac{\partial}{\partial y}\left[\mu\left(\frac{\partial w}{\partial y} + \frac{\partial v}{\partial z}\right)\right] + \frac{\partial}{\partial z}\left(\lambda \vec{V} \cdot \vec{V} + 2\mu \frac{\partial w}{\partial z}\right) + +\rho f_z$

  (3.2)

The all equations presented above constitute the Navier-Stokes equations.

These, together with the law of conservation of energy, constitute the three fundamental conservation laws, which can be reformulated into the following equations:

- Continuity equation: $\frac{D\rho}{Dt} + \rho \frac{\partial U_i}{\partial x_i} = 0$ (3.3)

  in the case of compressible fluid: $\frac{\partial U_i}{\partial x_i} = 0$ (3.4)

- Momentum equation: $\rho \frac{\partial U_j}{\partial t} + \rho U_i \frac{\partial U_j}{\partial x_i} = -\frac{\partial P}{\partial x_j} - \frac{\partial \tau_{ij}}{\partial x_i} + \rho g_j$ (3.5)

  if the fluid is compressible: $\rho \frac{\partial U_j}{\partial t} + \rho U_i \frac{\partial U_j}{\partial x_i} = -\frac{\partial P}{\partial x_j} - \mu \frac{\partial^2 U_j}{\partial x_i^2} + \rho g_j$ (3.6)

  Where: $\tau_{ij} = -\mu\left(\frac{\partial U_j}{\partial x_i} + \frac{\partial U_i}{\partial x_j}\right) + \frac{2}{3}\delta_{ij}\mu \frac{\partial U_k}{\partial x_k}$ (3.7)

- Energy equation: $\rho c_\mu \frac{\partial T}{\partial t} + \rho c_\mu U_i \frac{\partial T}{\partial x_i} = -P \frac{\partial U_i}{\partial x_i} + \lambda \frac{\partial^2 T}{\partial x_i{}^2} - \tau_{ij} \frac{\partial U_j}{\partial x_i}$ (3.8)

  where the first term at first member represents the local variation in time, the second term at first member is the momentum convection, the first term at

second member is the surface force, the second term at second member is the momentum exchange and the last term constitutes the mass force.

The Navier-Stokes equations can be rewritten in one form:

- $\frac{\partial(\rho\Phi)}{\partial x} + \frac{\partial}{\partial x_i}\left(\rho U_i \Phi - \Gamma_\Phi \frac{\partial \Phi}{\partial x_i}\right) = q_\Phi$ (3.9)

Substituting Φ = 1, Uj, T, we return to the 3 equations just described, which constitute a set of coupled, non-linear partial differential equations that cannot be solved analytically. For this reason, numerical techniques are used, such as CFD, which discretizes them into algebraic equations.

Different methods can be used for this purpose: finite difference method (FDM), finite element method (FEM), finite volume method (FVM).[66]

3.1.2 Methods for solving partial differential equations

In the FDM method, partial differential equations (PDEs) are solved using polynomials and Taylor series, while the FEM and FVM techniques are based on the integration of PDEs. The FEM method is characterized by the division of the domain into finite elements, and the equations are reworked using a weak formulation. In FVM, the integral form of the equations is calculated on each volume into which the domain is divided.[67] FDM is the simplest technique, but is not suitable for use with complex geometries and conditions, unlike FEM, which, however, entails higher computational costs, whereas the FVM technique can be used with complex geometries and is particularly effective when using a structured mesh, which is a mesh organized in rows and columns, within which points are identified by index [Figure 36].

Distinguished from these are the unstructured meshes, which are not characterized by a particular organization, which allows them a better adaptation to complex shapes, but are less efficient than the previous ones from a computational point of view.[68]

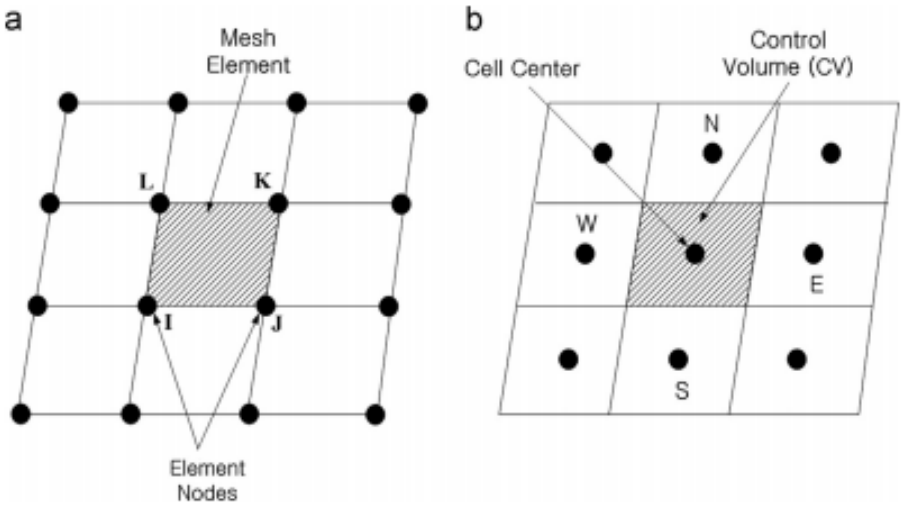

Figure 36 – a) FEM and b) FVM applied to a structured mesh

Jeong and Seong[67] carried out a study in which they compared FEM and FVM methods, using software based on these methods for analysing the same model. In particular, Ansys CFX, Ansys Fluent and ADINA were used. The first two are based on the FVM method, but CFX involves the use of a scheme in which the flow information is calculated at the cell vertices, whereas in Fluent this process takes place in the centre of the cell. With Fluent it is possible to choose between different calculation techniques based on density or coupled pressure, whereas CFX offers only one option. ADINA uses the FEM method instead. Meshes with different types of elements were used for the analysis. It turned out that in contrast to the FVM method, which led to the same solutions regardless of the mesh type, the FEM method only provided optimal flow information in the case of meshes with hexahedral elements, whereas it showed limitations with tetrahedral elements. This method also led to higher computational costs and was more time-consuming than the FVM.

O'Callaghan et al.[69] performed a blood flow analysis in a femoral artery, using both methods, specifically using FLUENT and ADINA. They concluded that the FVM method led to results that were more in line with those expected on the basis of the theoretical data [Figure 37].

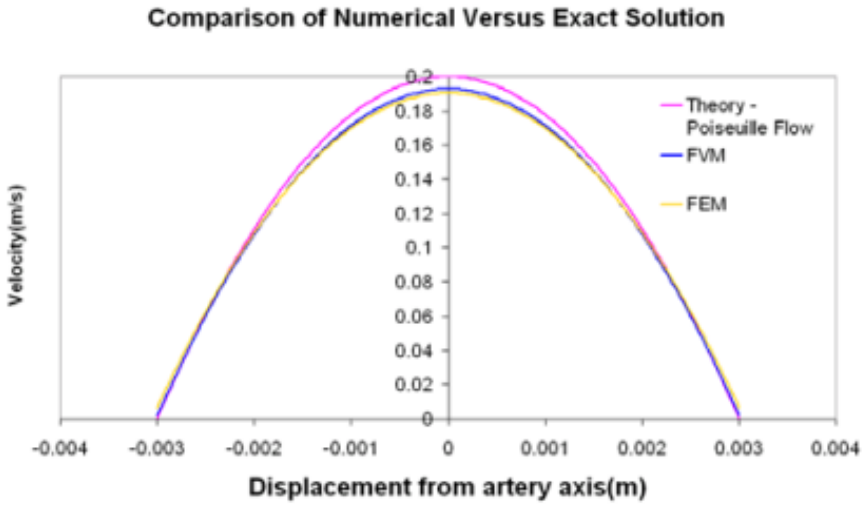

Figure 37 – velocity profile in a femoral artery according to theory and from data obtained with FEM and FVM, in the study conducted by O'Callaghan et al. [69]

Juretic and Gosman[70] carried out a study centred on the analysis of the error produced by the truncation that occurs during the discretization process conducted with the FVM method, in the case of meshes with quadrangular, triangular and hexagonal elements, in a 2D environment. They came to the conclusion that the coupling between the faces of each cell reduces the error generated, making the quadrangular meshes the most accurate.

Comparisons of the two methods can also be found in the literature with applications not related to the biomedical environment, such as the study conducted by Molina-Aiz et al.[71] about natural ventilation in greenhouses using CFD in two dimensions. Their research showed that the FVM method used with the Fluent software enabled information to be obtained in half the time and with 10 times less memory than when using the FEM method.

3.1.2.1 The finite volume method (FVM)

If we consider the flow through a volume V enclosed by a surface S described by the vector n, we can write the surface equilibrium [Figure 38]:

- $\int_S (\Phi \vec{v} \cdot \vec{n}) dS$ (3.10)

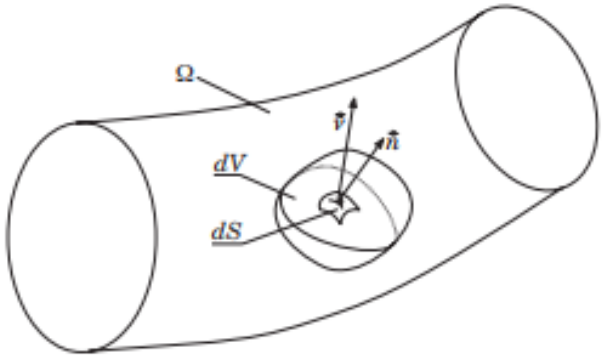

Figure 38 – A control volume[72]

And the volumetric equilibrium[72]:

- $\int_V (\Phi) dV$ (3.11)

The same principle can be applied to conservation laws and written in the form of an integral:

- $\frac{d}{dt}\int_V u(x,t)dV + \int_A f(u) \cdot n \, dA - \int_V S(u,x,t)dV = 0$ (3.12)

Where u(x,t) represents the variation of the quantity under consideration within the volume V, which when added to the flow occurring at the boundary A, yields the production rate S(u, x, t). If a constant volume is considered, it is possible via Gauss's theorem to arrive at the formulation:

- $\int_V \nabla \cdot f \, dV = \int_A f \cdot n \, dA$ (3.13)

↓

- $\int_V \left(\frac{\partial u}{\partial t} + \nabla \cdot f(u) - S\right) dV = 0$ (3.14)

For the integral to be zero:

- $\frac{\partial u}{\partial t} + \nabla \cdot f(u) - S = 0$ (3.15)

This is defined as the strong form of the equation. There is also the weak form, which is obtained via the weighted residue method:

- $\int_V \left[\left(\frac{\partial u}{\partial t} - S\right)\omega(x) - f(u) \cdot \nabla\omega(x)\right] dV + \int_A f \cdot n\, \omega(x)\, dA = 0$ (3.16)

As explained above, to solve PDEs it is therefore necessary to discretize them, with the creation of a mesh. Consider a function of a variable u(x), whose domain is constituted by the points x_i (i = 1, . . . , N), for simplicity considered equidistant from each other, then the solution will be given by the approximation of the discrete value assumed by this variable at the points $u_i \approx u(x_i)$; i = 1, . . . N and considering the distance ratios between the points $u_{i+1} \approx u(x_{i+1}) = u(x_i + \Delta x)$ [Figure 39].

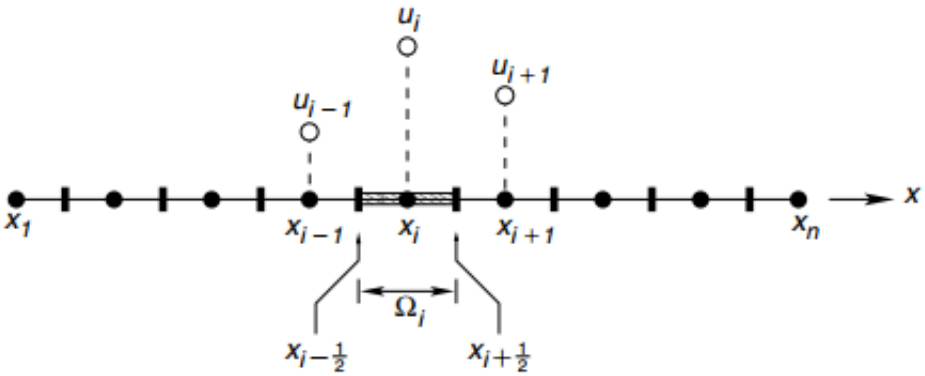

Figure 39 – Division of the domain in x_i points[63]

In the FVM method we work with the integrated form of the PDEs just seen, in particular, starting from their strong form and considering a control volume 'i', we obtain:

- $\int_{x_{i-\frac{1}{2}}}^{x_{i+\frac{1}{2}}} u_t \, dx + \int_{x_{i-\frac{1}{2}}}^{x_{i+\frac{1}{2}}} f_x(u)dx = 0$ (3.17)

Where:

- $\int_{x_{i-\frac{1}{2}}}^{x_{i+\frac{1}{2}}} f_x(u)dx = f(u_{i+\left(\frac{1}{2}\right)}) - f(u_{i-\left(\frac{1}{2}\right)})$ (3.18)

While the first term can be rewritten via the midpoint rule, arriving at:

- $u_{t|i}\left(x_{i+\frac{1}{2}} - x_{i-\frac{1}{2}}\right) + f\left(u_{i+\frac{1}{2}}\right) - f\left(u_{i-\frac{1}{2}}\right) = 0$ (3.19)

If the flux between adjacent cells is equal, a conservative pattern is obtained.

The same result can also be reached by starting from the weak form of PDEs and considering the weight w(x) = 1 for xi- 1/2≤ x ≤ xi+1/2 , otherwise w(x) = 0.[63]

3.1.2.2 FVM: algorithms for resolution

To solve the equations, it is necessary to proceed iteratively. There are various schemes for doing this, among them SIMPLE (Semi-Implicit Method for the Pressure Linked Equations) is an algorithm created by Patankar and Spalding used for systems based on the pressure-velocity coupling. SIMPLEC is a variation of the previous algorithm, while PISO (Pressure Implicit with Splitting of Operators) is an algorithm that involves a non-iterative time-marching procedure.

Writing the equation 3.9 as follows:

- $\frac{\partial}{\partial t}(\rho\phi) + \nabla \cdot (\rho V\phi) = \nabla \cdot \Gamma_\phi \nabla \phi + S_\phi$ (3.20)

Where, if we substitute ϕ with the velocity component u_i , or with a unit value, we obtain the momentum and continuity equation respectively:

- $\frac{\partial}{\partial y}(\rho\phi) + \nabla \cdot (\rho V u_i) = -\nabla p + \nabla \cdot (\mu \nabla u_i) + S_c + S_p u_i$ (3.21)
- $\frac{\partial \rho}{\partial t} + \nabla \cdot (\rho V) = 0$ (3.22)

Where p and μ are respectively the pressure and the dynamic viscosity and $S_c + S_p u_i$ is the linearised source term. Using a staggered mesh [Figure 40], the equations are reformulated as follows:

- $\left(a_e + \frac{\rho \Delta V}{\Delta t}\right) u_e = \sum_{nb} a_{nb} u_{nb} + A_e(p_P - p_E) + S_c \Delta V + \frac{\rho^o \Delta V}{\Delta t}\, u_e^o$ (3.23)
- $\left(a_n + \frac{\rho \Delta V}{\Delta t}\right) v_n = \sum_{nb} a_{nb} v_{nb} + A_n(p_P - p_N) + S_c \Delta V + \frac{\rho^o \Delta V}{\Delta t}\, v_n^o$ (3.24)

where subscripts n, e, s, w represent neighbouring cells (nb).[73,74]

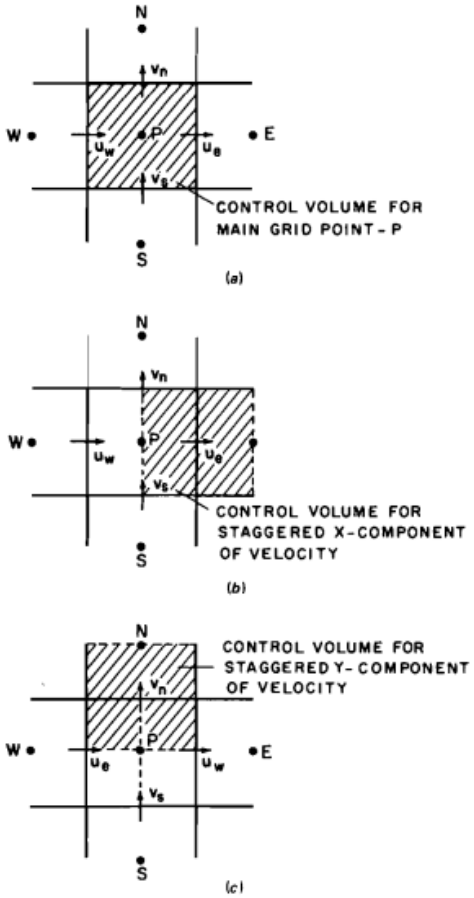

Figure 40 – Staggered-mesh scheme for: a) pressure; b) x-component of velocity; c) y-component of velocity[74]

They represent the non-stationary momentum equations calculated for a finite volume, their stationary equivalents can be calculated using the time-marching technique. The equations can be reformulated as follows[73,74]:

- $\bar{a}_e u_e = \sum a_{nb} u_{nb} + A_e(p_p - p_E) + b_e$ (3.25)
- $\bar{a}_n v_n = \sum a_{nb} v_{nb} + A_n(p_p - p_N) + b_n$ (3.26)

3.1.2.2.1 SIMPLE algorithm

If we subtract a guessed pressure field p*, velocities u* and v* from the equations seen, we obtain:

- $\bar{a}_e u'_e = \sum a_{nb} u'_{nb} + A_e(p'_P - p'_E)$ (3.27)
- $\bar{a}_n v'_n = \sum a_{nb} v'_{nb} + A_n(p'_P - p'_N)$ (3.28)

With:

- $u' = u - u*$ (3.29)
- $v' = v - v*$ (3.30)
- $p' = p - p*$ (3.31)

if we substitute:

- $d_e = \frac{A_e}{\bar{a}_e}$ (3.32)

and

- $d_n = \frac{A_n}{\bar{a}_n}$ (3.33)

The velocity correction equations are obtained:

- $u_e = u_e^* + d_e(p'_P - p'_E)$ (3.34)

- $v_n = v_n^* + d_n(p'_P - p'_N)$ (3.35)

Substituting this equation into the continuity equation:

- $\frac{(\rho_p - \rho_p^0)\Delta V}{\Delta t} + \rho_e u_e A_e - \rho_w u_w A_w + \rho_n u_n A_n - \rho_s u_s A_s = 0$ (3.36)

The pressure correction is obtained:

- $a_p p'_p = a_E p'_E + a_w p'_w + a_N p'_N + a_S p'_S + b$ (3.37)

The velocity and pressure correction equations can then be solved iteratively, updating the new pressure and velocity values at each iteration until convergence is achieved.[73,74]

3.1.2.2.2 SIMPLEC algorithm

The SIMPLEC algorithm works in the same way as SIMPLE, but in this case the correction factor takes the form:

- $d_e = \frac{A_e}{\bar{a}_e - \sum a_{nb}}$ (3.38)

And

- $d_n = \frac{A_n}{\bar{a}_n - \sum a_{nb}}$ (3.39)

3.1.2.2.3 PISO algorithm

The PISO algorithm works by making predictions and corrections at each time step. By indicating the previous step with the superscript n, the current step with *, the first correction with ** and the third correction with ***, it is possible to rewrite the equations seen above as:

- $\bar{a}_e u_e^* = \sum a_{nb} u_{nb}^* + A_e(p_P^n - p_E^n) + b_e^n$ (3.40)

and subsequently:

- $\bar{a}_e u_e^{**} = \sum a_{nb} u_{nb}^* + A_e(p_P^* - p_E^*) + b_e^n$ (3.41)

Subtracting the two equations:

- $u_e^{**} = \hat{u}_e - d_e(p_P^* - p_E^*)$ (3.42)

Where:

- $\hat{u}_e = u_e^* - d_e(p_P^n - p_E^n)$ (3.43)

Substituted into the continuity equation, the predictive pressure equation is obtained:

- $a_p p_p = a_E p_E + a_w p_w + a_N p_N + a_S p_S + b$ (3.44)

Subtracting instead the previous equation:

- $\bar{a}_e u_e^{**} = \sum a_{nb} u_{nb}^* + A_e(p_P^* - p_E^*) + b_e^n$ (3.41)

And

- $\bar{a}_e u_e^{***} = \sum a_{nb} u_{nb}^{**} + A_e(p_P^{**} - p_E^{**}) + b_e^n$ (3.45)

The corrective equation for velocity is obtained:

- $u_e^{***} = \hat{u}_e - d_e(p_P^{**} - p_E^{**})$ (3.46)

Where:

- $\hat{u}_e = u_e^{**} + \frac{\{\sum a_{nb}(u_{nb}^{**} - u_{nb}^*)\}}{\tilde{a}_e} - d_e(p_P^n - p_E^n)$ (3.47)

Substituting into the continuity equation gives the corrective equation for pressure.

In summary, through the previous time step, the coefficients for writing the predictive equations for velocity are obtained. The coefficients for the pressure predictive equation are then calculated. The velocity correction is made and with the new values, the pressure correction is obtained and then it's possible to move on to the next step.[73,74]

3.1.2.2.4 Biomedical applications: case study

Examples of their applications can be found in the literature, such as the research of Hodis et al.[75] who conducted numerical modelling of cerebral aneurysms, using geometries obtained through clinical imaging and segmented using Mimics software. Simulations were conducted with the Ansys Fluent 13 software, which uses the FVM method. The setup involved a pressure-based solver with velocity coupling realised with the SIMPLE algorithm, the use of the QUICK scheme for spatial discretization, while Least Squares Cell Based was used for gradient estimation and a second-order scheme was chosen for pressure interpolation.

Cito et al.[76] used CFD to analyse the flow within the giant aneurysm of the internal carotid artery. The simulations were performed using Ansys Fluent 12, choosing a pressure-velocity coupling given by the SIMPLE algorithm and a second-order scheme for discretization. In order to achieve convergence, residual analysis was performed, with the condition of obtaining the value 10-5. With regard to fluid characterisation, laminar motion was assumed and Newtonian blood was considered, with viscosity and density values of 0.04 Poise and 1.0 g/cm3 respectively.

Bressloff and Hameed[77] used the Ansys Fluent 12.1.4 solver for the design of vascular stents using a pressure-based method, a PISO scheme, least-squares cell-based gradients for spatial discretization, used the STANDARD method for pressure and second-order upwind for momentum.

3.2 The custom made pulse duplicator: experimental section

In this section, the experimental investigation conducted on a new pulse duplicator model will be presented. The customised pulse duplicator was developed as a result of the need to create a system capable of testing a new mitral valve prototype, which is currently being developed at the Ri.MED foundation working on the Biomitral project. The aim of the pulse duplicator is therefore to reproduce the cardiac cycle and the physiological environment of mitral valve. This is what was analysed in this thesis project, by subjecting the design of the new pulse duplicator model, realized by Post-Doc. Joan D. Laubrie, to CFD analysis and evaluating the preliminary and final design. To this purpose, the Ansys Fluent 2022 R2 software was used, which operates through the finite volume method, as seen previously. The simulations were conducted with a computer running Windows 10 Pro 64-bit operating system and Intel(R) Xeon(R) E-2174G CPU at 3.80 GHZ.

The pulse duplicator design was realised in parallel with its circuit equivalent, which was built using the model presented by Lanzarone et.al[78] as a reference [Figure 41], making modifications and revising it.

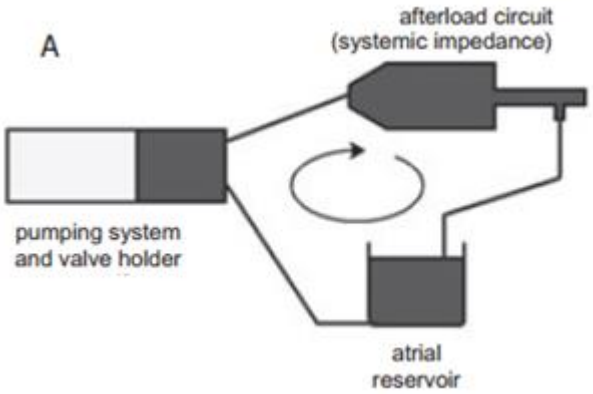

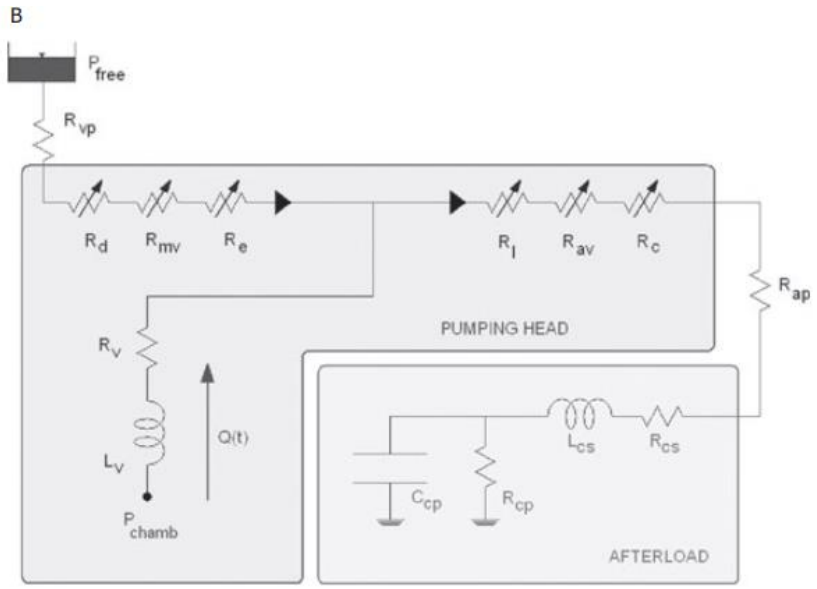

Figure 41 – Pulse duplicator model realized by Lanzarone et.al A) schems of mock loop; B) lumped model.[78]

The custom-made pulse duplicator consists of a pumping system formed by a hydraulic cylinder with a piston, an area that mimics the atrium, the mitral valve housing, a chamber representing the ventricle, the aortic valve housing and the afterload circuit [Figures 42].

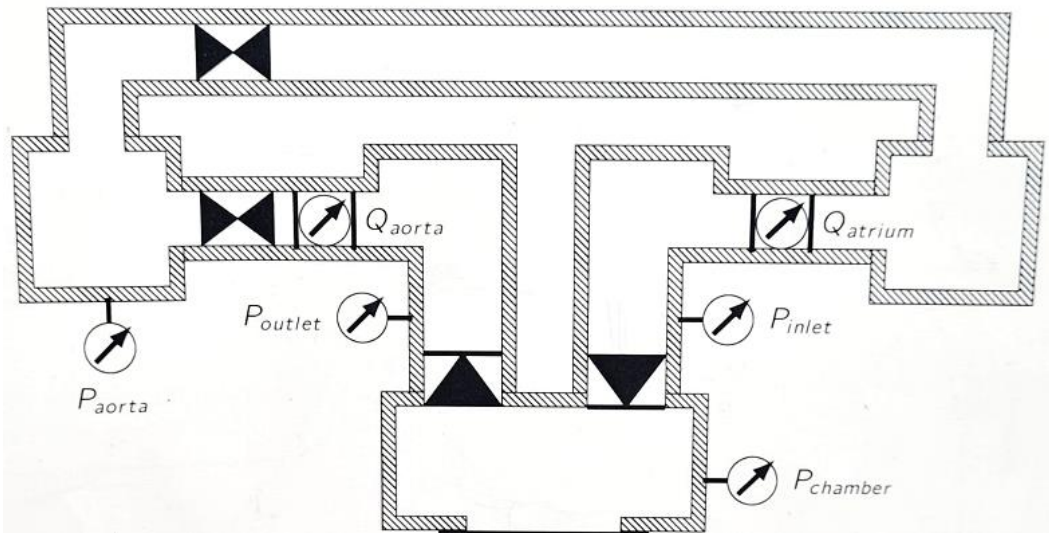

Figure 42 – Mock loop of the custom-made pulse duplicator

Its circuit equivalent, consisting of resistors, inductors and capacitors, is shown in the figure below [Figure 43]:

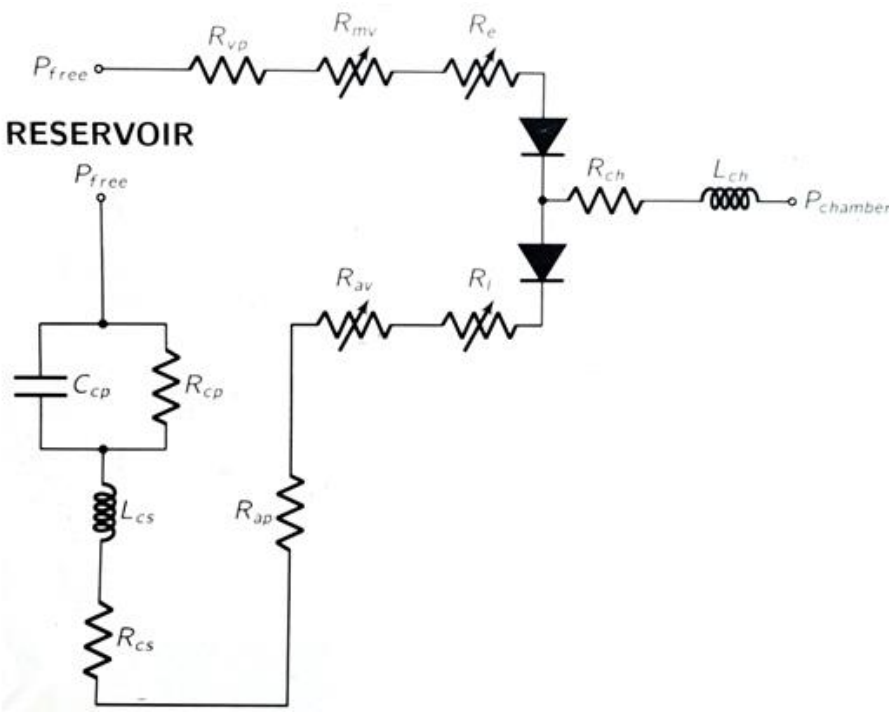

Figure 43 – Circuit model of custom-made pulse duplicator

Where:

- P_{free} : pressure due to the geodetic contribution of the atrial reservoir;
- R_{vp} : resistance of the venous suction pipe connecting the reservoir with the chamber;
- R_{mv} : resistance of the mitral valve;
- R_e : resistance of the cross-sectional variation at the ventricular chamber inlet;
- R_{ch}, L_{ch} : resistance and inertance of the ventricular chamber;
- $P_{chamber}$: pressure in the ventricular chamber;
- R_I : resistance due to the cross-sectional variation at the ventricular chamber outlet;
- R_{av} : resistance of the aortic valve;
- R_{ap} : resistance of the arterial pipe connecting the chamber with the afterload circuit;
- $R_{cs}, R_{cp}, L_{cs}, C_{cp}$: resistances, inertance and compliance of the afterload circuit;

A 2D CFD analysis was conducted, analysing 3 different pulse duplicator designs [Figure 44]:

1. Model No. 0: a simplified version, consisting of the atrium, ventricular chamber and mitral valve.
2. Model No. 1: preliminary version of the pulse duplicator, comprising the atrial chamber, ventricle, mitral and aortic valve and afterload pathway;
3. Model No. 2: final version of the pulse duplicator, comprising atrium, ventricle, mitral and aortic valve and afterload pathway; differs from model No. 1 in its measurements and the assumptions made about the mitral valve;

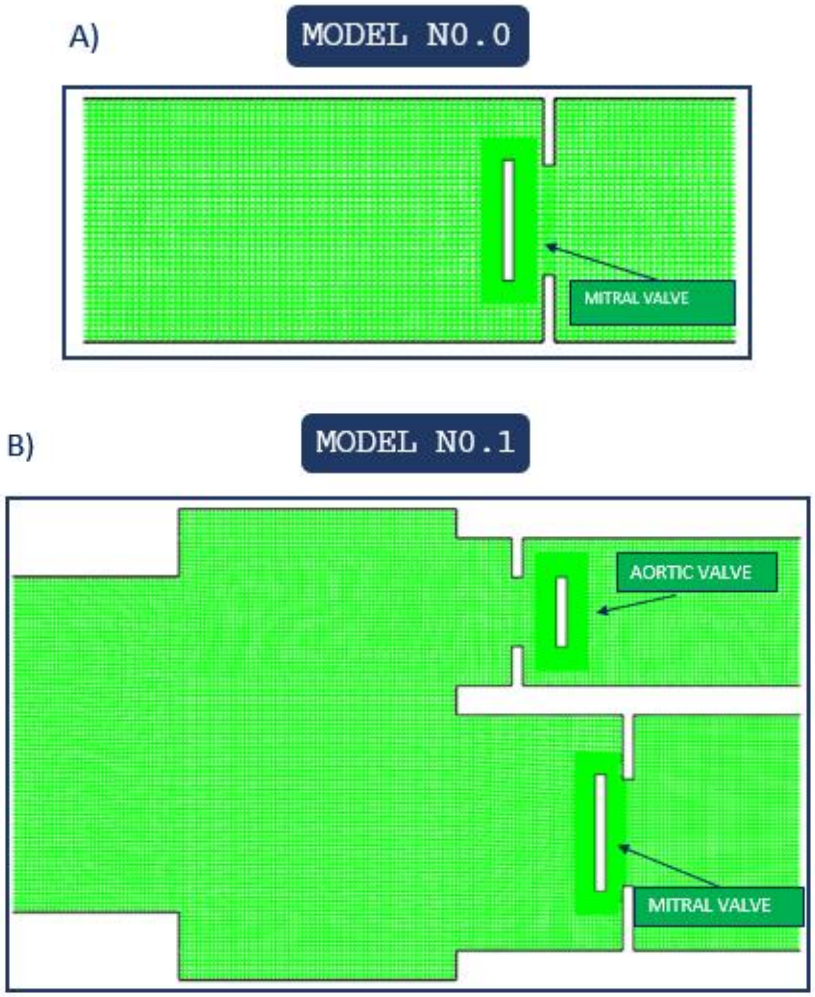

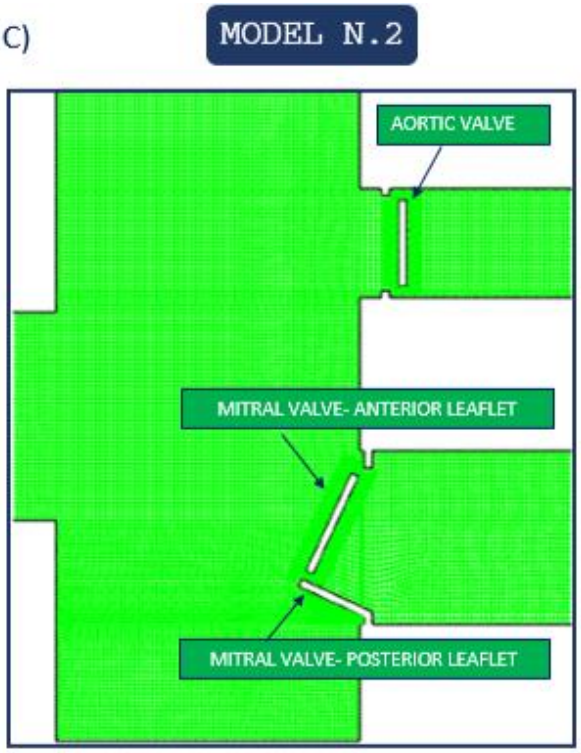

Figure 44 – The custom mad pulse duplicator CAD; A) model No.0 ; B) Model No.1; C) Model No.2

The first step of the analysis was the creation of the CAD models, which was followed by the discretization through the creation of the mesh.

For each model, simulations were then conducted, in which the cardiac cycle was reproduced in its systole and diastole phases, considering a flow rate of 9L and 60 bpm, and the rotational and translational motion of the mitral valve within the pulse duplicator was analysed under the relevant conditions, using the dynamic mesh technique. This technique makes it possible to study systems in which moving bodies cause a change in the shape of the domain and its boundaries.[79]

All the steps will be shown in the following paragraphs.

3.2.1 Model No. 0: a simplified model of pulse duplicator

In any CFD analysis, the first step is to identify the problem and convert it into a model capable of representing its characteristics (physical, chemical, etc.). Considering the complexity of the system under study, it is necessary for its resolution to make

assumptions and simplifications. To this end, it is necessary to have the appropriate knowledge and skills to make choices that do not compromise the quality of the results.[64] A simplified model of the pulse duplicator was therefore first studied in order to establish which criteria and parameters are most suitable for conducting optimal simulations, and then on the basis of these, to move on to the analysis of the complete pulse duplicator model.

Model no. 0 is therefore presented in this section.

Ansys Workbench 2022 R2 was used to create the CAD model and mesh. Two separate CADs were designed: one for the mitral valve and the other for the chambers. In fact, in order to use the dynamic mesh technique, it is necessary that the regions where relative movement is expected between zones of the domain, are modelled separately and that their contact occurs through interfaces.[79]

In this simplified case study, it was decided to work only on the atrium and part of the ventricle, leaving out the aortic valve, as the main purpose of creating the pulse duplicator is to identify an environment that is physiologically appropriate for the mitral valve. Therefore, a CAD drawing was created for the simplified model that respected the measurements of the complete original model as closely as possible. In the figure below, the CAD for the atrial and ventricular chamber is shown with the corresponding measurements in [cm] [Figure 45].

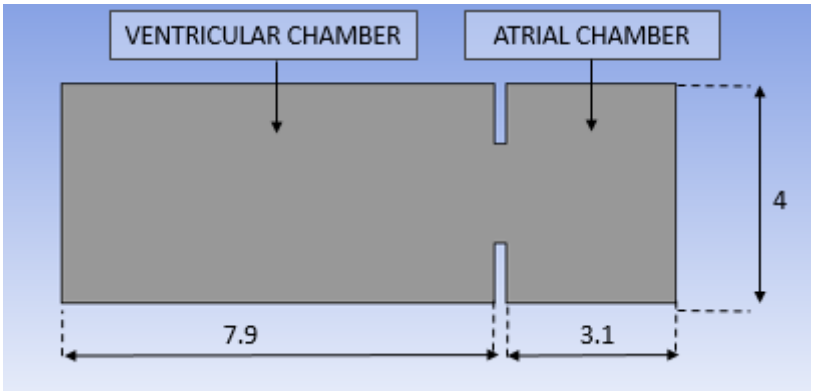

Figure 45 – Model No.0 : CAD design chambers and measurements [cm].

A simplified CAD model of the mitral valve was then created considering only the anterior leaflet, since it is this that makes a greater contribution to valve closure during systole than the posterior leaflet[18]. [Figure 46]. In anticipation of the use of dynamic mesh, the CAD was realised by considering the valve as a rigid structure, and creating a domain around it, that will serve to create the interface region with the chamber domain.

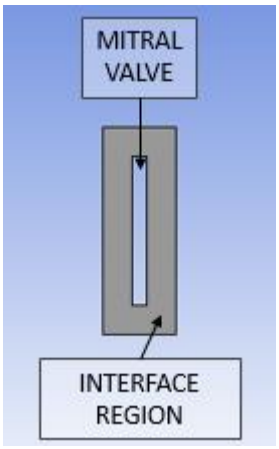

Figure 46 - Model No.0 : CAD of mitral valve

The mesh for both CAD models [Figure 47,48] was then realised, using quadrangular elements because they allow a lower error at higher accuracy.[70]

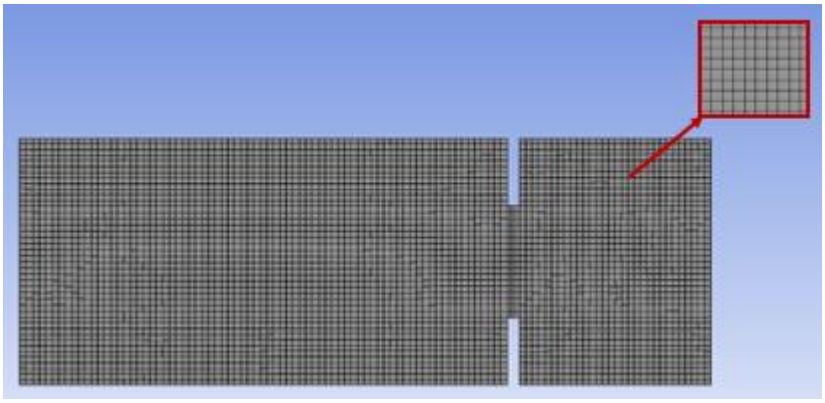

Figure 47 – Model of atrial and ventricle chambers discretized with quadrangular mesh

In both the chambers model and the mitral valve model, the mesh obtained has an element discretization quality of 99%.

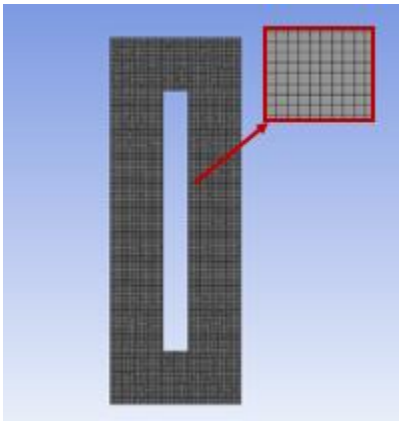

Figure 48 – Mitral valve model discretized with quadrangular mesh

At this point, the boundaries of the domain were identified, establishing the inlet and outlet regions, the walls and the fluid domain. The two models were then imported into Ansys Fluent 2022 R2, where they were overlaid to form a single system, through the identification of the interface region, referred to on Fluent as 'overset' [Figure 49].

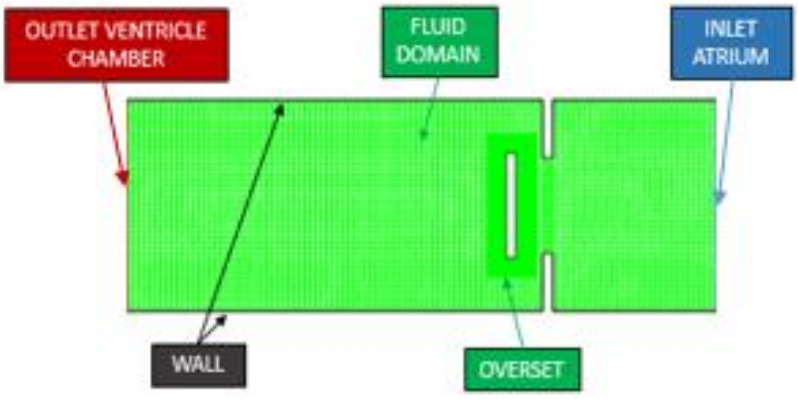

Figure 49 – Boundary regions of Model No.0

With regard to fluid characteristics, a density and dynamic viscosity value of ρ = 1060 Kg/m3 and μ = $3.4 \cdot 10^{-3}$ Pa*s were used to model the blood, which fall within the range found in the literature[80,81,82,83]. The k-ε model, which has also been used in other studies of flow analysis with prosthetic valves, was used as the viscous model[11,84]. In such, the flow is modelled following the transport equations for the kinetic energy of turbulence and its dissipation rate:

- $\frac{\partial}{\partial t}(\rho k) + \frac{\partial}{\partial x_i}(\rho k u_i) = \frac{\partial}{\partial x_j}\left[\left(\mu + \frac{\mu_t}{\sigma_k}\right)\frac{\partial k}{\partial x_j}\right] + G_k + G_b - \rho\varepsilon - Y_M + S_K$ (3.47)
- $\frac{\partial}{\partial t}(\rho \varepsilon) + \frac{\partial}{\partial x_i}(\rho \varepsilon u_i) = \frac{\partial}{\partial x_j}\left[\left(\mu + \frac{\mu_t}{\sigma_\varepsilon}\right)\frac{\partial \varepsilon}{\partial x_j}\right] + C_{1\varepsilon}\frac{\epsilon}{k}(G_k + C_{3\varepsilon}G_b) - C_{2\varepsilon}\rho\frac{\epsilon^2}{k} + S_\varepsilon$ (3.48)

Where G is a factor that takes into account average velocity gradients, Y_M takes into account the fluctuating dilatation, $\sigma_k$and $\sigma_\varepsilon$rappresent the Prandtl number, S_K and S_ε express the source and the C terms are costants[79].

The boundary conditions were then imposed, which were calculated by applying the equation of conservation of mass and energy between two points within the circuit used to model the pulse duplicator [Figure 43] and taking into account the dissipative components present in the pulse duplicator model:

- $C\frac{dP}{dt} + Q_2 - Q_1 = 0$ (3.49)
- $L\frac{dQ}{dt} + RQ + P_2 - P_1$ (3.50)

Where C, R and L represent the capacitances, resistances and inductances of the circuit and Q and P are the pressure and flow values between two different points in the circuit. The values obtained are shown in the following figure, where P_free represent the reservoir pressure values given as input to the inlet region of the atrium, while P_chamb_systole and P_chamb_diastole represent the pressure values applied to the outlet region of the ventricular chamber during the period of systole and diastole respectively [Figure 50]:

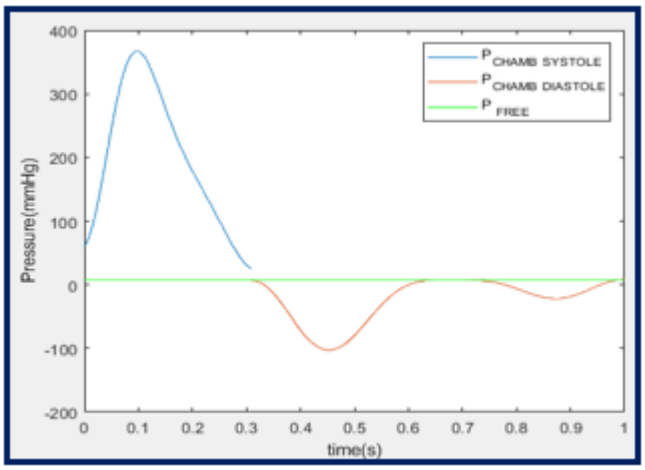

Figure 50 – Pressure values obtained numerically from the pulse duplicator circuit

The numerically obtained values were compared with the values physiologically present in the heart[85] [Figure 51] and then scaled by a factor chosen so as to obtain values close to the physiological ones [Figure 52]:

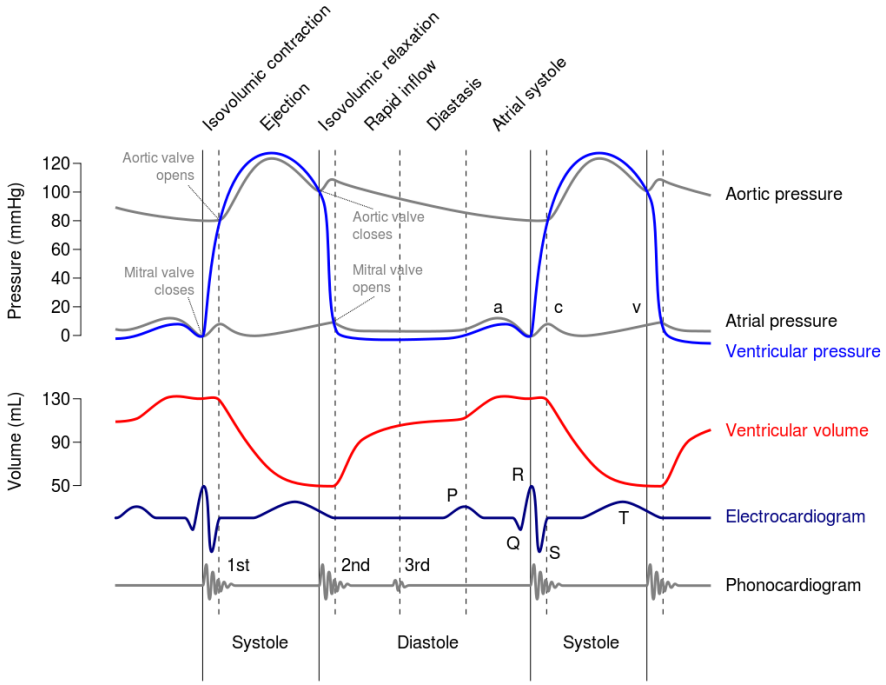

Figure 51 – Wiggers diagram;[85]

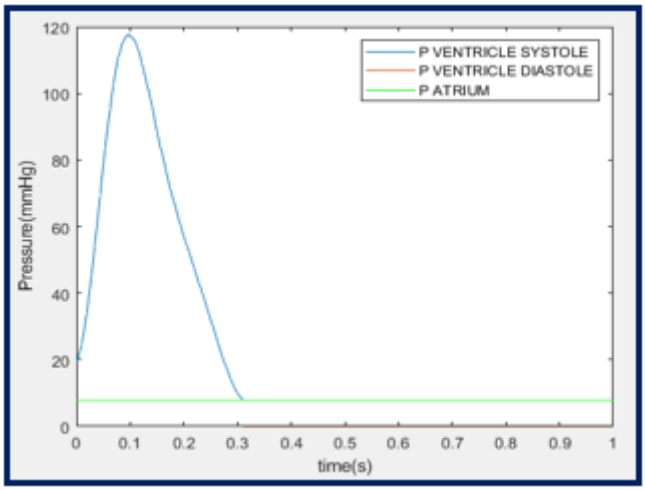

Figure 52 – Boundary conditions applied to the inlet and outlet region

No-slip boundary conditions were used for the walls.

To simulate the motion of the mitral valve, the 6DOF method was used, which allows the translational and rotational motion of a body to be calculated through the equations:

- $\vec{v}_G = \frac{1}{m}\sum \bar{f}_G$ (3.51)
- $\vec{\omega}_B = L^{-1}(\sum \vec{M}_B - \vec{\omega}_B \times L\vec{\omega}_B)$ (3.52)

Where the outputs correspond to the translational motion of the centre of gravity and the rotational motion, while the inputs represent the mass, the force of gravity in the first equation, and tensor of inertia, momentum and angular velocity, in the second one[79].

Finally, algorithms were selected to solve the problem. The SIMPLE method was used for the velocity-pressure coupling, while for the spatial discretization, the Least Squares Cell Based scheme was used for the gradient, the Second Order method for the pressure and Second Order Upwind for the momentum, turbulence and dissipation rate. The latter method allows for second-order accuracy, achieved through a Taylor Series expansion where the value associated with each cell is calculated by:

- $\phi_f = \phi + \nabla\phi \cdot \bar{r}$ (3.53)

where the first and third terms at the second member represent the value associated with the centroid and its displacement vector respectively, and the second term is the gradient. The latter using Least Squares Cell Based method is calculated through the following equation which considers the gradient between two cells and C_0 and C_1 along the vector Δr_i [79]:

- $(\forall \phi)_{C_o} \cdot \Delta r_i = (\phi_{C_i} - \phi_{C_0})$ (3.54)

3.2.2 Model No. 1 and Model No.2: the preliminary and final design of pulse duplicator

After elaborating a simplified model, the relative CAD of the original pulse duplicator was realised for 2 different configurations developed by the designer:

- Model No.1, which constitutes the preliminary version;
- Model No. 2, which represents its final version;

Again, Ansys Workbench was used for CAD design and mesh creation, and as in the previous case, separate models were built for chambers and valves in order to be able to use the dynamic mesh method.

The CAD for model no. 1 includes a chamber that mimics the atrium, a chamber for the ventricle, a region representing the connection to the pumping system and an area representing the afterfload circuit, as shown in the following figures along with the releted measurements in [cm][Figure 53].

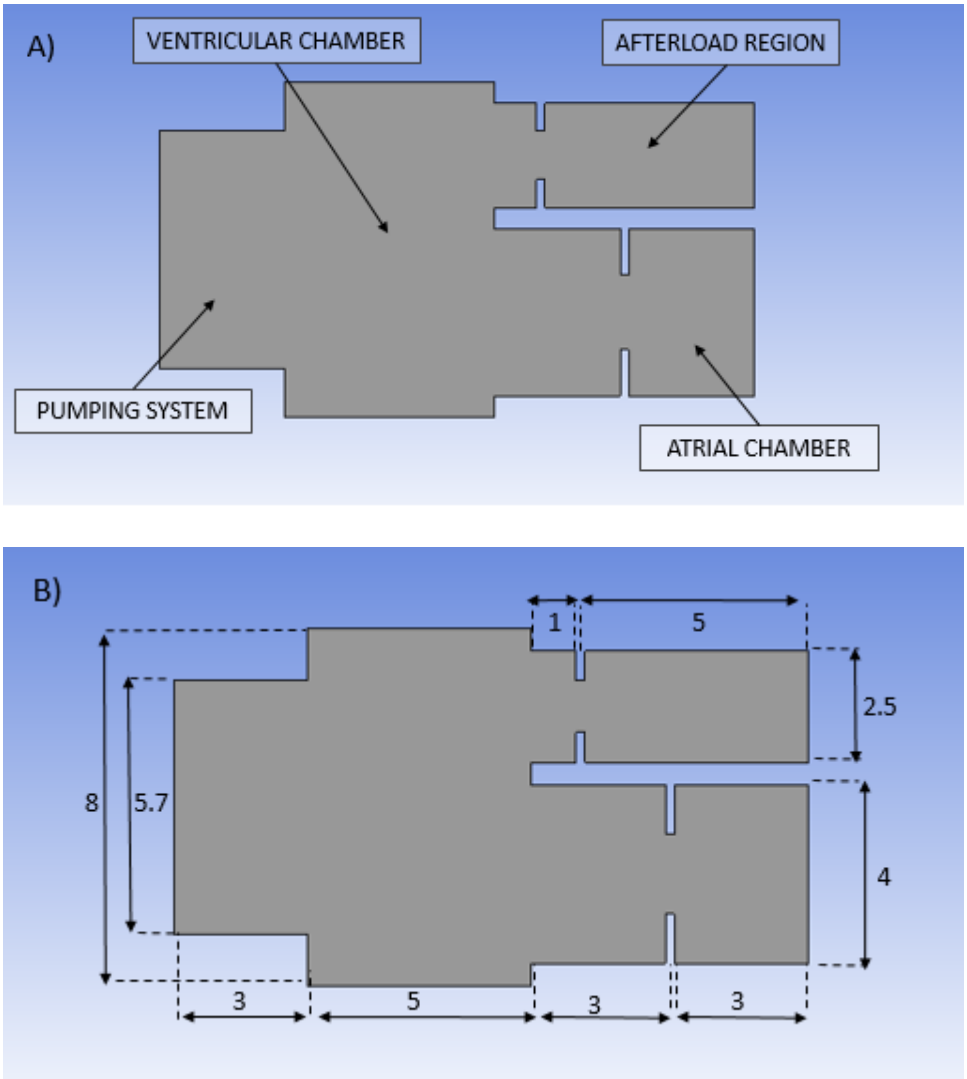

Figure 53 – Model No.1: a) chambers component CAD and b) related measures in [cm]

For the CAD of the mitral valve, the same considerations were made as for the previous model, representing only the anterior leaflet.

The model of the aortic valve has also been simplified [Figure 54], considering a single leaflet, since this valve is not the main object of investigation, and its presence is mainly linked to a better reproduction of the environment with which the mitral valve interacts.

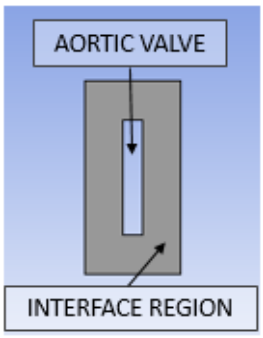

Figure 54 – Model No.1: aortic valve CAD

The CAD of model no. 2 is formed by the same chambers as the model just seen, which are the atrium, the ventricle, the region connected to the pumping system and the afterload area, but this design differs from the previous one in terms of measurements, as shown in the figure below [Figure 55]. For the aortic valve, the same considerations were made as for the previous model, while for the mitral valve, the posterior leaflet was also included. Its design was made taking into account the fact that its radial length is shorter than that of the anterior leaflet[21]. Furthermore, taking into account the fact that, as explained above, it contributes less to the closure of the valve, it was decided to consider it as a fixed element and not a movable one, which will therefore be incorporated into the design of the chamber [Figure 55].

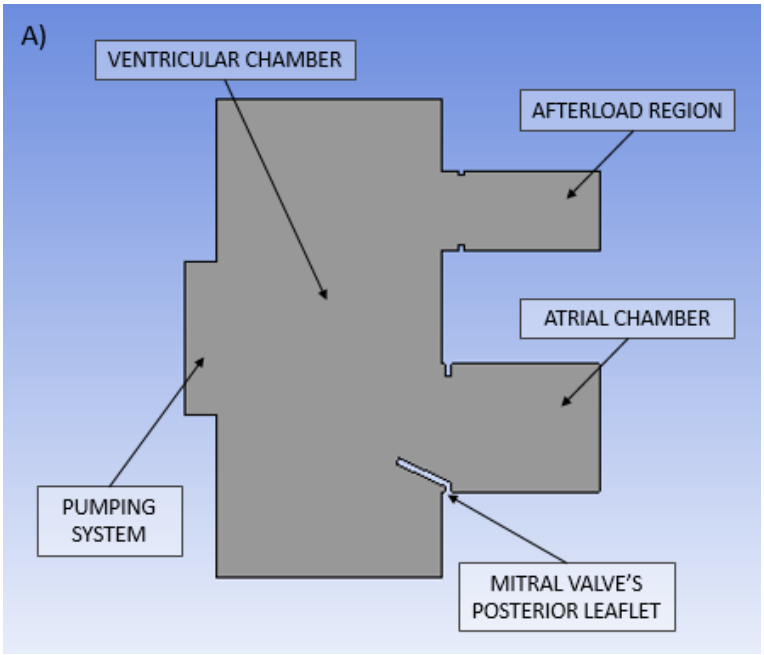

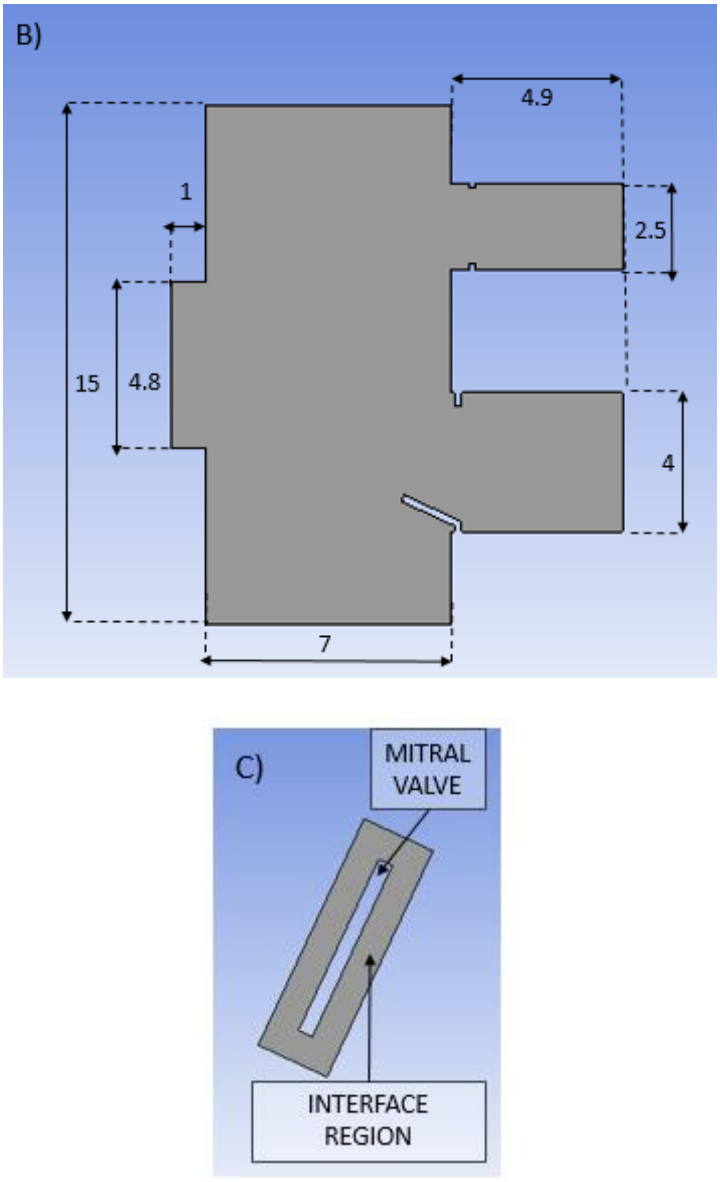

Figure 55 – Model No.2: CAD images of a) chambers with mitral valve posterior leaflets; b) related misures in [cm]; c) mitral valve

For both model no. 1 and model no. 2, a mesh with quadrangular elements was created, achieving a mesh quality of 99% in both cases [Figures 56,57].

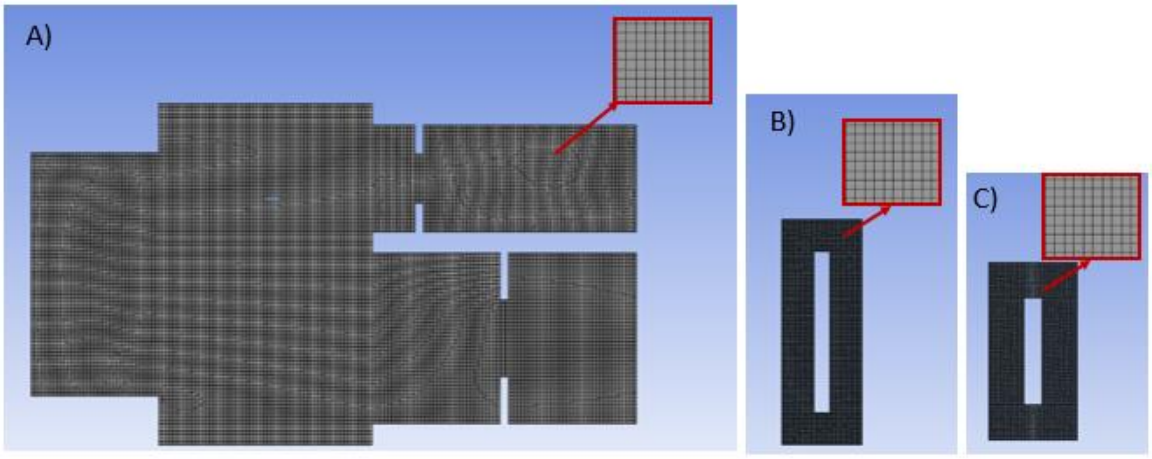

Figure 56 – Model n.1: a) chambers, b) mitral valve and c) aortic valve mesh

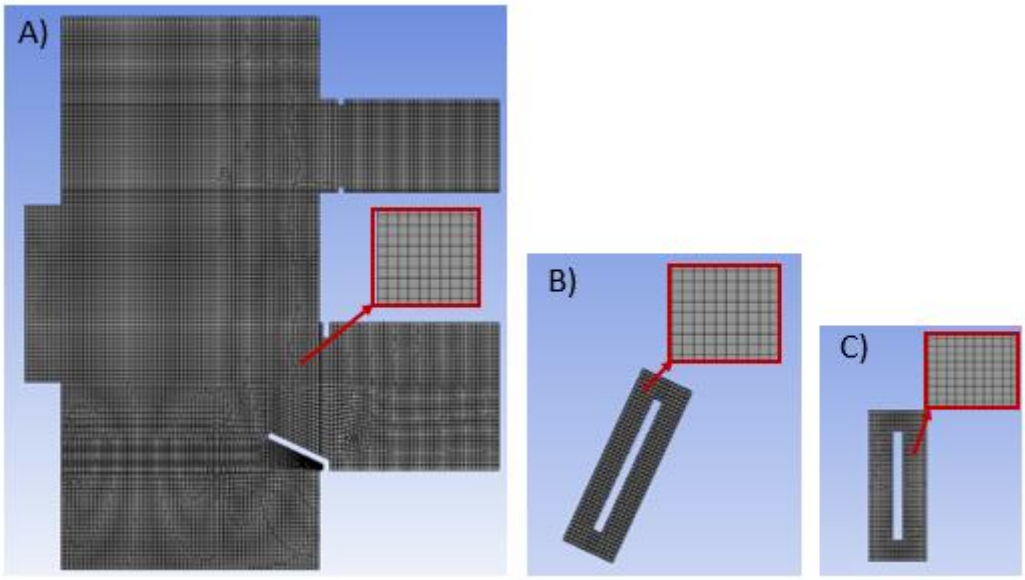

Figure 57 – Model n.2: a) chambers, b) mitral valve and c) aortic valve mesh

The inlet regions were then identified, corresponding for both models to the atrium and the area connected to the pumping system and the ventricle. The aortic region connected with the afterload area was selected as the outlet region. On Fluent, the valve models were then overlaid on the chamber models via the overset regions [Figure 58].

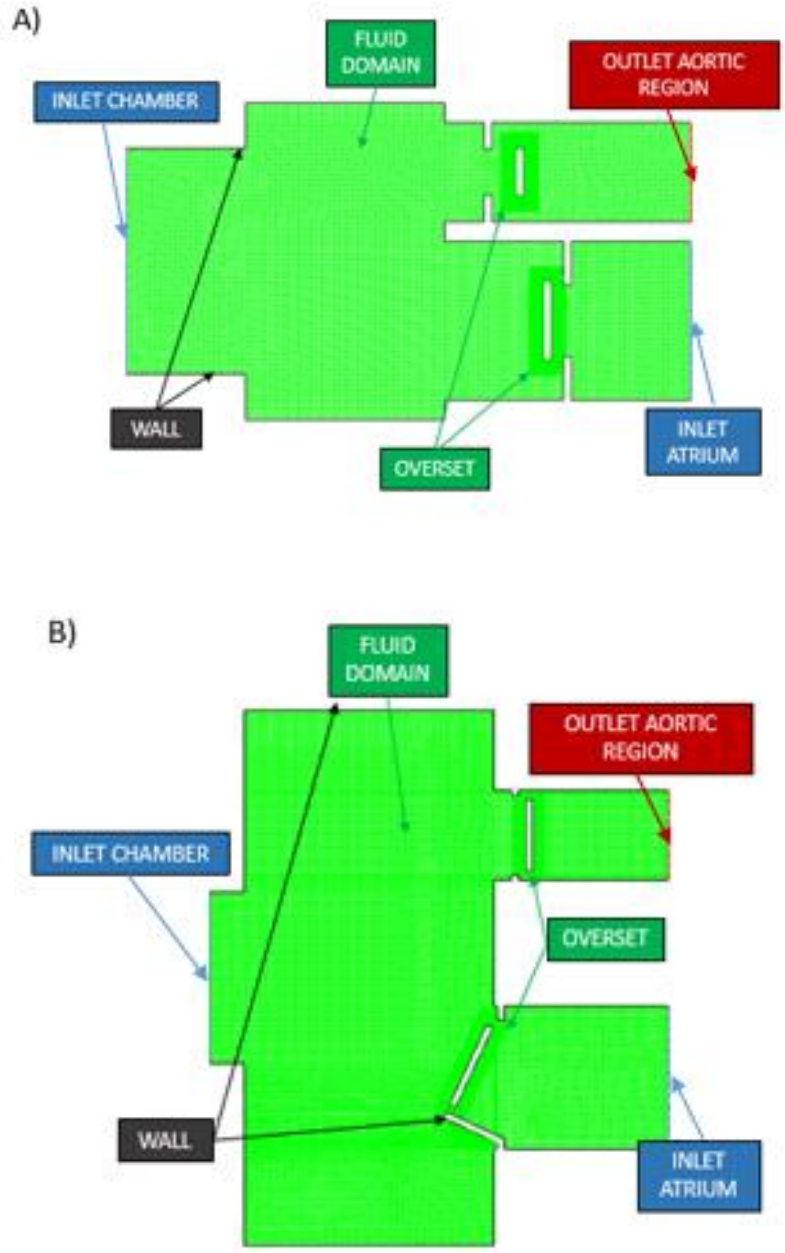

Figure 58 – boundary regions for a) model no.1 and b) model no.2

The boundary conditions were then calculated as in the previous case by applying the equations (3.49) and (3.50) to the pulse duplicator equivalent circuit and scaling the values obtained by a factor such that physiologically similar values were obtained [Figure 59]. The pressure values obtained were then used as boundary conditions assigned to the corresponding regions in the following manner:

- P_free was given as input to the atrium inlet region;

- P_chamb_systole and P_chamb_diastole were assigned to the inlet region located at the pumping system connected to the ventricular chamber during systole and diastole, respectively;
- P_E systole and P_E systole were used as boundary conditions for the outlet region;

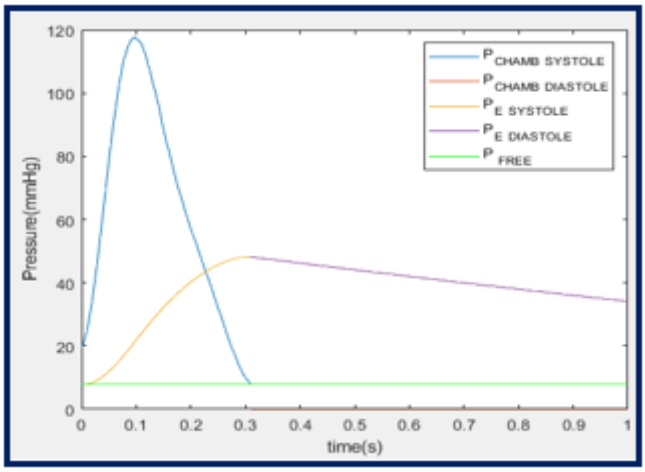

Figure 59 – Boundary conditions for model no.1 and model no.2

For both models, as for model no.0 seen above, the k-epsilon model was used to model the fluid and dynamic density and viscosity values equal to: ρ = 1060 Kg/m3 and μ = $3.4 \cdot 10^{-3}$ Pa*s.

The simulations were then conducted using the SIMPLE method and using the Second Order Upwind and Least Squares Cell Based schemes, as in the previous case, reproducing the overall cardiac cycle with a duration of 1s, considering the systole period of 0,31s and diastole for the remainder of the time, respectively. The motion of the mitral and aortic valves was allowed for using the 6DOF method.

Chapter 4

Results and discussion

4.1 General presentation of the analysis conducted

All three models shown above were investigated by means of CFD simulation, in which the cardiac cycle was reproduced in its phases of systole and diastole, considering a total duration of 1 s, of which 0.31 s for systole and 0.69 s for diastole respectively, for flow rates of 9L.

The movement obtained for the mitral valve in the respective conditions within the pulse duplicator was then analysed. In particular, both its rotational and translational movement were investigated, as it was shown that the mitral valve, and in particular its annulus, during the cardiac cycle not only changes its size, but also performs a translational movement that increases the efficiency of blood flow in the cardiac chambers[86,87].

The simulations were conducted using the pressure values obtained by considering the equivalent pulse duplicator circuit as boundary conditions and then scaled to approach the physiological values. Other possible boundary conditions were also studied, including pressure values obtained without a scaling factor; in other cases, velocity values were used as input instead of pressure. Only the results obtained with the first conditions just described will be shown below, as the investigations conducted led to the conclusion that these were the most appropriate conditions to use.

Finally, the velocity values obtained near the mitral valve and in the ventricular chamber were analysed. In addition, in order to evaluate the influence of the location of the pumping system in relation to the ventricular chamber, a different configuration of its position in model No.2 was also examined.

Ansys Fluent 2022 R2 and Matlab R2021a were used to perform the post-processing of the obtained data.

4.2 Model No. 0: results for rotational movement

The cardiac cycle in the two phases of systole and diastole in model no. 0 was reproduced by means of fluid-dynamic simulation. The pressure values obtained with the pulse duplicator circuit model (and scaled by a factor to approximate the pressure values physiologically present in the corresponding chambers of the heart) were used as boundary conditions (boundary conditions shown in figure 52 in chapter 3). Using the dynamic mesh method, the mitral valve was allowed to make a rotational movement. The analysis was conducted by means of a fluid-dynamic simulation, which achieved convergence, with values of the residuals shown in Table 1.

	VALUE	ABSOLUTE CRITERIA	CONVERGENCE STATUS
CONTINUITY	2.875×10^{-6}	0.001	converged
X-VELOCITY	1.559×10^{-4}	0.001	converged
Y-VELOCITY	1.397×10^{-4}	0.001	converged
K	3.105×10^{-4}	0.001	converged
ε	2.203×10^{-4}	0.001	converged

Table 1 - model no. 0: convergence of residuals in the simulation of rotational motion of the mitral valve

The following figure shows two images of the pulse duplicator relating to two different instants of the simulation [Figure 60]. The first image corresponding to the instant 0.26 s shows the mitral valve correctly closed during the period of systole, while the second image represents the instant 0.75 s corresponding to the period of diastole, in which the mitral valve is correctly open and the flow from the atrial chamber to the ventricular chamber is flowing. It is important to point out that during the construction phase of the model, it was not possible to place the valve in a completely closed position with respect to the passage orifice between the chambers, as the dynamic mesh method does not allow this[88]. This limitation of the method results in the valve not being able to close completely during systole and thus in the passage of a limited amount of flow between the chambers. For the reproduction of diastole, on the other hand, there are no

limitations as the valve rotates appropriately around the fixed centre of rotation, allowing the flow to pass correctly. There is also a ring vortex near the mitral valve in the vicinity of the ventricle, the formation of which has been demonstrated to be physiologically present in the heart.[89]

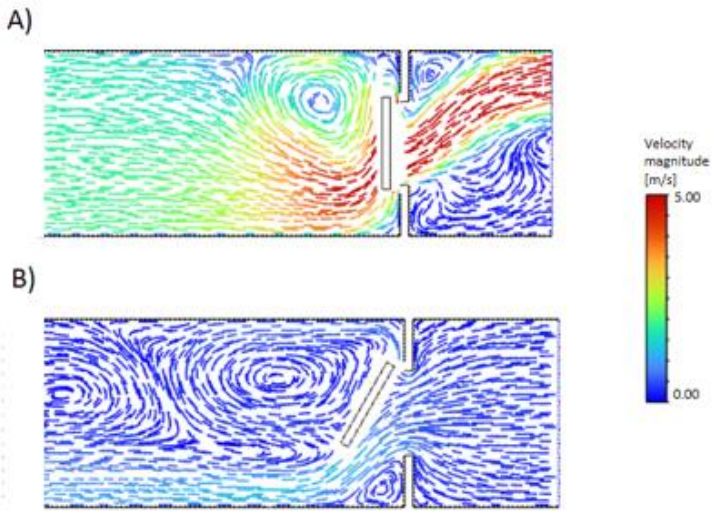

Figure 60 – Model no. 0: velocity flow line in the rotational valve model for A) systole (time instant 0.25 s) and B) diastole (time instant 0.75). Lines drawn in dark red indicate out-of-scale velocity values

The following figure shows the velocity profiles calculated near the mitral valve (before and after the mitral valve, respectively) for the period of systole and diastole [Figure 61].

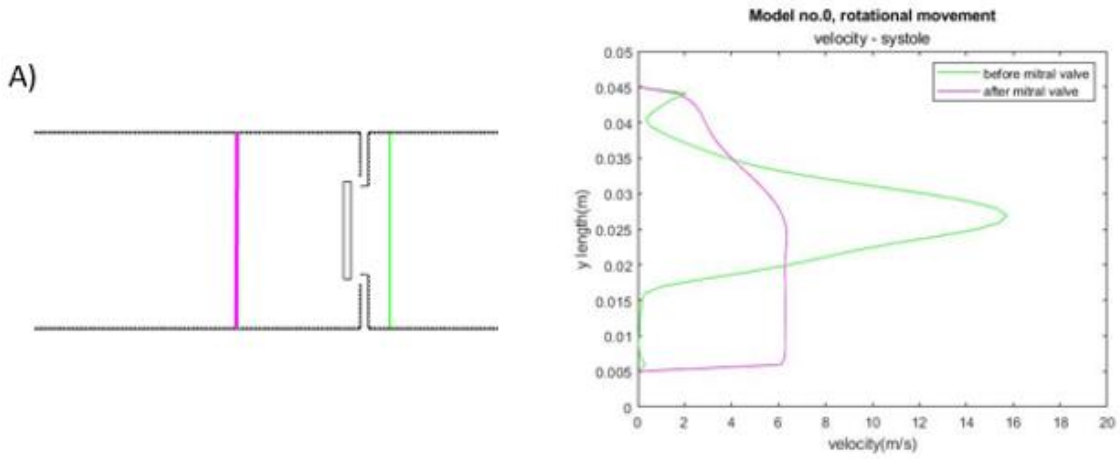

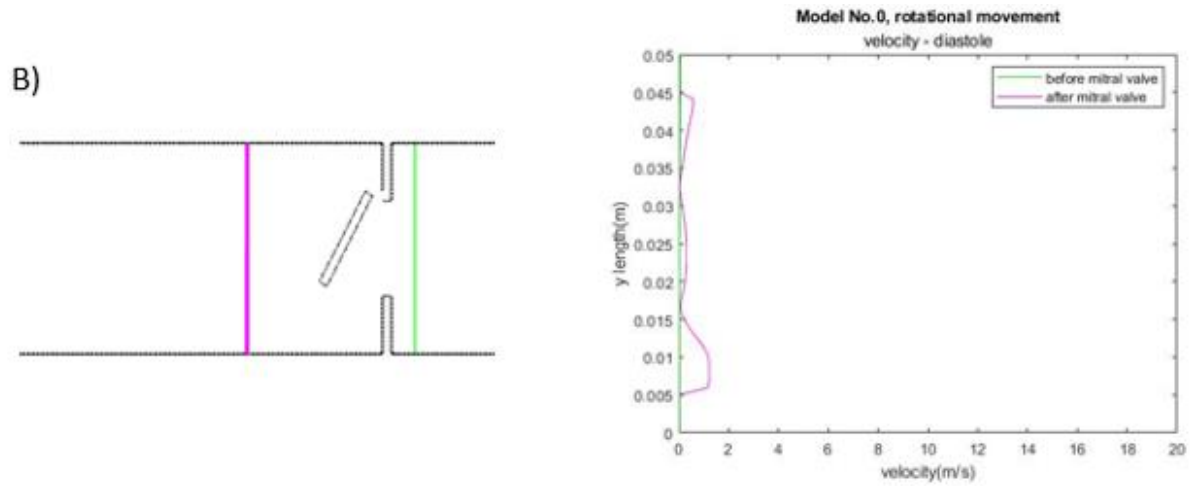

Figure 61 – Model No. 0: graphs showing velocity , in case of rotational motion, at the mitral valve as a function of channel length y, for A) the period of systole and B) diastole. In green are the velocity values located before the mitral valve and in magenta the velocity values after the valve.

From the graphs in Figure 61, it can be noted that during systole, the mitral valve is subjected to significantly high velocity gradients, whereas during diastole, velocity values are within the physiological range of 0.5- 1.7 m/s.[17,86] It is conceivable that the high velocity values during systole may be related to the valve not closing completely and thus the non-physiological passage of blood through a very small opening, which causes the velocity to increase.

4.3 Model No. 0: results for traslational movement

In addition to the rotational movement of the mitral valve, its translational movement within the pulse duplicator was also investigated, using the same boundary conditions. [Figure 52, Chapter 3]. The simulation conducted achieved convergence, with the value of residuals shown in Table 2.

	VALUE	ABSOLUTE CRITERIA	CONVERGENCE STATUS
CONTINUITY	4.153×10^{-4}	0.001	converged
X-VELOCITY	3.152×10^{-4}	0.001	converged
Y-VELOCITY	3.125×10^{-4}	0.001	converged
K	3.972×10^{-4}	0.001	converged
ε	6.617×10^{-4}	0.001	converged

Table 2 - model no. 0: convergence of residuals in the simulation of traslational motion of the mitral valve

As can be seen in the figure below [Figure 62], during systole the mitral valve moved correctly in the direction of the orifice that connects the atrium and ventricle and a correct overlap and therefore excellent closure was achieved. During diastole, the valve moved in the direction of the ventricle, allowing the orifice to open and the flow to pass.

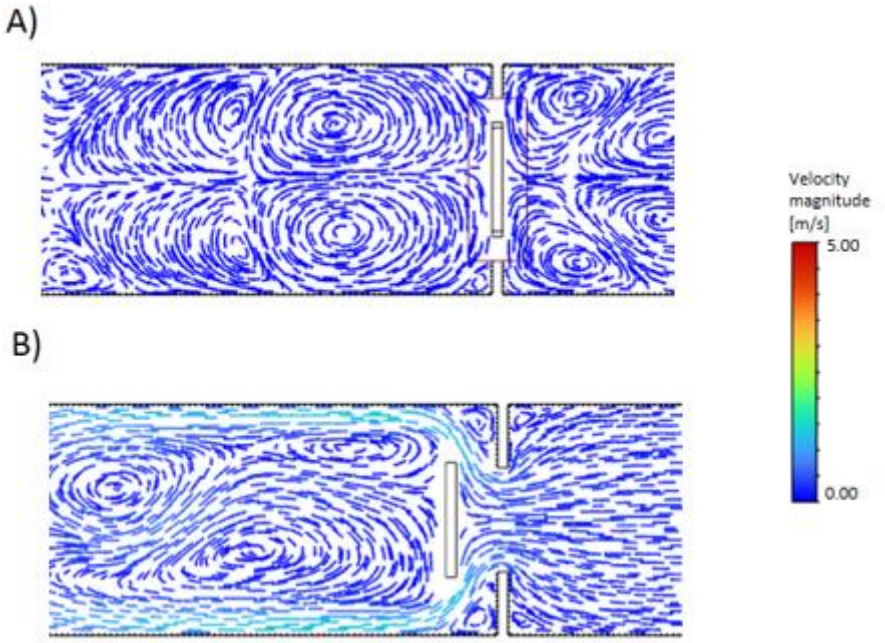

Figure 62 – Model no. 0: velocity flow line in the traslational valve model for A) systole (time instant 0.25 s) and B) diastole (time instant 0.75)

It is possible to make a comparison with the rotational case seen previously, where it was not possible to obtain a complete closure of the valve, as it was only allowed a movement around the centre of rotation (corresponding to its upper right-hand corner) and its closure configuration corresponded to the position realised during the CAD construction phase, where it was not possible to carry out a perfect overlap with the orifice and therefore a closure, as this was not compatible with the subsequent use of the dynamic mesh method, as explained previously.

In the case of translational movement, on the other hand, starting from the same initial configuration of the valve separated from the orifice, by reproducing its translational movement it was possible to achieve perfect closure.

It is important to note that in this case, physiological velocity values are present in the proximity of the mitral valve even during the systolic phase [Figure 63]. This could be considered a factor supporting the hypothesis previously made about the high velocity values obtained during the systolic phase in relation to imperfect valve closure.

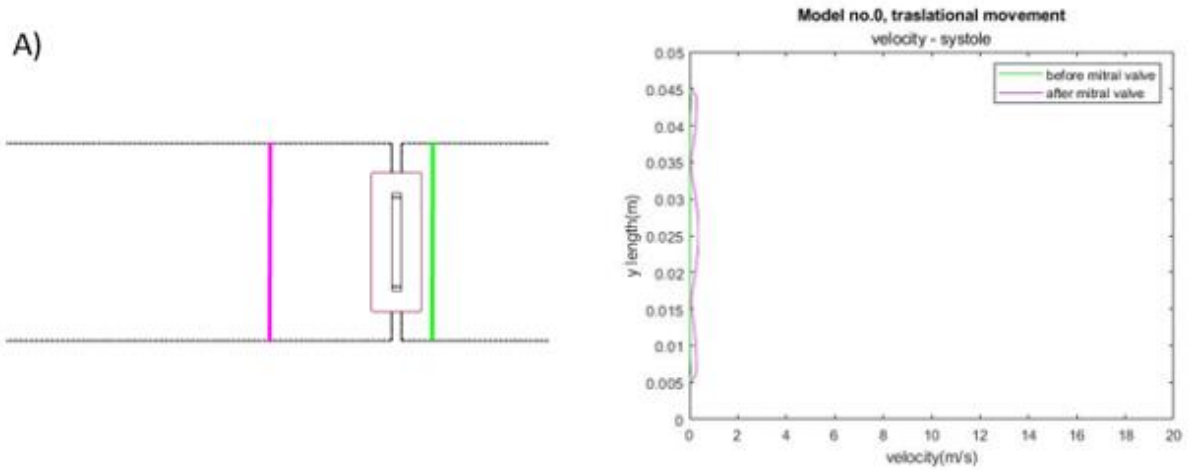

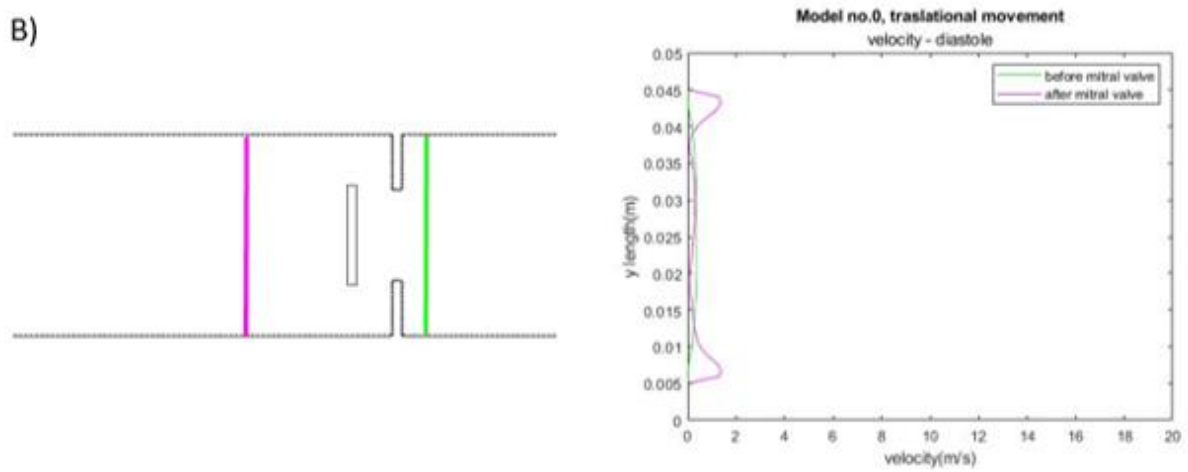

Figure 63 – Model No. 0: graphs showing velocity profiles, in case of translational motion, at the mitral valve as a function of channel length y, for A) the period of systole and B) diastole. In green are the velocity values located before the mitral valve and in magenta the velocity values after the valve.

4.4 Model No. 1 and Model No. 2 : results

Once the analysis on the simplified model had been carried out, the investigation was performed on models no.1 and no.2, taking into account the information acquired. For both models, the simulations conducted by simulating the rotational movement of the mitral valve will be shown, as this is the main movement performed physiologically and therefore the main object of investigation. Below are shown in Table 3 and Table 4, the values of the residuals obtained for the simulations concerning model no.1 and model no.2 respectively.

	VALUE	ABSOLUTE CRITERIA	CONVERGENCE STATUS
CONTINUITY	9.985×10^{-5}	0.001	converged
X-VELOCITY	2.297×10^{-4}	0.001	converged
Y-VELOCITY	1.689×10^{-4}	0.001	converged
K	3.332×10^{-4}	0.001	converged
ε	4.338×10^{-4}	0.001	converged

Table 3 - model no. 1: convergence of residuals in the simulation of rotational motion of the mitral valve

	VALUE	ABSOLUTE CRITERIA	CONVERGENCE STATUS
CONTINUITY	3.870×10^{-5}	0.001	converged
X-VELOCITY	4.829×10^{-4}	0.001	converged
Y-VELOCITY	4.502×10^{-4}	0.001	converged
K	5.602×10^{-4}	0.001	converged
ε	9.029×10^{-4}	0.001	converged

Table 4 - model no. 1: convergence of residuals in the simulation of rotational motion of the mitral valve

Using the pressure values previously shown in figure 59 of chapter 3 as boundary conditions for both models, the following results were obtained, which are shown in figure 64 where it is possible to observe the mitral valve closed and the aortic valve opened during systole, and vice versa the mitral valve correctly opened and the aortic valve closed during diastole.

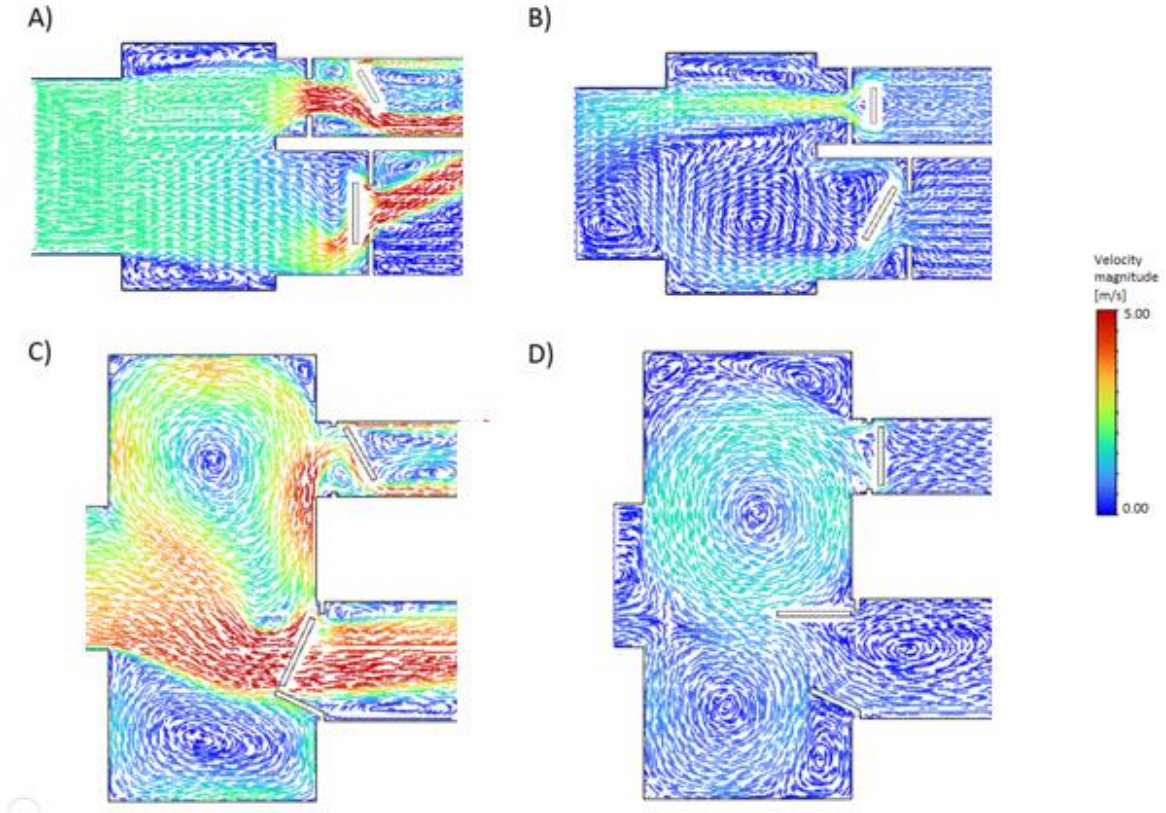

Figure 64 –Velocity flow line in the rotational valve model for A-B) Model no. 1 , systole (time instant 0.25) and diastole (time instant 0.75) and for C-D) Model no.2 , systole (time instant 0.25) and diastole (time instant 0.75) Lines drawn in dark red indicate out-of-scale velocity values

As in the case of the simplified rotational model, also with model no.1 and model no.2 during systole, high velocity values are present in the pulse duplicator, whereas during diastole, physiological values return. [Figures 65,66].

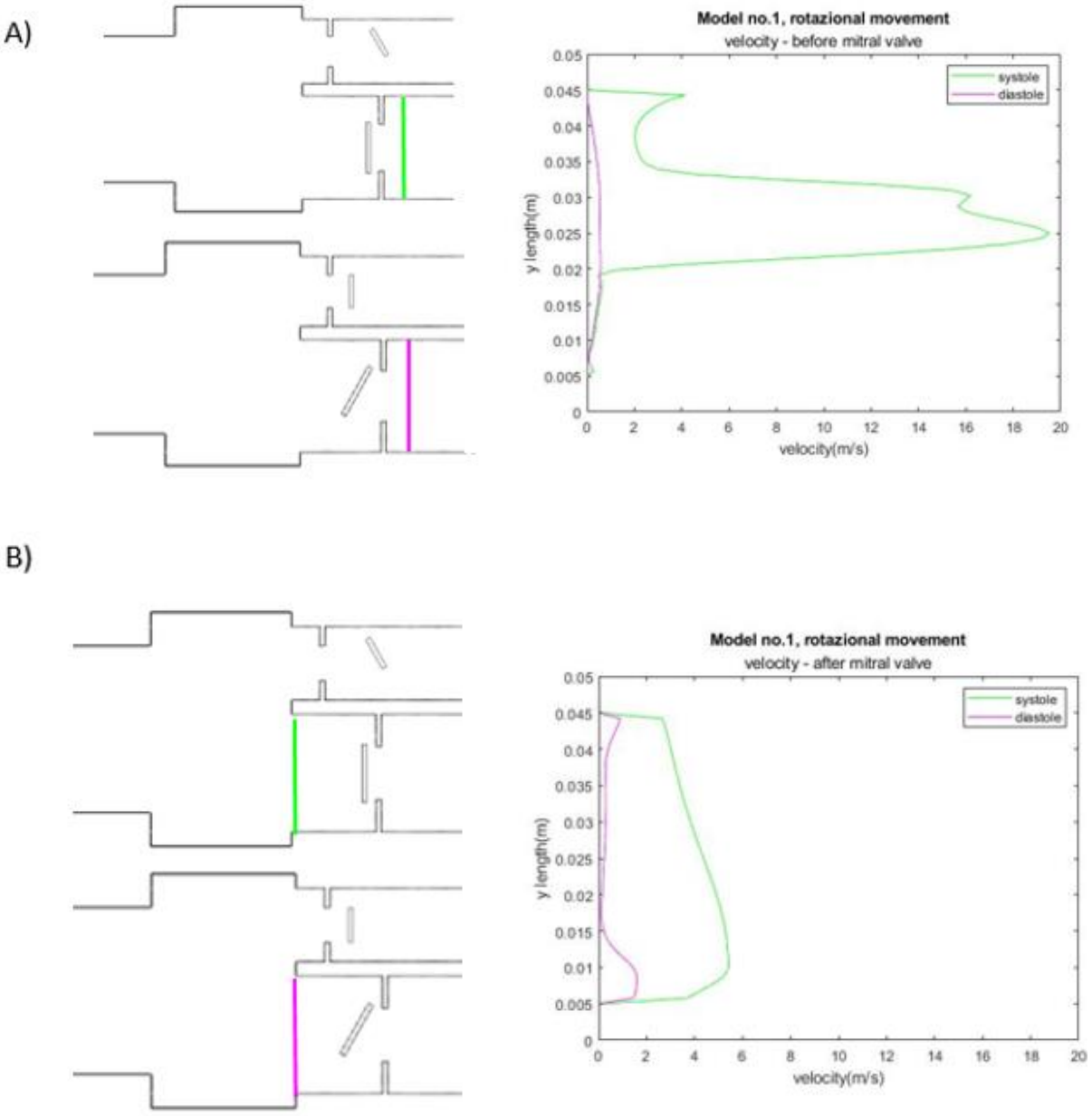

Figure 65 – Model No. 1: graphs showing velocity profiles, in case of rotational motion, at the mitral valve as a function of channel length y, considering A) the velocity values located before the mitral valve and B) after the mitral valve, for systole (green lines) and diastole (magenta lines).

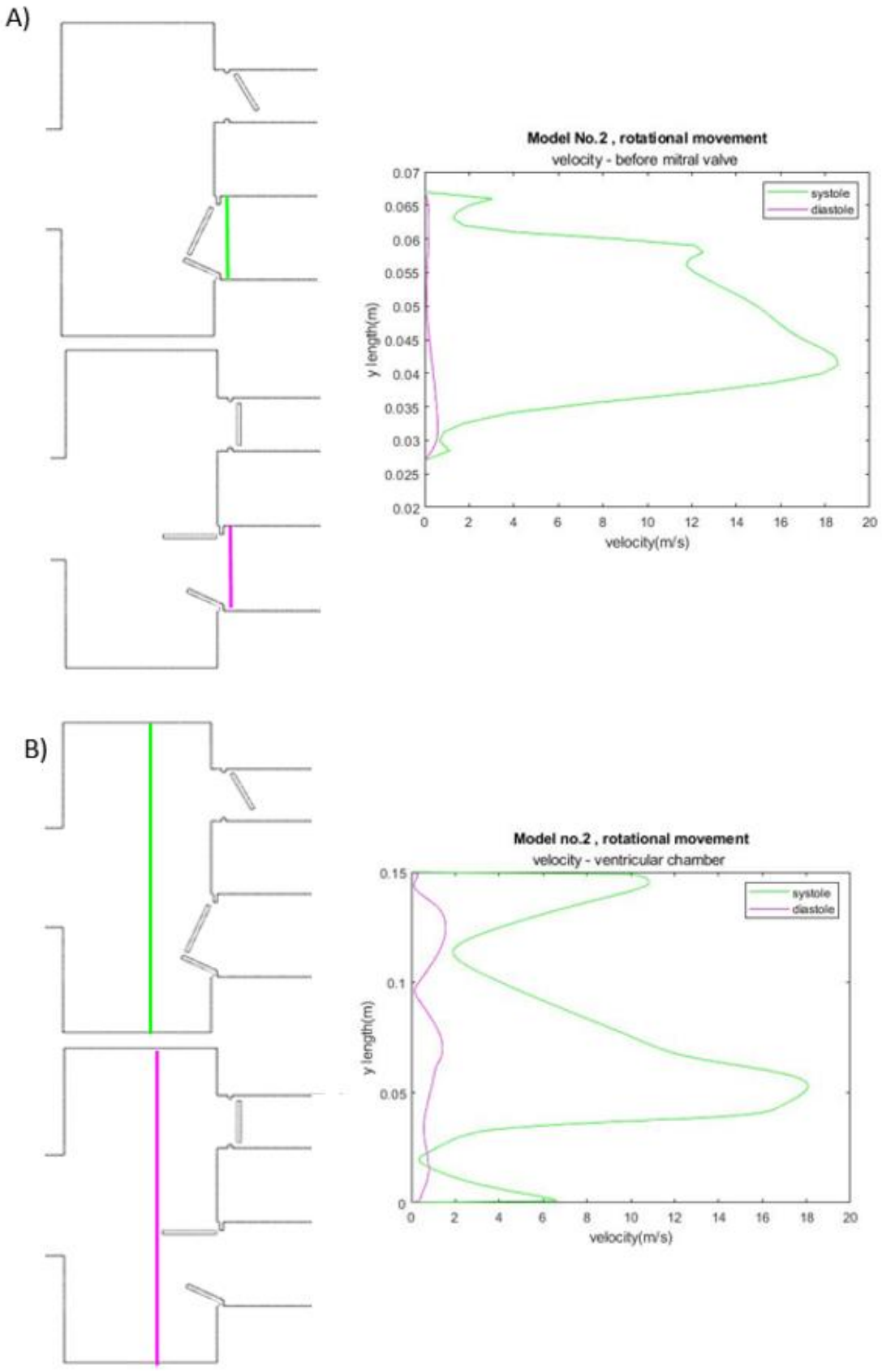

Figure 66 – Model No. 2: graphs showing velocity profiles, in case of rotational motion, at the mitral valve as a function of channel length y, considering A) the velocity values located before the mitral valve and B) after the mitral valve, in the ventricular chamber, for systole (green lines) and diastole (magenta lines).

Until now, it has been assumed that the high values present during systole were related to imperfect valve closure. Other hypotheses were also made, investigating other factors as well, making further investigations in which the boundary conditions were modified, or changing the position of the inlet connected to the pumping system to see if its location affected the values obtained in any way. In particular, its position was modified in model no.2 as this constitutes the final design of the pulse duplicator and therefore the model in which it is most important to obtain good haemodynamics. To this end, the area connected to the pumping system was positioned at the top of the ventricular chamber as shown in figure 67.

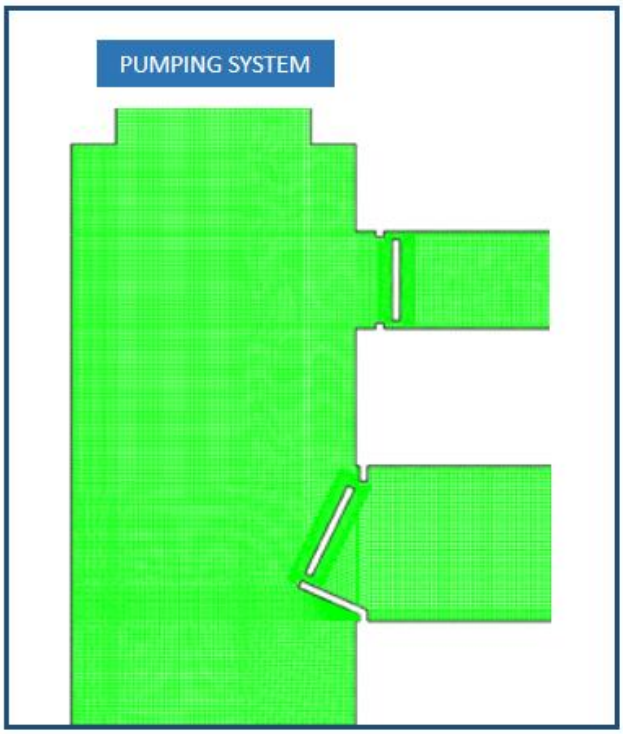

Figure 67 - New configuration of model no.2 with pumping system inlet positioned at the top of the ventricle

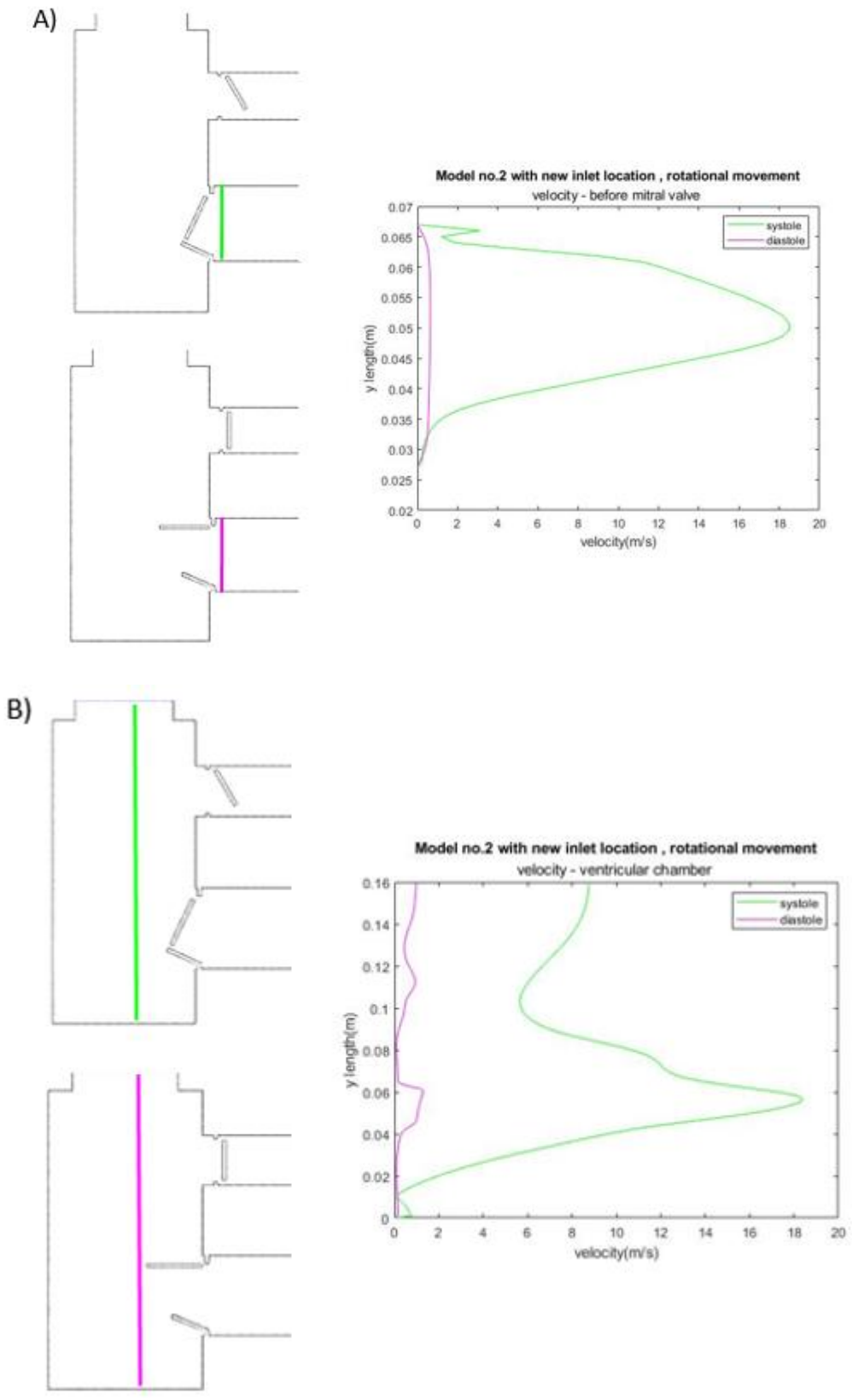

Figure 68 – Model No. 2: graphs showing velocity profiles, in case of rotational motion, at the mitral valve as a function of channel length y, considering A) the velocity values located before the mitral valve and B) after the mitral valve, in the ventricular chamber, for systole (green lines) and diastole (magenta lines).

Despite the modification implemented, high velocity values still occur during systole, only to return to physiological values during diastole as in the previous model [Figure 68]. Other configurations of the inlet were analysed with the same results, so these results are most likely to be attributable to the limitations of the dynamic mesh method. In order to confirm this hypothesis and thus ultimately exclude the incorrect functioning of the design, a greater depth of investigation could be achieved by using a 3D model and another analysis technique. To this end, the CAD of the 3D model based on the final design was prepared [Figure 69], the investigation of which is beyond the scope of this thesis and is left to the members of the Cardiovascular Tissue Engineering Laboratory who will subsequently continue their investigation of the pulse duplicator.

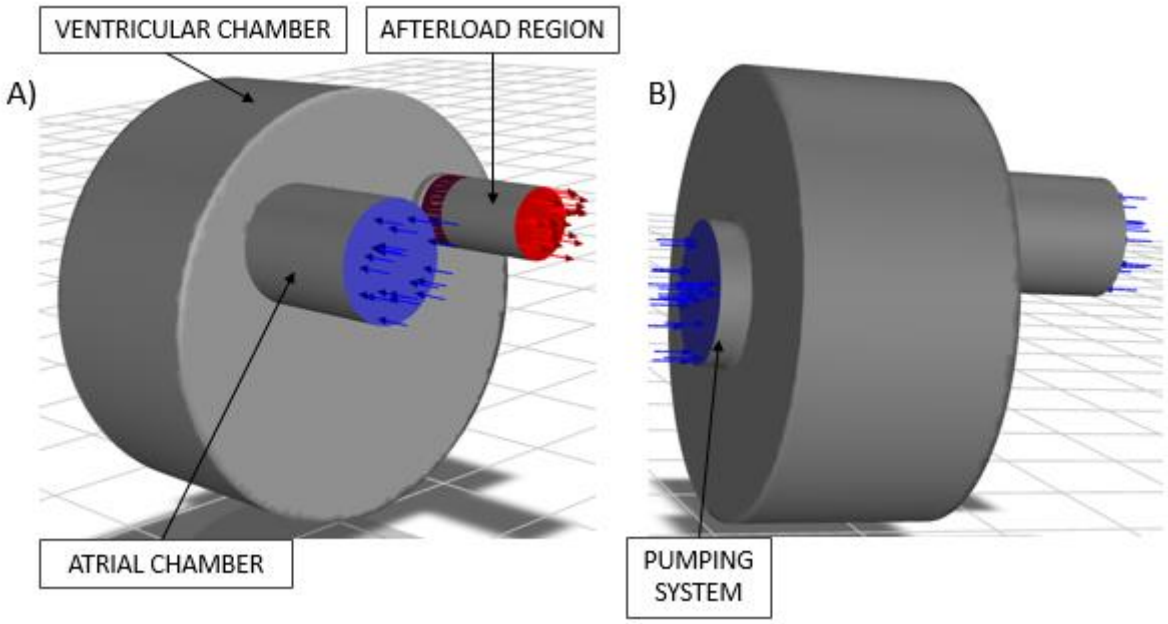

Figure 69 – 3D model 3d model of the final pulse duplicator design A) front and B) side view.

Chapter 5

Conclusion

A new Pulse Duplicator model was analysed with CFD analysis. This model was developed by Cardiovascular Tissue Engineering Laboratory (Ri.MED Foundation) and will be used as the environment in which to analyse a new mitral valve model currently being developed by the Biomitral project. The aim of this thesis was therefore to study the new pulse duplicator model consisting of the atrium and ventricle chamber and capable of housing both the mitral and aortic valves. In particular, the aim was to investigate its function from a fluid-dynamic point of view. To this end, the potential of Computational Fluid Dynamics was exploited and simulations were conducted using the Ansys Fluent 2022 R2 numerical solver based on the finite-volume method, in which the preliminary and final design of the pulse duplicator was examined and a simplified model used as the basis for the investigation was created. As a first step, CAD models of each design were produced for each component, which were then subjected to domain discretization by creating a mesh composed of quadrangular elements. The discretized CAD drawings were then imported into the Fluent environment where, through the creation of overset interfaces, it was possible to overlap the components and construct the complete model. At this point, the cardiac cycle was reproduced in its systole and diastole phases, using as boundary conditions the pressure values obtained by applying the laws of conservation of mass and energy to two points of the pulse duplicator's equivalent circuit consisting of resistors, inductances and capacitances modelling the various zones. The pressure values obtained were then scaled in accordance with the physiological values and used as input for the boundary conditions. Using the dynamic mesh method, it was possible to investigate the behaviour of the mitral valve under the conditions described, and in particular by reproducing translational and rotational motion in different phases. From the results obtained, it is possible to state that the pulse duplicator is able to correctly reproduce the period of diastole and thus the physiologically suitable environment for the mitral valve in this phase, while it presents difficulties during systole, in which high velocity values occur. However, these values

could be related to some limitations of the dynamic mesh method, so it is recommended that lab members (who will continue the study) investigate this further in order to exclude the incorrect performance of the pulse duplicator. A more in-depth investigation using a 3D model of the pulse duplicator is therefore suggested, of which the CAD model is provided, and a method other than the dynamic mesh is recommended for analysis, perhaps using the FSI method, bearing in mind that in vitro experimentation must always be added to the computational investigation.

Bibliography

1. Doost, S. N., Ghista, D., Su, B., Zhong, L. & Morsi, Y. S. Heart blood flow simulation: A perspective review. *Biomed. Eng. Online* **15**, (2016).
2. Dahlöf, B. Cardiovascular Disease Risk Factors: Epidemiology and Risk Assessment. *Am. J. Cardiol.* **105**, 3A-9A (2010).
3. Andersson, C. & Vasan, R. S. Epidemiology of cardiovascular disease in young individuals. *Nature Reviews Cardiology* vol. 15 230–240 at https://doi.org/10.1038/nrcardio.2017.154 (2018).
4. Tissue engineering of cardiovascular structures.
5. Sacks, M. S., David Merryman, W. & Schmidt, D. E. On the biomechanics of heart valve function. *Journal of Biomechanics* vol. 42 1804–1824 at https://doi.org/10.1016/j.jbiomech.2009.05.015 (2009).
6. Marom, G. & Einav, S. New insights into valve hemodynamics. *Rambam Maimonides Medical Journal* vol. 11 at https://doi.org/10.5041/RMMJ.10400 (2020).
7. Nishimura, R. A., Vahanian, A., Eleid, M. F. & Mack, M. J. Mitral valve disease - Current management and future challenges. *The Lancet* vol. 387 1324–1334 at https://doi.org/10.1016/S0140-6736(16)00558-4 (2016).
8. Manzoni, E., Rampazzo, M., Di Micco, L. & Susin, F. M. Characterization of Left Ventricular Hemodynamics in a Pulse Duplicator through Phase Plane Analysis. in *IFAC-PapersOnLine* vol. 55 139–144 (Elsevier B.V., 2022).
9. Yoganathan, A. P., Chandran, K. B. & Sotiropoulos, F. Flow in prosthetic heart valves: State-of-the-art and future directions. *Ann. Biomed. Eng.* **33**, 1689–1694 (2005).
10. Kaule, S. *et al.* Pulsatile flow testing of heart valve prostheses in vitro. *Curr. Dir. Biomed. Eng.* **8**, 683–686 (2022).
11. V, M. C. Computational Fluid Dynamics Simulation of the dynamics of a tilting disc heart valve prosthesis during the opening and fully open phases. *Artic. Int. J. Sci. Eng. Res.* **5**, (2014).
12. Ho, S. Y. Cardiac Anatomy: The Essentials. *Cardiol. Plus* **5**, 148–154 (2020).
13. Humphreyl, J. D. & Mcculloch, A. D. *The Cardiovascular System-Anatomy, Physiology and Cell Biology*.
14. Stefanovska, A. & Bračič, M. Physics of the human cardiovascular system. *Contemp. Phys.* **40**, 31–55 (1999).
15. A Review of Cardiac Anatomy and Physiology.
16. Meschini, V., Viola, F. & Verzicco, R. Heart rate effects on the ventricular hemodynamics and mitral valve kinematics. *Comput. Fluids* **197**, (2020).

17. Sacks, M. S. & Yoganathan, A. P. Heart valve function: A biomechanical perspective. *Philosophical Transactions of the Royal Society B: Biological Sciences* vol. 362 1369–1391 at https://doi.org/10.1098/rstb.2007.2122 (2007).

18. Misfeld, M. & Sievers, H. H. Heart valve macro- and microstructure. *Philosophical Transactions of the Royal Society B: Biological Sciences* vol. 362 1421–1436 at https://doi.org/10.1098/rstb.2007.2125 (2007).

19. Gao, H. *et al.* Modelling Mitral Valvular Dynamics-current trend and future directions. *Int. J. Numer. Meth. Biomed. Engng* (2858) doi:10.1002/cnm.cnm2858.

20. Kunzelman, K. S., Einstein, D. R. & Cochran, R. P. Fluid-structure interaction models of the mitral valve: Function in normal and pathological states. *Philos. Trans. R. Soc. B Biol. Sci.* **362**, 1393–1406 (2007).

21. Topilsky, Y. Mitral Regurgitation: Anatomy, Physiology, and Pathophysiology—Lessons Learned From Surgery and Cardiac Imaging. *Frontiers in Cardiovascular Medicine* vol. 7 at https://doi.org/10.3389/fcvm.2020.00084 (2020).

22. Lau, K. D., Diaz, V., Scambler, P. & Burriesci, G. Mitral valve dynamics in structural and fluid-structure interaction models. *Med. Eng. Phys.* **32**, 1057–1064 (2010).

23. Katsi, V. *et al.* Aortic valve: anatomy and structure and the role of vasculature in the degenerative process. *Acta Cardiologica* vol. 76 335–348 at https://doi.org/10.1080/00015385.2020.1746053 (2021).

24. Piazza, N. *et al.* Anatomy of the aortic valvar complex and its implications for transcatheter implantation of the aortic valve. *Circulation. Cardiovascular interventions* vol. 1 74–81 at https://doi.org/10.1161/CIRCINTERVENTIONS.108.780858 (2008).

25. Jonas, S. N., Kligerman, S. J., Burke, A. P., Frazier, A. A. & White, C. S. Pulmonary valve anatomy and abnormalities: A pictorial essay of radiography, computed tomography (CT), and magnetic resonance imaging (MRI). *J. Thorac. Imaging* **31**, W4–W12 (2016).

26. Hinton, R. B. & Yutzey, K. E. Heart valve structure and function in development and disease. *Annu. Rev. Physiol.* **73**, 29–46 (2011).

27. Hahn, R. T., Waxman, A. B., Denti, P. & Delhaas, T. Anatomic Relationship of the Complex Tricuspid Valve, Right Ventricle, and Pulmonary Vasculature: A Review. *JAMA Cardiology* vol. 4 478–487 at https://doi.org/10.1001/jamacardio.2019.0535 (2019).

28. Rostagno, C. Heart valve disease in elderly. *World J. Cardiol.* **11**, 71–83 (2019).

29. Nkomo, V. T. *et al.* Burden of valvular heart diseases: a population-based study. *www.thelancet.com* **368**, (2006).

30. Levine, R. A. *et al.* Mitral valve disease-morphology and mechanisms. *Nature Reviews Cardiology* vol. 12 689–710 at https://doi.org/10.1038/nrcardio.2015.161 (2015).

31. Harb, S. C. & Griffin, B. P. Mitral Valve Disease: a Comprehensive Review. *Current Cardiology Reports* vol. 19 at https://doi.org/10.1007/s11886-017-0883-5 (2017).

32. Ross, J., Guest Editor, F., Rapaport, E. & Francisco, S. *Symposium on the Effects of Surgical Treatment on the Natural History of Acquired Heart Disease. Part II. Aortic and Mitral Valve Disease Natural History of Aortic and Mitral Valve Disease*.

33. Coffey, S., Cairns, B. J. & Iung, B. The modern epidemiology of heart valve disease. doi:10.1136/heartjnl-2014.

34. Bland, E. F. D. & Jones, D. *Rheumatic Fever and Rheumatic Heart Disease A Twenty Year Report on 1009 Patients Followed Since Childhood*. http://ahajournals.org.

35. O'Donnell, A. & Yutz, K. E. Mechanisms of heart valve development and disease. *Development (Cambridge)* vol. 147 at https://doi.org/10.1242/dev.183020 (2020).

36. Harky, A. *et al.* Mitral valve diseases: Pathophysiology and interventions. *Progress in Cardiovascular Diseases* vol. 67 98–104 at https://doi.org/10.1016/j.pcad.2021.03.008 (2021).

37. Yoganathan, A. & Fotis Sotiropoulos. *Using Computational Fluid Dynamics to Examine the Hemodynamics of Artificial Heart Valves*. (2004).

38. Kiris, C., Kwak, D., Rogers, S. & Chang, L.-D. *Computational Approach for Probing the Flow Through Artificial Heart Devices*. http://biomechanical.asmedigitalcollection.asme.org/ (1997).

39. Ge, L., Leo, H. L., Sotiropoulos, F. & Yoganathan, A. P. Flow in a mechanical bileaflet heart valve at laminar and near-peak systole flow rates: CFD simulations and experiments. *J. Biomech. Eng.* **127**, 782–797 (2005).

40. Studies of Platelet and Fibrinogen Kinetics in Patients with Prosthetic Heart Valves.

41. Skoularigis, J., Essop, M. R., Skudicky, D., Middlemost, S. J. & Sareli, P. Frequency and severity of intravascular hemolysis after left-sided cardiac valve replacement with medtronic hall and St. Jude medical prostheses, and influence of prosthetic type, position, size and number. *Am. J. Cardiol.* **71**, 587–591 (1993).

42. Toma, M., Singh-Gryzbon, S., Frankini, E., Wei, Z. & Yoganathan, A. P. Clinical Impact of Computational Heart Valve Models. *Materials* vol. 15 at https://doi.org/10.3390/ma15093302 (2022).

43. Bartoli-Leonard, F. & Aikawa, E. Heart Valve Disease: Challenges and New Opportunities. *Front. Cardiovasc. Med.* **7**, (2020).

44. Basri, E. I. *et al. Computational Fluid Dynamics Study in Biomedical Applications: A Review*. https://www.researchgate.net/publication/309389664 (2016).

45. Dhotre, M. T., Nere, N. K., Vedantam, S. & Tabib, M. Advances in computational fluid dynamics. *International Journal of Chemical Engineering* at https://doi.org/10.1155/2013/917373 (2013).

46. DeCampli, W. M., Ricardo Argueta-Morales, I., Divo, E. & Kassab, A. J.

Computational fluid dynamics in congenital heart disease. in *Cardiology in the Young* vol. 22 800–808 (2012).

47. Morris, P. D. *et al.* Computational fluid dynamics modelling in cardiovascular medicine. doi:10.1136/heartjnl.

48. Lee, J. H. *et al.* Fluid–Structure Interaction Models of Bioprosthetic Heart Valve Dynamics in an Experimental Pulse Duplicator. *Ann. Biomed. Eng.* **48**, 1475–1490 (2020).

49. Kelly, S. G. D. *Computational Fluid Dynamics Insights in the Design of Mechanical Heart Valves*. (2002).

50. Chan, B. T., Lim, E., Chee, K. H. & Abu Osman, N. A. Review on CFD simulation in heart with dilated cardiomyopathy and myocardial infarction. *Computers in Biology and Medicine* vol. 43 377–385 at https://doi.org/10.1016/j.compbiomed.2013.01.013 (2013).

51. Ge, L., Jones, S. C., Sotiropoulos, F., Healy, T. M. & Yoganathan, A. P. Numerical Simulation of Flow in Mechanical Heart Valves: Grid Resolution and the Assumption of Flow Symmetry. *J. Biomech. Eng.* **125**, 709–718 (2003).

52. McQueen, D. M. & Peskin, C. S. *COMPUTER-ASSISTED DESIGN OF BUTTERFLY BILEAFLET VALVES FOR THE MITRAL POSITION*. *Cardiovasc Surg* vol. 19 (1985).

53. Lai, Y. G., Chandran, K. B. & Lemmon, J. *A Numerical Simulation of Mechanical Heart Valve Closure Fluid Dynamics*. *Journal of Biomechanics* vol. 35 (2002).

54. King, M. J., David, T. & Fisher, J. An Initial Parametric Study on Fluid Flow Through Bileaflet Mechanical Heart Valves Using Computational Fluid Dynamics. *Proc. Inst. Mech. Eng. Part H J. Eng. Med.* **208**, 63–72 (1994).

55. Collia, D., Zovatto, L. & Pedrizzetti, G. Analysis of mitral valve regurgitation by computational fluid dynamics. *APL Bioeng.* **3**, (2019).

56. Bjork, V. o, Intonti, F. & Meissl, A. *A MECHANICAL PULSE DUPLICATOR FOR TESTING PROSTHETIC MITRAL AND AORTIC VALVES*. *Thorax* (1962).

57. Duran, C. G., Gunning, A. J. & Mcmillan, T. *A Simple Versatile Pulse Duplicator*. *Thorax* http://thorax.bmj.com/ (1964).

58. Rodriguez, R. A., Dellimore, K. H. & Müller, J. H. Evaluating the Performance of Cardiac Pulse Duplicators Through the Concept of Fidelity. *Cardiovasc. Eng. Technol.* **10**, 423–436 (2019).

59. Haaf, P. *et al.* A novel pulse duplicator system: Evaluation of different valve prostheses. *Thorac. Cardiovasc. Surg.* **57**, 10–17 (2009).

60. Fredrick Cornhill, J. *An Aortic-Left Ventricular Pulse Duplicator Used in Testing Prosthetic Aortic Heart Valves*.

61. Verdonck, P. R., Van Nooten, G. J. & Van Belleghem, Y. *Pulse Duplicator Hydrodynamics of Four Different Bileaflet Valves in the Mitral Position*. *Cardiovascular Surgery* vol. 5 (1997).

62. Mashari, A. *et al.* Hemodynamic Testing of Patient-Specific Mitral Valves Using a Pulse Duplicator: A Clinical Application of Three-Dimensional Printing. *Journal of Cardiothoracic and Vascular Anesthesia* vol. 30 1278–1285 at https://doi.org/10.1053/j.jvca.2016.01.013 (2016).

63. Peiró, J. & Sherwin, S. *8.2 FINITE DIFFERENCE, FINITE ELEMENT AND FINITE VOLUME METHODS FOR PARTIAL DIFFERENTIAL EQUATIONS*.

64. Versteeg, H. K. & Malalasekera, W. *An Introduction to Computational Fluid Dynamics Second Edition*. www.pearsoned.co.uk/versteeg.

65. Al-Baali, A. G. A. G. & Farid, M. M. Fundamentals Of Computational Fluid Dynamics. in *Food Engineering Series* 33–44 (Springer, 2006). doi:10.1007/0-387-31129-7_4.

66. Zawawi, M. H. *et al.* A review: Fundamentals of computational fluid dynamics (CFD). in *AIP Conference Proceedings* vol. 2030 (American Institute of Physics Inc., 2018).

67. Jeong, W. & Seong, J. Comparison of effects on technical variances of computational fluid dynamics (CFD) software based on finite element and finite volume methods. *Int. J. Mech. Sci.* **78**, 19–26 (2014).

68. Harrild, D. M. & Henriquez, C. S. *A Finite Volume Model of Cardiac Propagation*. *Annals of Biomedical Engineering* vol. 25 (1997).

69. O'Callaghan, S., Walsh, M. & McGloughlin, T. Comparison of finite volume, finite element and theoretical predictions of blood flow through an idealised femoral artery. *2003 Summer Bioeng. Conf.* 417–417 (2003).

70. Juretić, F. & Gosman, A. D. Error analysis of the finite-volume method with respect to mesh type. *Numer. Heat Transf. Part B Fundam.* **57**, 414–439 (2010).

71. Molina-Aiz, F. D., Fatnassi, H., Boulard, T., Roy, J. C. & Valera, D. L. Comparison of finite element and finite volume methods for simulation of natural ventilation in greenhouses. *Comput. Electron. Agric.* **72**, 69–86 (2010).

72. Sobieski, W. *THE BASIC EQUATIONS OF FLUID MECHANICS IN FORM CHARACTERISTIC OF THE FINITE VOLUME METHOD*. *Abbrev.: Techn. Sc., No* vol. 14 (2011).

73. Acharya, S. *et al.* Pressure-based finite-volume methods in computational fluid dynamics. *Journal of Heat Transfer* vol. 129 407–424 at https://doi.org/10.1115/1.2716419 (2007).

74. Jang, D. S., Jetli, R. & Acharya, S. Comparison of the piso, simpler, and simplec algorithms for the treatment of the pressure-velocity coupling in steady flow problems. *Numer. Heat Transf.* **10**, 209–228 (1986).

75. Hodis, S., Kallmes, D. F. & Dragomir-Daescu, D. *CFD Challenge Solution Using the Commercial Finite Volume Solver Fluent*. http://www.asme.org/about-asme/terms-of-use (2012).

76. Cito, S., Pallares, J., Vernet, A. & Cuesta, I. *CFD Challenge: Giant Internal Carotid Artery Aneurysm Simulation Using the Commercial Finite Volume Solver Fluent*. http://proceedings.asmedigitalcollection.asme.org/pdfaccess.ashx?url=/data/conferences/asmep/75456/ (2012).

77. Bressloff, N. W. & Hameed, A. T. *CFD Challenge: Solutions Using the Mesher, Harpoon, and the Finite Volume Solver, Fluent*. http://www.asme.org/about-asme/terms-of-use (2012).

78. Lanzarone, E., Vismara, R. & Fiore, G. B. A new pulsatile volumetric device with biomorphic valves for the in vitro study of the cardiovascular system. *Artif. Organs* **33**, 1048–1062 (2009).

79. *ANSYS FLUENT Theory Guide*. http://www.ansys.com (2011).

80. A three-dimensional analysis of flow in the pivot regions of an ATS bileaflet valve.

81. Aluri, S. & Chandran, K. B. Numerical simulation of mechanical mitral heart valve closure. *Ann. Biomed. Eng.* **29**, 665–676 (2001).

82. Dedè, L., Menghini, F. & Quarteroni, A. Computational fluid dynamics of blood flow in an idealized left human heart. *Int. j. numer. method. biomed. eng.* **37**, 1–24 (2021).

83. Adi A. Basri, Mohamed Zubair , Ahmad F.A. Aziz., Rosli M. Ali, Masaaki Tamagawa, K. A. A. Computational Fluid Dynamics Study of the Aortic Valve Opening on Hemodynamics Characteristics. in (2014).

84. Bajgrowicz, M. *CFD SIMULATION OF BLOOD FLOW THROUGH ARTIFICIAL HEART VALVES. XIII th Youth Symposium on Experimental Solid Mechanics*.

85. Vucinic, D., Yang, T. & Aksenov, A. A. *Human Heart Blood Flow Simulations Based on CFD*. www.ijfht.com (2016).

86. Yoganathan, A. P., He, Z. & Jones, S. C. Fluid mechanics of heart valves. *Annual Review of Biomedical Engineering* vol. 6 331–362 at https://doi.org/10.1146/annurev.bioeng.6.040803.140111 (2004).

87. Simonson, J. S. & Schiller, N. B. Descent of the Base of the Left Ventricle: An Echocardiographic Index of Left Ventricular function. *J. Am. Soc. Echocardiogr.* **2**, 25–35 (1989).

88. Dumont, K., Stijnen, J. M. A., Vierendeels, J., van de Vosse, F. N. & Verdonck, P. R. Validation of a fluid-structure interaction model of a heart valve using the dynamic mesh method in fluent. *Comput. Methods Biomech. Biomed. Engin.* **7**, 139–146 (2004).

89. Sotiropoulos, F., Le, T. B. & Gilmanov, A. Fluid Mechanics of Heart Valves and Their Replacements. *Annu. Rev. Fluid Mech.* **48**, 259–283 (2016).